

# On the nature of Mersenne fluctuations<sup>☆,☆☆</sup>

U. Merkel\*

<sup>a</sup> Universitätsstr. 38, 70569 Stuttgart, Germany

---

## Abstract

The article introduces crotons, multifaceted pre-geometric objects that occur both as labels encoded on the boundary of a “volume” and as complementary aspects of geometric fluctuations within that volume. If you think of crotons as linear combinations, then the scalars used are croton base numbers. Croton base numbers can be combined to form the amplitudes and phases of Mersenne fluctuations which, in turn, form qphyla. Volume normally requires space or space-time as a prerequisite; in a pregeometric setting, however, “volume” is represented by a qphyletic assembly. Various stages of pre-geometric refinement, expressed through the aspects crotonic amplitude or phase, combine to eventually form and/or dissolve sphere-packed chunks of Euclidean space. A time-like crotonic refinement is a rough analog of temporal resolution in tenacious time; a space-like crotonic refinement corresponds to spatial resolution in sustained space. The analogy suggests the existence of a conceptual link between the ever-expanding scope of Mersenne fluctuations and the creation and lifetime patterns of massive elementary particles, an idea that is exploited to substantiate our previously proposed preon model of subnuclear structure.

*Keywords:* pre-geometry, crotons, Mersenne fluctuations, qphyla, continued fractions, kissing numbers, Magnus equation, preons, up-type and down-type interordinal bounds

*2010 MSC:* 06B15, 11A55, 11H99

*PACS:* 12.50.Ch, 12.60.Rc

---

<sup>☆</sup>This document deepens aspects addressed in a previous article titled “Parafermi algebra and interordinality” (see [Merkel]).

<sup>☆☆</sup>In “Parafermi algebra and interordinality”, the central theme was the implications raised by the special case that two parafermi algebras are of Mersenne-wise neighboring orders. The present document is meant to be largely self-contained, but an in-depth study of the previous work is helpful and therefore recommended.

\*Corresponding author

*Email address:* [merkel.u8@googlemail.com](mailto:merkel.u8@googlemail.com) (U. Merkel)

## Part I

### 1. Introduction

Crotons are pregeometric objects that emerge both as labels encoded on the boundary of a “volume” and as complementary aspects of geometric fluctuations within that volume. To express their multifacetedness, the name *croton* was chosen, after Crotos, son of Pan and Eupheme, who, once a mortal 3D being, was put in sky by Muses as the celestial fixture Sagittarius. The term volume is normally linked to the categories space or space-time. In a pre-geometric setting, more basic categories are needed – Mersenne fluctuations and qphyla. Both require various stages of *pregeometric refinement* which, expressed through the complementary aspects croton amplitude and phase, combine to eventually form – or dissolve – real geometric objects. Advancing from mark  $n$  to  $n+1$  thus, in what follows, means a time-like refinement  $2^{-n}c \mapsto 2^{-n-1}c$  (roughly the analog of an exponential increase of temporal resolution in tenacious time), and an increase from  $\alpha$  to mark  $\alpha+1$  a space-like refinement  $\frac{a}{b_\alpha} \mapsto \frac{a}{b_\alpha + b_{\alpha+1}^{-1}}$  ( $b_\alpha, b_{\alpha+1} > 0$ ) (analogous to increase of spatial resolution in sustained space). On the boundary, these increases find expression in additionally encoded labels.

In a previous work [Merkel], basic croton components have been identified, though at the time the name croton was not yet used. The starting point was the equivalence between a Mersennian identity, distilled from the special case that two parafermi algebras [Green] are of neighboring orders  $p = 2^i - 1$ ,  $p' = p^{i+1} - 1$  (order marked by parenthesized superscript):

$$\frac{1}{2} \{ \mathbf{b}^{(p')}, \mathbf{1}^{\otimes n} \otimes \mathbf{b}^{(1)} \} = \mathbf{b}^{(p)} \otimes \mathbf{1}, \quad (1)$$

and the identities<sup>1</sup>

$$(\mathbf{f}^{(p')})^2 = \mathbf{f}^{(p)} \otimes \mathbf{1}, \quad (2)$$

$$(\mathbf{h}^{(p')})^2 = \mathbf{h}^{(p)} \otimes \mathbf{1}. \quad (3)$$

Leaving the details to Appendix A, the way croton base numbers are derived and how they are subdivided into bases pop out naturally when the matrix elements of  $\mathbf{f}^{(p)}$  and  $\mathbf{h}^{(p)}$  are constructed. Crotons, conceived of as linear combinations, use the following croton base numbers as scalars (underlining explained later): for  $i = 2$ ,  $G^{(3)} = 1$ ,  $J^{(3)} = 1$ ; for  $i = 3$ ,  $G^{(7)} = \underline{1}$ ,  $(J_\rho^{(7)}) = (-\underline{1}, 3)$ ; for  $i = 4$ ,  $(G_\rho^{(15)}) = (3, \underline{5}, 11, 17, 41, 113)$ ,  $(J_\rho^{(15)}) = (-\underline{5}, 15, -43, 149)$ , to name only the first few (singletons and bases). They are instructive enough to show how label encoding works on the boundary.

---

<sup>1</sup> where  $\mathbf{f}^{(1)} \equiv \mathbf{b}^{(1)} = \begin{pmatrix} 0 & 0 \\ 1 & 0 \end{pmatrix}$ ,  $c_3 = \begin{pmatrix} 0 & 1 \\ -1 & 0 \end{pmatrix}$ ,  $c_2 = \begin{pmatrix} 0 & 1 \\ 1 & 0 \end{pmatrix}$ ,  $\mathbf{1} = \begin{pmatrix} 1 & 0 \\ 0 & 1 \end{pmatrix}$ :  
 $\mathbf{f}^{(p)} \equiv \mathbf{1}^{\otimes i-1} \otimes \mathbf{b}^{(1)} + (G_{\mu\nu}^{(p)}) \otimes c_3$ ,  $\mathbf{h}^{(p)} \equiv \mathbf{1}^{\otimes i-1} \otimes \mathbf{b}^{(1)} + (J_{\mu\nu}^{(p)}) \otimes c_2$ ,  $(i = 2, 3, \dots)$

## 2. Crotons on the boundary

We first concentrate on order  $p = 15$ , dropping the parenthesized superscript and just asking the reader to bear in mind that the crotons examined belong to  $i = \log_2(p + 1) = 4$ . Our boundary is then defined by the  $3^T - 1$  outer nodes of a  $T$ -cube complex,  $T$  being the number of croton base numbers to handle:  $T = 6$  for  $(G_\rho) = (3, \underline{5}, 11, 17, 41, 113)$ , and  $T = 4$  for  $(J_\rho) = (-\underline{5}, 15, -43, 149)$ . Let the  $x$ -th node out of the  $728 = 3^6 - 1$  of the first boundary bear the label  $\Gamma_x = E_x^\rho G_\rho$ , and, correspondingly, the  $y$ -th node out of the  $80 = 3^4 - 1$  of the second boundary the label  $\chi_y = E_y^\rho J_\rho$  (summation convention, and  $E$  denoting all non-null  $T$ -tuples out of  $3^T$  possible from  $-1, 0, 1$ ). It's easy to see that the total of labels form a croton field in either case:  $\Gamma$  and  $\chi$ . The fact aside that nodes can be grouped into pairs bearing values of opposite sign, field values may occur multiply, for instance  $6 = (0, -1, 1, 0, 0, 0) \cdot G^t = (0, 0, -1, 1, 0, 0) \cdot G^t$ . With each field defined on its own boundary, it's far from obvious they should have anything in common. Yet, as we assume either one deals with a distinct crotonic aspect –  $\Gamma$  with the global perspective,  $\chi$  with the integration of  $\Gamma$  with the local  $T$ -cube complexes  $\Lambda_\alpha^{(n)}$  to be introduced in 7.3 – we have to find ways of considering them side by side.

### 2.1. Croton field duality and complementarity

We may, for instance, ask how many distinct labels there can be expressed *potentially*, neglecting mere sign reversals. Counting from 1 on and taking as the highest conceivable value the sum of croton base numbers in absolute terms, we arrive at the number 190 of potential labels from  $G$ . Out of these, 170 are realized as node labels  $\Gamma_x$ . Those not realizable are 20 in number:  $7, 34, 48, \dots, 189$ . The converse holds true for the  $J$  case. Of 212 potentially attainable labels, 40 are realized by  $\chi_y$  (sign-reversals included, that's the stock of nodes), leaving 172 labels in potential status.

A comparable situation arises when we bunch together croton base numbers that are rooted in neighboring Mersenne orders, a process we have previously termed *interordinal* to express this kind of hybridization. We now have  $T = 7$  for  $(G_\rho^{(7,15)}) = (\underline{1}, 3, \underline{5}, 11, 17, 41, 113)$ , and  $T = 6$  for  $(J_\rho^{(7,15)}) = (-\underline{1}, 3, -\underline{5}, 15, -43, 149)$ . Neglecting sign reversals and counting again from 1 on, we get 191 potential labels from the enlarged  $G$  and 216 from the enlarged  $J$ . All of the 191s' bunch are realized as  $\Gamma_x$  on the expanded boundary's nodes; but a singularity also springs up,  $0 = (1, 0, 1, 1, -1, 0, 0) \cdot G^t$ . By contrast, 202 out of the 216s' bunch are realized as  $\chi_y$ , on another expanded boundary's nodes and with no singularity popping up, leaving 14 in potential status:  $68, 69, \dots, 81$ . The conclusion is that the fields are dual to each other with respect to realizability of labels on the boundary. The duality is controlled by two quantities, Catalan number  $C_{q\pm 1}$  and the number  $5 \cdot 2^{i-r}$  ( $q \in \{1, 3\}, r \in \{2, 3\}$ ):

*Intraordinal case:*

$$\begin{aligned} \# \Gamma_x = 170 &\xleftrightarrow{C_2} \# \neg \chi_y = 172 \\ \# \chi_y = 40 &\xleftrightarrow{5 \cdot 2^2} \# \neg \Gamma_x = 20. \end{aligned} \quad (4)$$

*Interordinal case:*

$$\begin{aligned} \# \Gamma_x = 192^* &\xleftrightarrow{5 \cdot 2} \# \chi_y = 202 \\ \# \neg \chi_y = 14 &\xleftrightarrow{C_4} \# \neg \Gamma_x = 0. \end{aligned} \quad (5)$$

(\*The singularity assignment included.) The key role in that duality is taken by the quantity  $C_q$  ( $q = (p - 3)/4$ ) around which the croton base numbers for a specific basis of order  $p$  are built (hence the underlining of  $C_q$  in Sect. 3.1 where the bases of order 31 are presented):

*Intraordinal case:*

$$G_\rho^{(15)} \xleftrightarrow{C_3 \text{ sign reversal}} J_\varrho^{(15)} \quad (6)$$

*Interordinal case:*

$$G_\delta^{(7,15)} \xleftrightarrow{C_1, C_3 \text{ sign reversals}} J_\vartheta^{(7,15)}. \quad (7)$$

### 3. Crotons in the volume

For “volume” as the term is used here, a multitude of Mersenne fluctuations are constitutive. They assume a descriptive  $\wedge$  shape when amplitude is plotted versus “time”. Nodes on legs of a  $\wedge$  each bear a croton amplitude  $\varphi_{\alpha_{n \mp r}}^{(n \mp r)} \in \mathbb{N}$  that emerges with a specific time-like and space-like refinement — on the left leg  $n - r, \alpha_{n-r}$ , on the right  $n + r, \alpha_{n+r}$  — and the peak amplitude is reached at  $n, \alpha_n$ . The left-leg structure is given by

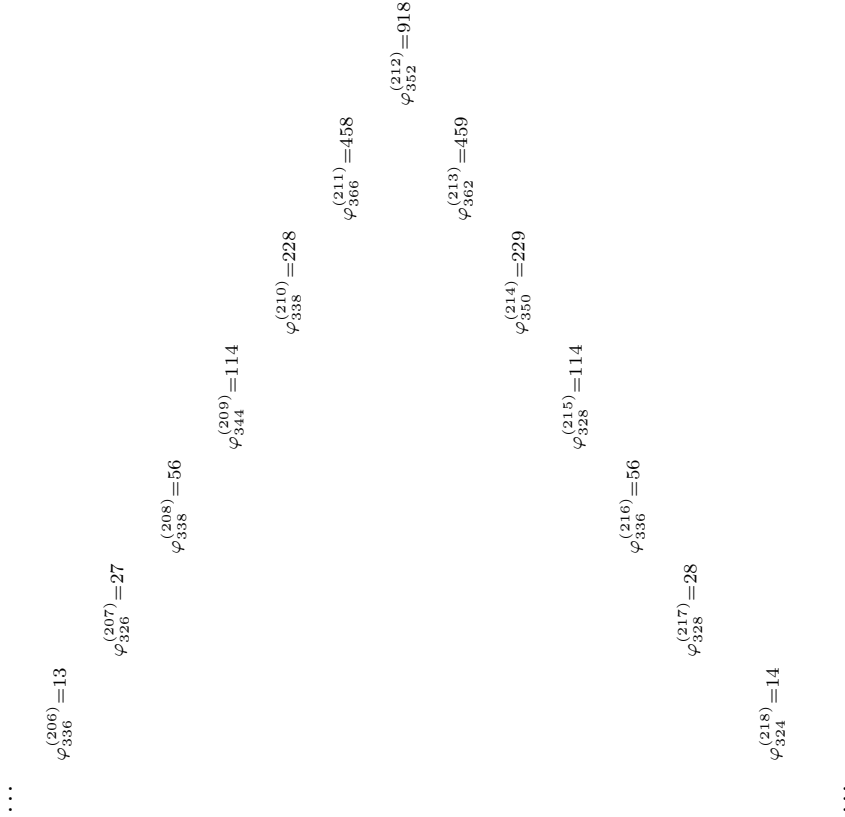
$$\varphi_{\alpha_{n-r+1}}^{(n-r+1)} = 2\varphi_{\alpha_{n-r}}^{(n-r)} + \delta + \epsilon, \quad (8)$$

the right-leg structure by

$$\varphi_{\alpha_{n+r+1}}^{(n+r+1)} = \left\lfloor \varphi_{\alpha_{n+r}}^{(n+r)} / 2 \right\rfloor - \delta \quad (9)$$

( $\delta \in \{0, 1\}$ ,  $\epsilon \in \{-1, 0, 1\}$ ), under the constraint of a maximal croton-amplitude shift between  $n - r$  and  $n + r$  of 1:  $|\varphi_{\alpha_{n-r}}^{(n-r)} - \varphi_{\alpha_{n+r}}^{(n+r)}| \leq 1$  ( $r < n, r \in \mathbb{N}_0$ ). A typical Mersenne fluctuation is shown in Fig. 1:

Figure 1: A geometric fluctuation of Mersenne type



We can stay in the (“time”,amplitude) coordinate system and observe how fluctuations which share amplitudes that differ maximally by  $\delta$  at each node but peak at different heights, organize into what we have previously termed *qphylum*.<sup>2</sup>

---

<sup>2</sup> One such qphylum would for instance house (peaks in boldface) the Mersenne fluctuations  
 $(\dots, 17, 35, 72, 145, 291, 584, \mathbf{1170}, 585, 292, 145, 72, 35, 17, \dots)$ ,  
 $(\dots, 18, 36, 72, 145, 291, 584, 1169, \mathbf{2340}, 1170, 585, 292, 145, 72, 36, 18, \dots)$ ,  
 $(\dots, 17, 35, 72, 146, 292, 584, 1169, 2340, \mathbf{4681}, 2340, 1169, 584, 292, 145, 72, 36, 17, \dots)$  etc. However, the Mersenne fluctuation  $(\dots, 584, 1168, 2337, 4676, \mathbf{9351}, 4675, 2336, 1168, 583, \dots)$  definitely belongs to a different qphylum — one worth mentioning also because it is one of the rare instances where overt inversion of the  $\epsilon$  term occurs: increase from 4676 to 9351 implies  $\delta = 0, \epsilon = -1$  (see Eq. (8)).

Figure 2: A prototype qphylum

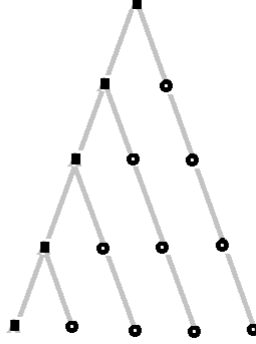
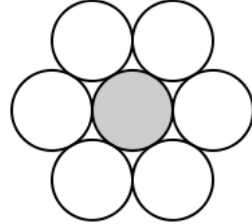


Figure 3: 1-sphere packing with our without centerpiece



Seen top-down, a qphylum is a left-complete binary tree, that is: a rooted tree whose root node and left child nodes have left and right child nodes, while right child nodes have only right child nodes, as shown in Fig. 2. Typically, qphylogenetically related amplitudes are rooted in different time-like and space-like refinements; nodes of a qphylum thus are associated with a set of frozen-in pre-geometric ‘‘time’’ and ‘‘space’’ signatures.<sup>3</sup> ‘‘Volume’’ then becomes the assembly of all distinct qphylla. But let us go back one step and ask what it means when an amplitude in a given fluctuation reaches a certain level. If that level coincides with  $L_m + 1$  or  $L_m$ , where  $L_m$  denotes the kissing number of  $m$ -dimensional

---

<sup>3</sup>As for unfreezing, see piece in 7.3 titled ‘Link between local and global implementation.’

Euclidean space, it could mean that a chunk of space containing an  $(m - 1)$ -sphere packing *with* or *without* centerpiece was created in that fluctuation – or dissolved if the amplitude did not peak: crotons which wax and wane. As an example, Fig. 1 shows a fluctuation that peaks at 918, a quantity considered to be the proper kissing number of 13-dimensional Euclidean space. A chunk of  $13D$ -space containing 918 12-spheres certainly is hard to visualize, so a  $2D$  version may suffice to give a first impression (see Fig. 3).

### 3.1. Connecting boundary and volume croton data

We may ask if and how the peak amplitude 918 is related to a label  $\Gamma_x$  on the boundary. Certainly it is a realizable label, and one realizable *intraordinarily*: All kissing numbers lying – on the basis of  $(G_\rho^{(15)})$  – in the range of potentially attainable labels can be seen to be realizable *intraordinarily*, and this holds true too for the current basis, the 18-tuple<sup>4</sup>  $(G_\rho^{(31)}) = (19, 43, 115, 155, \underline{429}, \dots, 1275, \dots, 4819, 4905, \dots)$  where 918 belongs:  $918 = (0, 1, 1, 0, -1, 0, \dots, 1, 0, \dots, 1, -1, 0, \dots) \cdot (G^{(31)})^t$ . The crucial question is, Do we require *all* croton amplitudes from a given Mersenne fluctuation with one of them “geometrizing” to have counterparts in *intraordinarily* realizable labels on the boundary, in a narrow interpretation of the holographic principle? Amplitudes “on the way/from there” may at least in principle be amenable to an answer. And, what does this mean for Mersenne fluctuations “making detours” which presumably are by far in the majority? If one of the croton amplitudes, call it *pivotal*, comes only close and does not “geometrize”, it is because some residual Mersenne fluctuations co-evolve in *different* qphylla. Yet, with sufficiently tight space-like and time-like refinement constraints, fluctuations that are inter-qphyletically linked to the pivotal fluctuation can be identified and examined. See the example below where one of the residual partial amplitudes is 102 as  $n - 2 = 1556$ , and the pivotal amplitude 5219, together with a second residual partial amplitude 24, is closing in on  $L_{17}(= 5346)$  as  $n = 1558$ :

---

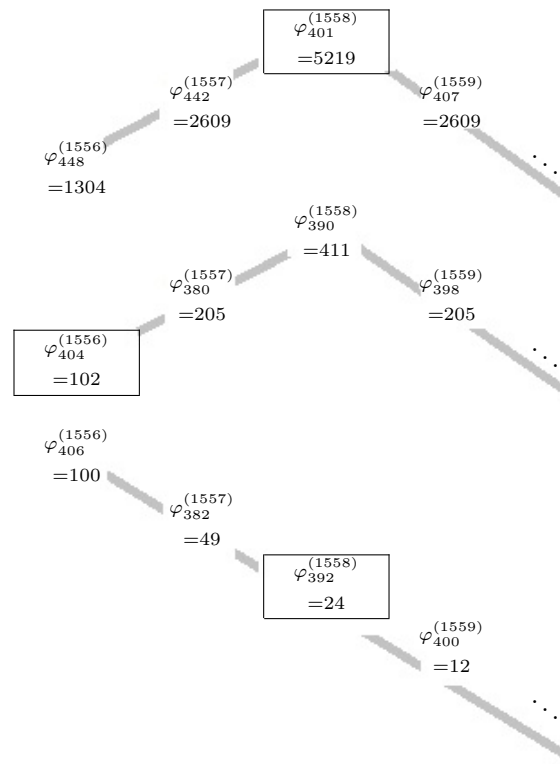
<sup>4</sup> in full length, the tuple reads

$$(G_\rho^{(31)}) = (19, 43, 115, 155, \underline{429}, 1275, 1595, 1633, 4819, 4905, 15067, 15297, 18627, 58781, 189371, 227089, 737953, 2430289);$$

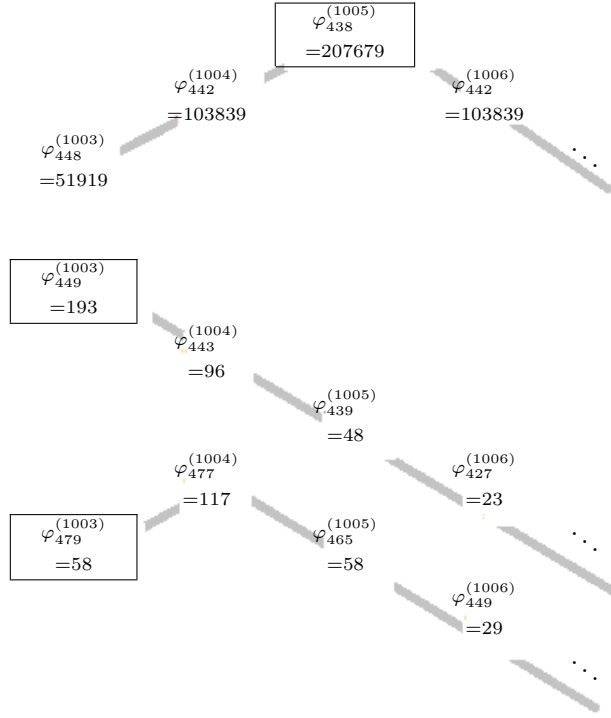
its origin and the origin of the tuple

$$(J_\rho^{(31)}) = (13, -41, 117, 143, \underline{-429}, 1319, 1343, 1547, -4823, -4903, 15547, 17989, 18269, -58791, 194993, 223573, -747765, 2886235);$$

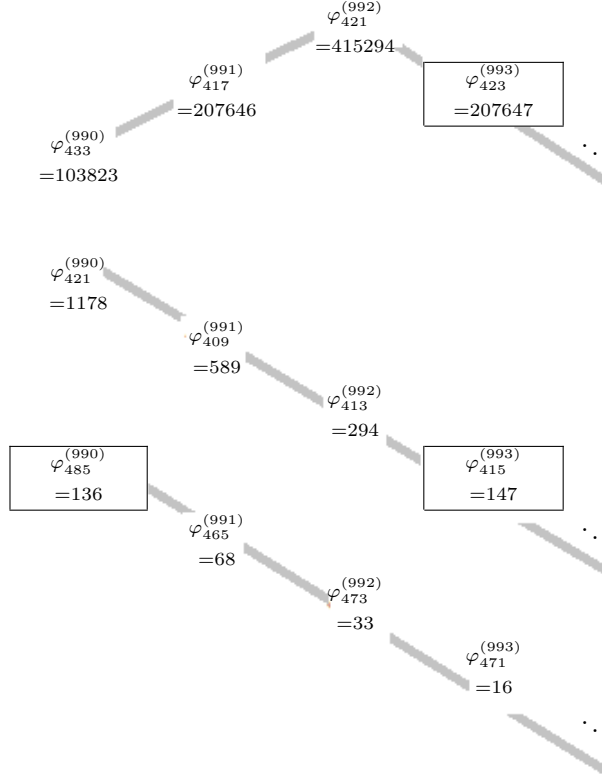
are elucidated in Appendix A; in Appendix B (see Table B.15 and B.16) various kissing numbers and kissing number-related croton amplitudes are tabularized, among them also the peak amplitude 918 from Fig.1.

Figure 4: Pivotal amplitude closing in on  $L_{17}(= 5346)$  plus two residual partial amplitudes

Another example is shown in Fig. 5 where two residual partial amplitudes attain the levels 58 and 193 respectively as  $n - 2 = 1003$ , allowing a pivotal amplitude 207679 to close in on  $L_{29}(= 207930)$  as  $n = 1005$ :

Figure 5: Pivotal amplitude closing in on  $L_{29}$  ( $= 207930$ ) plus two residual partial amplitudes

The pivotal amplitudes in Figs. 4 and 5 each coincide with the peak of their paternal fluctuation, but peak amplitude is not a necessary condition. Fig. 6 describes a situation where an  $(n \mp r)$ -pair of pivotal amplitudes on a fluctuation's legs are about to close in on  $L_{29}$ ; here, since only one time-like refinement lies between each candidate and the peak, one further time-like refinement also suffices to determine the residual partial amplitudes, where they originate and which of the two ‘leggy’ candidates 207646 and 207647 would have succeeded in filling the bill had it peaked:

Figure 6: Leggy pivot closing in on  $L_{29}(= 207930)$  plus two residual partial amplitudes

## 3.2. Croton phase and its inter-qphyletic role

“Phase” in the pre-geometric setting assumed here just means ‘having an ordinate value fluctuate between positions above and below an imaginary baseline,’ with consecutive marks on that line corresponding to stepwise increases of space-like refinement. That ordinate value, let us call it  $\psi_{\alpha_\psi}^{(n)}$  for a given “time” level  $n$ , is linked to the croton amplitude  $\varphi_{\alpha_\varphi}^{(n)}$  by the condition:

$$\text{if } |\psi_{\alpha_\psi}^{(n)}| = \varphi_{\alpha_\varphi}^{(n)} + \delta \text{ then } \psi_{\alpha_\psi}^{(n)} = \begin{cases} -\varphi_{\alpha_\varphi}^{(n)} - 1 & (\alpha_\psi \text{ even}) \\ \varphi_{\alpha_\varphi}^{(n)} + \delta & (\alpha_\psi \text{ odd}) \end{cases} \quad (\delta \in \{0, 1\}). \quad (10)$$

Whilst introducing croton phase in the volume now, the discussion will be limited to the fluctuations already considered in order to keep things as coherent as possible. Let us first follow two Mersenne fluctuations’ amplitudes (Fig. 6) and their associated  $\psi^{(n)}$ , one steering a pivotal, one a selected residual’s course:

Table 1: Pivotal and inter-qphyleticly accompanying residual fluctuation for  $987 \leq n \leq 997$ 

$n$	Pivot					Residue				
	$\varphi_P$	$\alpha_\varphi$	$\psi_P$	$\alpha_\psi$	$\Delta\alpha$	$\varphi_R$	$\alpha_\varphi$	$\psi_R$	$\alpha_\psi$	$\Delta\alpha$
987	12977	407	12977	437	30	9434	397	-9435	426	29
988	25955	411	-25956	418	7	4716	399	-4717	410	11
989	51911	397	51911	449	52	2357	385	-2358	438	53
990	103823	433	103824	441	8	1178	421	-1179	430	9
991	207646	417	207647	457	40	589	409	589	449	40
992	415294	421	415294	469	48	294	413	294	461	48
993	207647	423	207647	473	50	147	405	147	461	56
994	103823	443	103823	457	14	73	435	-74	446	11
995	51911	425	51912	453	28	36	413	36	445	32
996	25955	431	25955	477	46	17	417	17	461	44
997	12977	439	12978	469	30	8	427	8	457	30

From the table one can glean that, as the 991-th time-like refinement level is reached, the offsets  $\Delta\alpha (\equiv \alpha_\psi - \alpha_\varphi)$  under consideration get correlated for pivot and residual – first in  $\Delta\alpha = 40$ , then in  $\Delta\alpha = 48$  – signalling the residual amplitude’s share 147 to the target bill and concomitant decorrelation of  $\Delta\alpha$  as  $n = 993$ . The same holds true for the pivot’s and the largest residual’s amplitudes from Fig. 4 and their associated  $\psi^{(n)}$ : (1) correlation in  $\Delta\alpha = 20$  as  $n = 1003$ ; (2) correlation in  $\Delta\alpha = 22$  as  $n = 1004$ ; (3) residual amplitude’s (belated) contribution 193 and decorrelation of  $\Delta\alpha$  as  $n = 1005$  (see Table 2). So a first conclusion is that, from a volume point of view, target-seeking implies phase correlation irrespective of a pivotal amplitude’s coincidence with a peak or not.

Table 2: Pivotal and inter-qphyleticly accompanying residual fluctuation for  $1003 \leq n \leq 1005$ 

$n$	Pivot					Residue				
	$\varphi_P$	$\alpha_\varphi$	$\psi_P$	$\alpha_\psi$	$\Delta\alpha$	$\varphi_R$	$\alpha_\varphi$	$\psi_R$	$\alpha_\psi$	$\Delta\alpha$
1003	51919	448	-51920	468	20	193	449	194	469	20
1004	103839	442	103839	464	22	96	443	96	465	22
1005	207679	438	207679	443	5	48	439	48	445	6

There is more to croton phase than just that. Let us once more go back one step and consider the target-matching case first. If a croton amplitude reaches a level  $L_m + 1$  or  $L_m$ , it was assumed a chunk of  $m$ -dimensional Euclidean space containing an  $(m - 1)$ -sphere packing *with* or *without* centerpiece was created

in that fluctuation (or dissolved if the amplitude did not peak). Whether that creation succeeded depends on the quantity  $\delta \in \{0, 1\}$ : only if the amplitude  $\varphi$  peaks on  $L_m$  and the phase  $\psi$ , in absolute terms, on  $L_m + \delta$  ( $\delta \in \{0, 1\}$ ) can we be sure of successful creation; if  $\varphi < L_m$ , or if  $|\psi| > L_m + 1$ , we'd be uncertain whether to settle on success or state failure. There are situations where that criterion applies to more than one Mersenne fluctuation. See Table 3 which illuminates the stance of three detouring fluctuations:

Table 3: Co-occurrent fluctuations targeted at  $L_{29}(= 207930)$ ,  $L_{10}(= 336)$  and  $L_8(= 240)$ 

$n$	Pivot						Residue 1					
	$\varphi_P$	$\alpha_\varphi$	$\psi_P$	$\alpha_\psi$	$\Delta\alpha$		$\varphi_{R_1}$	$\alpha_\varphi$	$\psi_{R_1}$	$\alpha_\psi$	$\Delta\alpha$	
609	208430	72	-208431	72	0		10	58	-11	52	6	
											Residue 2	
											$\varphi_{R_2}$	$\alpha_\varphi$
											$\psi_{R_2}$	$\alpha_\psi$
609							66	78	66	83	5	

Contrary to the former examples of detouring, in the above there is only one time-like refinement that counts because the largest amplitude (still called pivot) overshoots as  $n = 609$ . The three fluctuations could, in a “covert conspiracy”, strive concurrently after three targets,  $\varphi_P + \varphi_{R_1} + \varphi_{R_2} = L_{29} + L_{10} + L_8$ , where  $L_{29} = 207930$ ,  $L_{10} = 336$  and  $L_8 = 240$ . Residuosity not only assumes a different meaning here, the space-like refinements get also symmetrized, one residual's being lower than the pivot's, the other one's higher, and the offsets in question get correlated as  $n = 609$ . Offset equality obviously is uncertain by a factor  $\delta = |\Delta\alpha_{R_2} - \Delta\alpha_{R_1}|$  ( $\delta \in \{0, 1\}$ ), and  $\delta = 1$  above since the phase inversions that enter at  $n = 609$  are followed only by two of the three contributors. A very similar example is shown in Table 4:

Table 4: Co-occurrent fluctuations targeted at  $L_{12}(= 756)$ ,  $L_{10}(= 336)$  and  $L_2(= 6)$ 

$n$	Pivot						Residue 1					
	$\varphi_P$	$\alpha_\varphi$	$\psi_P$	$\alpha_\psi$	$\Delta\alpha$		$\varphi_{R_1}$	$\alpha_\varphi$	$\psi_{R_1}$	$\alpha_\psi$	$\Delta\alpha$	
1000	758	239	758	269	30		335	356	-336	388	32	
											Residue 2	
											$\varphi_{R_2}$	$\alpha_\varphi$
											$\psi_{R_2}$	$\alpha_\psi$
1000							5	135	-6	168	33	

A natural question to ask is if the aforementioned amplitudes and phases and the conclusions drawn from them stand a boundary check.

### 3.3. Boundary check

Clearly, the boundary must be checked at this stage because it has yet to be decided if crotons from Mersenne fluctuations making a detour around a kissing number get encoded *intraordinarily* or *interordinarily*. We may put together the relevant facts here by starting with a recollection and extrapolating from there:

(1) Out of all  $\Gamma^{(15)}$  labels realizable on the basis of  $(G_\rho^{(15)})$  (the intraordinal case), one subset of labels can be extracted that encode croton amplitudes coincident with  $\pm L_m, \pm(L_m + 1)$  ( $m = 1, 2, \dots, 7$ ). Not  $\pm(L_2 + 1) = \pm 7$ , however. The complete realization (interordinal case) demands an enlarged basis  $(G_\rho^{(7,15)})$  that brings singular labels in its wake. On the basis of  $(J_\rho^{(15)})$ , no subset of  $\chi^{(15)}$  labels is able to encode  $L_m, L_m + 1$  ( $m = 1, 2, \dots, 7$ ) or sign reversed versions thereof; that encoding only catches up when the basis is enlarged to  $(J_\rho^{(7,15)})$ , facing us with two adamant cases yet:  $\pm(L_7 + 1) = \pm 127$  (realizable before) and  $\pm L_6, \pm(L_6 + 1)$  (unrealizable after); no singular labels are entailed. Altogether a complex picture.

(2) In contrast, singular labels spring up directly on the basis of either  $(G_\rho^{(31)})$  or  $(J_\rho^{(31)})$  (see Appendix A); a simplification that, in turn, pays off with *twofold*-realizable labels all the way up for croton amplitudes coincident with  $\pm L_m, \pm(L_m + 1)$  ( $m = 8, 9, \dots, 31$ ), also making up leeway to the former special cases  $m = 2, 6, 7$ .

So what can, on top of that, be checked is the realizability of our example *pivots* from Figs.4 to 6, including their associated  $\varphi_P$ . Because of what they are targeted at, it is decidable unequivocally where their images are to be sought:  $\Gamma^{(31)}$  and  $\chi^{(31)}$ , based on the 18-tuples  $(G_\rho^{(31)})$  and  $(J_\rho^{(31)})$ . The targets under discussion behave as one would expect:  $\pm L_{17} (= \pm 5346), \pm(L_{17} + 1)$  as well as  $\pm L_{29} (= \pm 207930), \pm(L_{29} + 1)$  are realizable altogether by  $\Gamma^{(31)}$  and  $\chi^{(31)}$ . The same statement holds true for our example pivots – 5219, 5220. And, peaking or not, amplitudes 207646, 207647 and 207679 are perfectly twofold-realizable either. Surprisingly, twofold-realizability holds out for the whole pivotal and residual stopovers and co-occurred targets mentioned in the discussion of detouring fluctuations. The holographic principle, according to which all volume quantities  $\varphi_P, \psi_P$  and  $\varphi_R, \psi_R$  from Tables 1 to 4 should have boundary counterparts,  $\varphi$  in  $\Gamma^{(31)}$ ,  $\psi$  in  $\chi^{(31)}$ , is exceedingly satisfied – the aforesaid quantities are invariably twofold-realizable (see Appendix A). Since the same encompassing holographicity also obtains for the stopovers in the target matching Mersenne fluctuation of Fig. 1, one can in summary say that amplitude and phase data from target-seeking Mersenne fluctuations in the volume have a perfect image on the boundary.

#### 4. Sources of Mersenne fluctuations

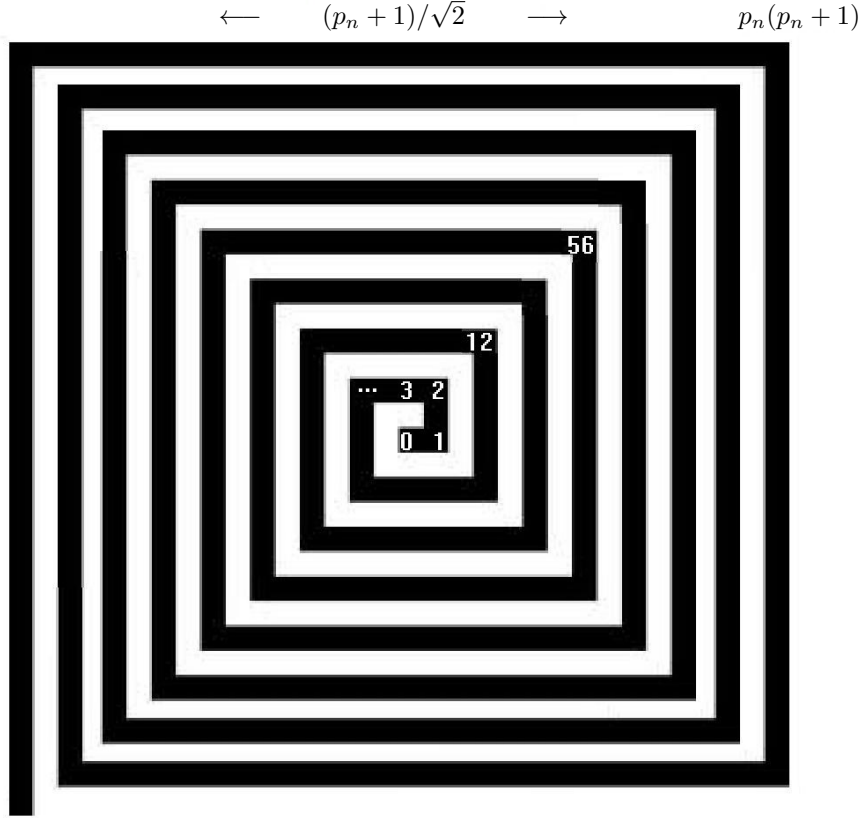
Thus far, examples of Mersenne fluctuations have been alleged without specifying their sources. What we expect from actual sources is that they reveal the conditions under which Mersenne fluctuations (1) develop and (2) grow into qphyla that in turn define “volume” in a pregeometric context. The apparatus employed here is continued fractions

$$b_0 + \frac{a_1|}{|b_1|} + \frac{a_2|}{|b_2|} + \frac{a_3|}{|b_3|} + \dots \quad (11)$$

where the shorthand  $[b_0; b_1, b_2, \dots]$  is used for the regular case ( $a_\alpha = 1$ ); a shorthand for the case  $a_0 = a_{2\mu-1} = 1, a_{2\mu} = -1$  will be given soon.

##### 4.1. The role of continued fractions in refinement

To illustrate the role of continued fractions in refinement, let us start with a time-honored example, the square spiral formed by the numbers  $\mathbb{N}_0$  accompanied by a generalization of  $p = 2^i - 1$  ( $i = 1, 2, \dots, 5$ ) to Mersenne numbers  $p_n \equiv 2^n - 1$  ( $n \in \mathbb{N}$ ). As indicated in Fig. 7, with  $B(,)$  the Beta function, the terms  $(C_{p_n} B(p_n, p_n + 1))^{-1} = p_n(p_n + 1)$  figure as marks on a subset of corners along the number pattern’s diagonal: For  $p_1$ , this is one corner away from the origin, for  $p_2$  two corners, and for  $p_n, p_{n-1} + 1$  corners generally. Taking the number of corners as a measure, we can say the square spiral is endowed with an *expansion* parameter:  $(p_{n-1} + 1)/\sqrt{2}$ , the radius of an inscribed circle of a square with side length  $(p_n + 1)/\sqrt{2}$ . That in turn is equivalent to saying a fixed irrational quantity  $\sqrt{2}$  gets refined in steps of powers of two,  $\left(\frac{2^n}{\sqrt{2}}\right)^{-1}$ . The denominators from a convergent’s regular continued fraction representation  $\left(\frac{2^n}{\sqrt{2}}\right)^{-1} \rightarrow [b_0^{(n)}; b_\alpha^{(n)}]$  then unveil the time-like and space-like aspects of refinement: One just proceeds from  $n$  to  $n + 1$  in the superscript of the denominators to follow the convergent’s *time*-like refinement, and follows its respective *space*-like refinements by proceeding from  $\alpha = 1$  to  $\alpha = 2$  to further increments of  $\alpha$  in the denominator subscripts ad infinitum.

Figure 7: Square spiral representation of  $\mathbb{N}_0$ 

#### 4.2. Mersenne fluctuations and randomness

The continued fraction representations  $\left(\frac{2^n}{\sqrt{2}}\right)^{-1} \rightarrow [b_0^{(n)}; b_\alpha^{(n)}]$  yield orderly Mersenne fluctuations. Moreover, allowing for (CFR)  $\left(\frac{2^n}{\sqrt{2}}\right)^{-1} \pm \mathbb{N} \rightarrow [\tilde{b}_0^{(n)}; \tilde{b}_\alpha^{(n)}]$ , amplitudes can conveniently be generalized to trajectories across lattice points via the identities  $b_\alpha^{(n)} = \tilde{b}_\alpha^{(n)}$  ( $\alpha > 2$ ). In both representations, however, denominators are confined to a period after which they repeat and lead to relatively modest target matching: Results are, at least for online CFR calculators with the typical limits  $n \leq 3324$ ,  $\alpha \leq 499$  restricted to the kissing numbers  $L_m$ ,  $m = 1, \dots, 13$  (see Table B.15). It was mentioned in the introduction that the bases  $G^{(p_n)}$ ,  $J^{(p_n)}$  are rooted in the matrix representations of the operators  $\mathbf{f}^{(p_n)}$ ,  $\mathbf{h}^{(p_n)}$ . In the same previous work that introduced them it was further noted that  $(\mathbf{f}^{(p_n)})^{p_n+1} = 0$ ,  $(\mathbf{h}^{(p_n)})^{p_n+1} = 0$ ,

and that the length of an arc on a cardioid parametrized by  $p_n$  shows similar behavior: After  $n$  steps taken in reverse, the cardioid's arclength too becomes zero:

$$(A_n, A_n) \equiv 2 \frac{A_n \cdot \text{co-}A_n}{A_n + \bar{A}_n} = A_{n-1} \quad \text{etc.} \quad (12)$$

where

$$\begin{aligned} A_n &= 4c \sin \frac{\pi}{p_n+1}, \\ \text{co-}A_n &= 4c \cos \frac{\pi}{p_n+1}, \quad (c \text{ a parameter}) \\ \bar{A}_n &= 4c - A_n. \end{aligned} \quad (13)$$

Normalizing to  $c = \frac{1}{4}$  in Eqs. (13) and associating a regular (CFR)  $A_n \rightarrow [\tau_0^{(n)}; \tau_1^{(n)}, \tau_2^{(n)}, \dots]$  to  $A_n$ , one notes that the denominator  $\tau_1$  satisfies

$$\tau_1^{(n+1)} = 2\tau_1^{(n)} + \delta_\tau^{(n)} \quad (\delta_\tau^{(n)} \in \{0, 1\}, n > 2). \quad (14)$$

In particular,  $\tau_1^{(n)}$  is the integer part of  $\frac{2^n}{\pi}$ :

$$\begin{aligned} \tau_1^{(4)} &= 5 & \tau_1^{(5)} &= 10 & \tau_1^{(6)} &= 20 & \tau_1^{(7)} &= 40 & \tau_1^{(8)} &= 81 \\ \frac{2^4}{\pi} &= 5.09 & \frac{2^5}{\pi} &= 10.18 & \frac{2^6}{\pi} &= 20.37 & \frac{2^7}{\pi} &= 40.74 & \frac{2^8}{\pi} &= 81.48 & \dots & (15) \end{aligned}$$

with  $\frac{2^n}{\pi}$  as a new expansion parameter. Again, we have an irrational quantity that allows for refinement in steps of powers of two, and the denominators from a convergent's regular (CFR)  $(\frac{2^n}{\pi})^{-1} \rightarrow [b_0^{(n)}; b_\alpha^{(n)}]$  show all the the time-like and space-like refinement characteristics constitutive for Mersenne fluctuations.<sup>5,6</sup> But contrary to the case of the square spiral, the cardioid has a *second* expansion parameter,  $c$ . It was previously shown [Merkel] that the croton base number  $C_{q_n}$  ( $q_n \equiv (p_n - 3)/4$ ) comes with the identity

$$-\lceil n/2 \rceil + \sum_{i=1}^{n-2} p_i = \lfloor \log_2 C_{q_n} \rfloor \quad (n > 3), \quad (16)$$

<sup>5</sup>With the option of treating denominators as croton amplitudes and generalizing them to trajectories via (CFR)  $(\frac{2^n}{\pi})^{-1} \pm \mathbb{N}_0 \rightarrow [b_0^{(n)}; \tilde{b}_\alpha^{(n)}]$ ;

<sup>6</sup>the clamp which connects the sources  $(\frac{2^n}{\pi})^{-1}$  and  $(\frac{2^n}{\sqrt{2}})^{-1}$  is the quantity  $\delta \in \{0, 1\}$  which links a specific denominator at  $n$  to the first denominator at  $n+1$ ; in Eq. (14),

$\delta_\tau^{(n)} = 1 - \left\lceil \frac{\tau_2^{(n)} - 1}{\tau_2^{(n)}} \right\rceil$ , while for (CFR)  $(\frac{2^n}{\sqrt{2}})^{-1} \rightarrow [b_0^{(n)}; b_\alpha^{(n)}]$  the analog to Eq. (14) is

$b_1^{(n+1)} = 2b_{\text{last}}^{(n)} + \delta_b^{(n)}$  and  $\delta_b^{(n)} = 1 - \left\lceil \frac{b_{\text{ntl}}^{(n)} - 1}{b_{\text{ntl}}^{(n)}} \right\rceil$ , with  $b_{\text{ntl}}^{(n)}$  and  $b_{\text{last}}^{(n)}$  respectively denoting the next-to-last and last denominator terminating a period ( $\sqrt{2}$  is an algebraic number).

which makes for an ideal candidate regarding second parametrizing via  $c$ . We can therefore conceive of the irrationals

$$\text{Type I : } \lfloor \log_2 C_{q_s} \rfloor \left( \frac{2^n}{\pi} \right)^{-1}, \quad (17)$$

$$\text{Type II : } \log_2(C_{q_s}) \left( \frac{2^n}{\pi} \right)^{-1}, \quad (18)$$

and

$$\text{Type III : } \log_2(C_{q_s}) \left( \left\lfloor \frac{2^n}{\pi} \right\rfloor \right)^{-1} (= \log_2(C_{q_s})/\tau_1^{(n)}). \quad (19)$$

The symmetry is not a perfect one: Mersenne fluctuations of type I or II (a shorthand saying they have their habitat in the CFR of irrationals of type I and II) are fully traceable – as are those based on  $\frac{2^n}{\sqrt{2}}$ . In contrast, rounding  $\frac{2^n}{\pi}$  to  $\left\lfloor \frac{2^n}{\pi} \right\rfloor (= \tau_1^{(n)})$  in the CFR of irrationals of type III leads to truncated Mersenne fluctuations, referred to as Mersenne fluctuations of type III. Truncation occurs whenever a sequence of like  $\delta$ 's that determine the upper row of Eq.(15) above breaks:  $\delta_\tau^{(n)} = \delta_\tau^{(n+1)} = \dots = \delta_\tau^{(n+i-1)} \neq \delta_\tau^{(n+i)}$ . Conversely, a Mersenne fluctuation of type III is given birth when a like delta sequence is initiated – to stay in the picture, when  $\delta_\tau^{(n-1)} \neq \delta_\tau^{(n)}$ . Truncated fluctuations can be hard to assign to a qphylum. The longer the fragment that coincides with a connected path in a qphylum the lesser the risk of misassignment; if only few predecessor and successor nodes are available to escort the insertion, assignment is fraught with uncertainty. Mersenne fluctuations of type III thus occupy a middle position between randomness and qphyletically founded “volume” definition.

#### 4.3. CFR aspect of the examples shown in Sect. 3

In agreement with the symbol choices of Sect. 3, a regular CFR associated with irrationals of type I, II or III will be denoted  $[\varphi_0; \varphi_1, \varphi_2, \dots]$ , while the alternating case corresponding to  $b_0 + \frac{1}{|b_1|} + \frac{-1}{|b_2|} + \frac{1}{|b_3|} + \dots$  is denoted  $[\psi_0; \psi_1, \psi_2, \dots]$ . With  $\log_2 C_{q_s}$  ( $q_s \equiv (2^s - 1)$ ) modulating the outcome of refinements, the start value of  $s$  must be 2 to guarantee a nonvanishing  $\log_2 C_{q_s}$  term; otherwise, the natural numbers  $s$  and  $n$  can be chosen freely due to a remarkable property: As was shown in Sect. 3, the amplitudes and phases produced by Mersenne fluctuations are by the holographic principle (hgp) linked to the croton bases underlying the boundary definition. The bases  $G^{(15)}, J^{(15)}, G^{(31)}, J^{(31)}$ , are in turn rooted in the square-matrix representations of  $\mathbf{f}^{(15)}, \mathbf{h}^{(15)}, \mathbf{f}^{(31)}, \mathbf{h}^{(31)}, \dots$  If peak amplitudes fit with boundary  $\Gamma^{(p)}$  at  $\log_2(p+1) = n_{\text{hgp}}$  (the same reasoning applies to  $\chi^{(p)}$ ), they can nevertheless originate in Mersenne fluctuations for which the margins  $n_{\min}, n_{\max} \gg n_{\text{hgp}}$  because of an in-built recursivity. Using the shorthands LL and UR for lower left and upper right square-matrix quadrants, the quadrant  $\text{LL}(\mathbf{f}^{(p)})$  can be shown to coincide with

the subquadrant  $UR(LL(\mathbf{f}^{(p')}))$ , a recursivity<sup>7</sup> that allows for arbitrarily large assignments  $n_{\min}, n_{\max}$  without impeding the amplitude's membership to  $\Gamma^{(p)}$ . The assignment of  $s$  is similarly open-ended; for technical reasons,<sup>8</sup> however, only fluctuations with  $n_{\max} \leq 3330$  and modulations  $\log_2 C_{qs}$  with a domain  $2 \leq s \leq 9$  could be considered.

In what follows, Mersenne fluctuations are listed in the order they occurred in the text. The fluctuation shown in Fig. 1 is taken from the CFR of  $\lfloor \log_2 C_3 \rfloor \cdot \left(\frac{2^n}{\pi}\right)^{-1}$  ( $= \frac{\pi}{2^{n-1}}$ ). The values  $\varphi_{\alpha}^{(n)}$  at  $n < 206$  and  $n > 218$  have been omitted. A principal limitation of the CFR approach becomes apparent at this point: The more frequent and closer to unity  $\varphi$  gets, the less can we tell its affinity.<sup>9</sup> The fact that  $\alpha \bmod 2$  must be invariant and offsets in  $\alpha$  not become too decorrelated from one stopover  $n$  to the next  $n + 1$  (see Fig. 1) is a help in telling right from wrong candidates, but that criterion fails if candidates satisfying  $\alpha \bmod 2$  equivalence come close to one another. Worst are instances of  $\varphi_{\alpha} = 1$  with like  $\alpha \bmod 2$  – they are truly legion.

The rest of the examples mentioned are, in the right order, based on the CFR of:

Footnote 2:	$\lfloor \log_2 C_{31} \rfloor \left(\frac{2^n}{\pi}\right)^{-1}$ ( $1488 \leq n \leq 1500$ );
	$\log_2 C_{31} \left(\frac{2^n}{\pi}\right)^{-1}$ ( $1068 \leq n \leq 1082$ );
	$\log_2 C_{31} \left(\frac{2^n}{\pi}\right)^{-1}$ ( $2012 \leq n \leq 2028$ );
	$\lfloor \log_2 C_{31} \rfloor \left(\frac{2^n}{\pi}\right)^{-1}$ ( $1951 \leq n \leq 1959$ );
Fig. 4:	$\lfloor \log_2 C_{127} \rfloor \left(\frac{2^n}{\pi}\right)^{-1}$ ( $1556 \leq n \leq 1559$ );
Fig. 5, Table 2:	$\log_2 C_3 \left(\frac{2^n}{\pi}\right)^{-1}$ ( $1003 \leq n \leq 1006$ );
Fig. 6, Table 1:	$\log_2 C_3 \left(\frac{2^n}{\pi}\right)^{-1}$ ( $987 \leq n \leq 997$ );
Table 3:	$\log_2 C_{511} \left(\frac{2^n}{\pi}\right)^{-1}$ ( $n = 609$ );
Table 4:	$\log_2 C_{127} \left(\frac{2^n}{\pi}\right)^{-1}$ ( $n = 1000$ ).

## 5. Conclusions

The notable thing about CFR-based Mersenne fluctuations is that whether the underlying irrational quantity to be refined is an algebraic or a transcendental number does not matter, as long as there exists an *interordinal* connection

---

<sup>7</sup>there are subsubquadrantal (SSQ) relationships that owe their existence to recursivity too and can be classified in accordance with the equations' (13) leading/next-to-leading CF denominator behavior: *interordinal* SSQ identities forming structural analogs of  $p' = 2p + 1$  can be classified as sine-like, and *intraordinal* SSQ identities forming structural analogs of  $p'' = 2p' + 1 = 2(2p + 1) + 1$  as cosine-like (see [Merkel] for details)

<sup>8</sup>online CF calculators command a scope of 499 denominators; with a value of  $\pi$  accurate to 1000 decimals, that makes for a limit  $n_{\max} \approx 1024$  at full coverage, and  $n_{\max} \approx 3030$  at lesser and lesser denominator production

<sup>9</sup>In Sect.6, we have postulated a mere 1-3D-space relatedness of  $\varphi_{\alpha} \leq 13$  – quasi as the *conditio sine qua non* of continuum illusion.

$b_1^{(n+1)} = 2b_x^{(n)} + \delta^{(n)}$  ( $\delta^{(n)} \in \{0, 1\}$ ).<sup>10</sup> The tables shown in Appendix B are the outcome of an in-depth study of denominators emerging with CFR-based Mersenne fluctuations. Table B.15 summarizes the results of scanning the CFRs  $\left(\frac{2^n}{\sqrt{2}}\right)^{-1} \rightarrow [b_0^{(n)}; b_\alpha^{(n)}]$  for kissing-number matches and hit frequencies, while Table B.16 summarizes the corresponding figures for Eqs. (17)-(19). Results for closest pivots and largest peaks are set in parentheses. A note on largest peaks: While those given in Table B.16 for type I and III, 12 986 152 and 9 996 953, are definitely beyond  $\Gamma^{(31)}$ ,  $\chi^{(31)}$  realizabilities,<sup>11</sup> the largest peak in Table B.15, 2 445 930, and the largest type-II peak in Table B.16, 3 614 855, are twofold-realizable in  $\Gamma^{(31)}$ ,  $\chi^{(31)}$ . That does not mean that a kissing number  $L_m$  they may have as target must have an image in both boundaries  $\Gamma^{(31)}$  and  $\chi^{(31)}$ . For example, many numbers realizable in  $\Gamma^{(15)}$ ,  $\chi^{(15)}$  may in theory become pivotal with respect to  $L_6$  ( $= 72$ ); but, although the numbers  $L_m$  ( $m = 1, \dots, 7$ ) are realizable in  $\Gamma^{(15)}$ ,  $L_6$  is not in  $\chi^{(15)}$  – it becomes (twofold-)realizable in  $\Gamma^{(31)}$ ,  $\chi^{(31)}$  at last. By the same token, it may be that peaks such as 2 445 930 and 3 614 855 become true pivots not until a target  $L_m$  for them realizable in  $\Gamma^{(63)}$ ,  $\chi^{(63)}$  is found. Unfortunately, kissing number candidates  $L_m$  ( $m > 31$ ) are, with the exception  $L_{48}$  ( $= 52 416 000$ ), notoriously uncertain. For the time being, more matches with  $L_m$  ( $m \leq 31$ ) and interesting pivots may only be obtained by enlarging the scope of  $s$ .

At the very beginning, however, there is a master Mersenne fluctuation that pauses at  $n = 1$ : If we take the geometrizing hypothesis via Mersenne fluctuations literally, the continued fraction  $[0; 1, \bar{2}]$  – a special case of (CFR)  $\left(\frac{2^n}{\sqrt{2}}\right)^{-1} \rightarrow [b_0^{(n)}; b_\alpha^{(n)}]$  for  $n = 1$  – means “recursive geometrization into a centerpiece-free pair of a 0-spheres” or, a self-similar laminar pattern “dash-space-dash” for all space-like refinements.

## Part II

### 6. Application to subatomic physics

The only ingredient that sounded physical thus far is the complementarity of amplitude and phase. Complementarity provides an excellent starting point for studying the conceptual link between Mersenne fluctuations, or qphyla – our pregeometric categories linked to increases in time-like and space-like refine-

---

<sup>10</sup>For (CFR)  $\left(\frac{2^n}{\sqrt{2}}\right)^{-1} \rightarrow [b_0^{(n)}; b_\alpha^{(n)}]$ ,  $b_x$  is the last denominator in a finite period, while the CFR of the cardioid-arc length-function argument  $\left(\frac{2^n}{\pi}\right)^{-1}$  has an infinite period, hence  $\tau_x = \tau_1$  in Eq. (14).

<sup>11</sup>the largest number realizable in  $\Gamma^{(31)}$  being 3 707 462, the largest in  $\chi^{(31)}$ , 4 177 840,

ment  $-$ , and the particle creation/lifetime patterns that arise with increases in temporal and spatial resolution for sustained geometry. As a prelude invoking atomic physics, let us examine the ratio of the electrical to the gravitational forces between a proton and an electron, where a first kind of complementarity comes into play. Consider the collections formed by  $m$  Magnus terms  $M_k \equiv (2k+1)^2(-x)^{k(k+1)/2}$  ( $0 < x < 1$ ) and the estimated number of protons in the universe,  $N = 10^{80}$ ,

$$\sum^{(m)} M_k (N - m + 1), \quad (20)$$

from which  $x$  is to be determined. The electrical force  $F_e$  is considered independent of  $N$ ; thus  $m = 1$ , *i.e.*, only one Magnus term is there to account for  $x_e$ . Assuming that the boundaries  $\Gamma^{(15)}$ ,  $\chi^{(15)}$  are sufficient for the proton-electron system, we make a choice of the triple  $(k, 2k+1, x_e^{-1})$  such that expression (20) forms a least upper bound to the observed ratio  $F_e/F_g$  under the constraint that only successive Mersenne numbers are being used. This is fulfilled for  $M_7(x_e) = 225(-x_e)^{28}$  with  $k = 7$ ,  $2k+1 = 15$ ,  $x_e^{-1} = 31$  where (20) assumes just the reasonable value  $M_7(1/31) \times 10^{80} \approx 3.92 \times 10^{40}$ . Thus

$$x_e = \frac{1}{31}.$$

In contrast, the gravitational force according to Mach's principle is dependent on all other gravitating bodies in the universe so that, in this case,  $m = N$  and expression (20) reduces to  $10^{80}$  Magnus sum terms, starting with  $k = 0$ , that are going to account for  $x_g$ . To good approximation,

$$x_g \approx \Lambda = 0.10765 \dots,$$

the so-called 'one-ninth' constant which is the unique exact solution of the full Magnus equation  $\sum_{k=0}^{\infty} (2k+1)^2(-x)^{k(k+1)/2} = 0$  ( $0 < x < 1$ ). Next, we come to the aforementioned croton complementarity, which plays the part of fine-tuning: 170 croton field values are representable on  $\Gamma^{(15)}$ , 40 on  $\chi^{(15)}$ ; but only the difference in the number of values represented seems to matter (Sect. 8), leaving  $2^{130}$  combinations for the power set of crotons compatible with charged particles. The only gravity-related croton, on the other hand, is  $\varphi = 13$ , each occurrence of which corresponds to a chunk, endowed with centerpiece, of the very 3D space whose curvature according to general relativity is equivalent to gravity. The power set allowing just two combinations in this case, one finds

$$\frac{2^{130}}{x_e} \div \frac{2}{x_g} \approx 2.27123 \times 10^{39}, \quad (21)$$

which coincides with the measured ratio  $F_e/F_g$  to five decimal places.

From the above we behold:  $\varphi = 13$  is key to providing a 3D scenery. In order for ever-expanding Mersenne fluctuations to allow for particulates,<sup>12</sup> a cloud of

---

<sup>12</sup> a generalization of amplitudes to trajectories was proposed in Sect. 4.2

crotons of amplitude  $\leq 13$  has to keep company with them which administer a background of 1-3D space chunks. The denser that cloud, the more convincing the impression of a persistent 3D continuum.

Now we are prepared for subatomic physics. We have seen that complementarity of boundary-field values affects the power set of croton combinations admissible in a situation, the theoretical upper bound for combinations of order 31 being  $2^{3^{18}-1}$ . It seems reasonable to associate  $\Gamma_x^{(31)} \notin \chi^{(31)}$  with nuclear phenomena – whose fundamental laws and constants are unknown and peculiarities such as the EMC effect and SRC plateaux [Higin] have remained puzzling to this day – and reserve non-complementary croton combinations – among them all those identified in the previous section (and summarized in Appendix A) as doubly representable on  $\Gamma^{(31)}$  and  $\chi^{(31)}$  – to quarks and preons. Magnus-type considerations cannot be expected to apply without qualification. A safe starting point is to presume that preons carry electric charge (see 7.1), an assumption that allows to associate crotonic activity to (para)fermionic forms of particulates, from superordinate levels such as protons and neutrons to quarks and quark constituents.

Oscar Wallace Greenberg envisaged a parafermionic nature of quarks. But with the advent of QCD, and the experimental findings, valid to this day, that quarks are pointlike down to  $10^{-20}$  m, preons, parafermionic or otherwise, have not found much acclaim among physicists. The consequence of the experimental standoff is that preons, if they exist, must inhabit extradimensions, do aggregate there and betray their origin only in short-lived resonances known as quark flavors. It is known that the up quark carries more momentum than the down quark, which makes it likely that even the two of them are not of the same dimensional origin. The following is not meant to be a worked out general model of hadronic matter – it just contemplates on the possible mathematical structure of the subatomic onion in the light of crotonic activity. In what follows we use the notation  $f_{n+1} (= 2^{n+1} - 1)$  to denote (para-)fermionic order and the symbols  $p_{\text{up}}^{(f_{n+1})}$  and  $p_{\text{down}}^{(f_{n+1})}$  for up-type and down-type preons of that order, respectively.

**Conjecture 1.** *Preons of order  $f_{n+1}$  are either up-type or down-type,  $p_{\text{up}}^{(f_{n+1})}$  or  $p_{\text{down}}^{(f_{n+1})}$ . The electric charge (in e) of up-type items is given by the expressions  $c_{\text{up}}^{(f_{n+1})} = (f_{n+1} - \sum_{s=0}^n f_s) / \prod_{r=1}^{n+1} f_r = (n+1) / \prod_{r=1}^{n+1} f_r$ , while down-type items have the charge  $c_{\text{down}}^{(f_{n+1})} = - \sum_{s=0}^n f_s / \prod_{r=1}^{n+1} f_r$  (see Table 5 below). The charge of up-type items transforms as  $c_{\text{up}}^{(f_n)} = (f_{n+1} - 1)c_{\text{up}}^{(f_{n+1})} + c_{\text{down}}^{(f_{n+1})}$  and the charge of down-type items as  $c_{\text{down}}^{(f_n)} = (f_n + 1)c_{\text{down}}^{(f_{n+1})} + f_n c_{\text{up}}^{(f_{n+1})}$ .*

Table 5: Mersennian preon charge model

$f_{n+1}$	up-type charge	down-type charge
1	1	0
3	$\frac{2}{3}$	$-\frac{1}{3}$
7	$\frac{3}{21}$	$-\frac{4}{21}$
15	$\frac{4}{315}$	$-\frac{11}{315}$
31	$\frac{5}{9765}$	$-\frac{26}{9765}$
63	$\frac{6}{615195}$	$-\frac{57}{615195}$
$\vdots$	$\vdots$	$\vdots$

For preon configurations enabling these charge transformations the shorthand

$$Q_{\text{up}}^{(f_n)} = (f_{n+1} - 1)p_{\text{up}}^{(f_{n+1})} + p_{\text{down}}^{(f_{n+1})}, \quad \bar{Q}_{\text{up}}^{(f_n)} = (f_{n+1} - 1)\bar{p}_{\text{up}}^{(f_{n+1})} + \bar{p}_{\text{down}}^{(f_{n+1})},$$

$$Q_{\text{down}}^{(f_n)} = (f_n + 1)p_{\text{down}}^{(f_{n+1})} + f_n p_{\text{up}}^{(f_{n+1})}, \quad \bar{Q}_{\text{down}}^{(f_n)} = (f_n + 1)\bar{p}_{\text{down}}^{(f_{n+1})} + f_n \bar{p}_{\text{up}}^{(f_{n+1})},$$

is used where the bar in  $\bar{p}$  indicates an antipreon of opposite electric charge. The Magnus formalism suggests a connection between  $f_{n+1}$  (or  $f_n$ ) and  $x_e^{-1} = 31$ . This does not only suffice for the proton and the neutron – if the greatest assignment eligible is  $f_{n+1} := x_e^{-1}$ , it suffices for three generations of quarks; and if  $f_n := x_e^{-1}$  is eligible, for a fourth generation as well. Proton and neutron are assigned the least root order:  $f_{n+1} = 3$ . They are named (1) configurations here:

$$Q_{\text{up}}^{(1)} \quad \text{proton (p) with charge 1,}$$

$$Q_{\text{down}}^{(1)} \quad \text{neutron (n) with charge 0.}$$

The valence quarks or quarks of generation 1 are considered (3) configurations:

$$Q_{\text{up}}^{(3)} \quad \text{up quark (u) with charge } \frac{2}{3},$$

$$Q_{\text{down}}^{(3)} \quad \text{down quark (d) with charge } -\frac{1}{3}.$$

Charm quark and strange quark (generation 2) have  $(7^2 3)$  configurations:

$$Q_{\text{up}}^{(7)} + \bar{Q}_{\text{down}}^{(7)} + \bar{Q}_{\text{down}}^{(3)} \quad \text{charm quark (c) with charge } \frac{2}{3},$$

$$Q_{\text{up}}^{(7)} + \bar{Q}_{\text{down}}^{(7)} + \bar{Q}_{\text{up}}^{(3)} \quad \text{strange quark (s) with charge } -\frac{1}{3},$$

and top quark and bottom quark (generation 3), with root order  $f_{n+1} = x_e^{-1} = 31$ , are represented by  $(15^2 7^2 3^2)$  configurations.<sup>13</sup>

$$(\bar{Q}_{\text{up}}^{(15)} + Q_{\text{down}}^{(15)} + \bar{Q}_{\text{up}}^{(7)}) + (\bar{Q}_{\text{up}}^{(7)} + Q_{\text{up}}^{(3)} + \bar{Q}_{\text{down}}^{(3)}) \quad \text{top quark (t) with charge } \frac{2}{3},$$

$$(\bar{Q}_{\text{up}}^{(15)} + Q_{\text{down}}^{(15)} + \bar{Q}_{\text{up}}^{(7)}) + (\bar{Q}_{\text{down}}^{(7)} + \bar{Q}_{\text{up}}^{(3)} + \bar{Q}_{\text{down}}^{(3)}) \quad \text{bottom qu.(b) with charge } -\frac{1}{3}.$$

How these configurations relate to targets of crotonic activity is propounded in our second conjecture:

**Conjecture 2.** *To qualify as constituents of a superordinate preon, hyperspheres must be used in numbers that divide the kissing number of the space they live in.*

This principle is best understood as a simile to the Magnus ansatz, where the intra-generational quark-mass ratios  $m_u/m_d$ ,  $m_c/m_s$  and  $m_t/m_b$  replace the dimensionless force ratio  $F_e/F_g$ . Quark mass is assumed to result from crotonic activity, and the configurations  $c,s$  and  $t,d$  make it clear that this activity has to cover extended spans of orders. Here, only leading-order crotonic activity is considered in deriving bounds for intra-generational mass ratios. This implies identifying where leading-order crotonic activity singles out space chunks that suit the up-type quark of a generation and other space chunks suiting the down-type quark. The kissing numbers<sup>14</sup> of the target spaces,  $L_{\text{up}}$  and  $L_{\text{down}}$ , must in turn show the divisibility properties demanded in Conjecture 2. But that's only a necessary condition. In the Magnus ansatz, assignment of successive Mersenne numbers to the triple  $(k, 2k+1, x_e^{-1})$  is essential to getting a handle on bounds. Here, the clue to successful bounds comes from a divisibility postulate for a generation's  $L_{\text{up}}$ : in addition to being divisible by  $f_{n+1} - 1$ ,  $L_{\text{up}}$  must contain a genuine prime factor  $P_\mu > 13$  (larger than the croton amplitude of  $3D$  space) such that

$$|P_\mu - L_{\mu_0 + \mu}| = 1 \quad (\mu = 1, 2, 3). \quad (22)$$

The task is for the  $\mu$ th generation completed when all its kissing numbers  $L_{\text{down}}$  – there are several – which are divisible by  $f_n + 1$  and have but prime factors

---

<sup>13</sup> The top quark's charge, for instance, ensues from the  $(15^2 7^2 3^2)$  transformations  $\frac{2}{3} = \left( \frac{30 \cdot (-5) + 1 \cdot 26}{9765} + \frac{16 \cdot (-26) + 15 \cdot 5}{9765} + \frac{14 \cdot (-4) + 1 \cdot 11}{315} \right) + \left( \frac{14 \cdot (-4) + 1 \cdot 11}{315} + \frac{6 \cdot 3 + 1 \cdot (-4)}{21} + \frac{4 \cdot 4 + 3 \cdot (-3)}{21} \right)$ ; corresponding transformations yield the charges of the remaining quarks.

<sup>14</sup> large kissing numbers are an active field of research [Cohn]; those used here are taken from <http://www.math.rwth-aachen.de/Gabriele.Nebe/LATTICES/kiss.html>

Table 6: Prime factors of  $(x_e)^{-1}$  kissing numbers; characteristic divisors determine up-type and down-type kissing numbers that bound measured intra-generational quark mass ratios from below

$m$	$L_m$	prime factorization	divisors t [b]	divisors c [s]	divisors u [d]
1	2	2			
2	6	$2 \times 3$			
3	12	$2^2 \times 3$			
4	24	$2^3 \times 3$			$[2^2]$
5	40	$2^3 \times 5$			$[2^2]$
6	72	$2^3 \times 3^2$			$[2^2]$
7	126	$2 \times 3^2 \times 7$			
8	240	$2^4 \times 3 \times 5$	$[2^4]$	$[2^3]$	$[2^2]$
9	272	$2^4 \times 17$	$[2^4]$	$[2^3]$	$[2^2]$
10	336	$2^4 \times 3 \times 7$	$[2^4]$	$[2^3]$	$[2^2]$
11	438	$2 \times 3 \times 73$			$2 \times 3$
12	756	$2^2 \times 3^3 \times 7$			
13	918	$2 \times 3^3 \times 17$			
14	1422	$2 \times 3^3 \times 79$			
15	2340	$2^2 \times 3^2 \times 5 \times 13$			
16	4320	$2^5 \times 3^3 \times 5$	$[2^4]$		
17	5346	$2 \times 3^5 \times 11$			
18	7398	$2 \times 3^3 \times 137$			
19	10668	$2^2 \times 3 \times 7 \times 127$		$2 \times 7$	
20	17400	$2^3 \times 3 \times 5^2 \times 29$			
21	27720	$2^3 \times 3^2 \times 5 \times 7 \times 11$			
22	49896	$2^3 \times 3^4 \times 7 \times 11$			
23	93150	$2 \times 3^4 \times 5^2 \times 23$			
24	196560	$2^4 \times 3^3 \times 5 \times 7 \times 13$			
25	197040	$2^4 \times 3 \times 5 \times 821$			
26	198480	$2^4 \times 3 \times 5 \times 827$			
27	199912	$2^3 \times 24989$			
28	204188	$2^2 \times 51047$			
29	207930	$2 \times 3 \times 5 \times 29 \times 239$	$2 \times 3 \times 5$		
30	219008	$2^7 \times 29 \times 59$			
31	230872	$2^3 \times 28859$			
	$\frac{L_{\text{up}}}{\Sigma L_{\text{down}}}$		$\approx 40.23$	$\approx 12.58$	$\approx 0.45$
	$\frac{m_{\text{up}}}{m_{\text{down}}}$		$\approx 41.86$	$\approx 13.58$	$\approx 0.48$

less  $P_\mu$  are identified. Then for each  $L_{\text{down}}$  found the single ratio  $\frac{L_{\text{up}}}{L_{\text{down}}}$  could be considered a bound to the ratio  $\frac{m_{\text{up}}}{m_{\text{down}}}$  in question. However, true to the Magnus ansatz, getting a fine-tuned result requires taking all contributors into account. The above table shows how, for each generation, a ratio  $\frac{L_{\text{up}}}{\sum L_{\text{down}}}$  can be deduced that bounds the respective measured ratio  $\frac{m_{\text{up}}}{m_{\text{down}}}$  from below.

Let us clear up the inner workings of the table, beginning with the third-generation quarks,  $\mathbf{t}$  and  $\mathbf{b}$ . With the top quark,  $f_5 - 1 = 30$  hyperspheres must fit in a chunk of space such that  $f_5 - 1$  and a prime factor  $P_3$  satisfying postulate (22) for some  $\mu_0$  divide its kissing number without rest. Both is the case for the spaces  $23D$  and  $29D$ , with the candidates  $(93150, 23)$  and  $(207930, 239)$  for  $(L_{\text{up}}, P_3)$ , respectively. Only by observing that the same selection rules must apply to the other generations are we able to decide that  $(207930, 239)$  (framed in the table) is the appropriate pair — a  $P_3 = L_4 - 1$  would not leave place for a  $P_2$  exceeding 13:  $L_3 \pm 1 = P_2 \not> 13$ . The bottom quark is collectively realized by all subspace chunks in which there are  $f_4 + 1 = 16$  hyperspheres such that  $f_4 + 1$  divides their kissing numbers without rest (marked by  $[]$ ) and the prime factors involved are less  $P_3 = 239$ . For the next lower generation, the pair suiting the up-type quark is from  $19D$ ,  $(10668, 127)$ , and for the first generation, that pair is from  $11D$ ,  $(438, 73)$ . In accordance with postulate (22), the  $P_\mu$  ( $\mu = 1, 2, 3$ ), specify a triple of successive kissing numbers,  $(72, 126, 240)$ . Unsurprisingly

$$\mu_0 = \log_2 (x_e^{-1} + 1). \quad (23)$$

The kissing numbers of the subspace chunks corresponding to down-type quarks  $\mathbf{s}$  and  $\mathbf{d}$  too satisfy the required divisibilities (again marked by  $[]$ ).

We now want to hint at the possible existence of a fourth quark generation.

Table 7: Quantities  $S_{\mu_0+\mu-1} := \sum_{m=1}^{\mu_0+\mu-1} (2^m - 1)$ ;  $L_{\mu_0+\mu}$ ;  $P_\mu$ ;  $\kappa(\mu) := 6 \text{Prime}(\mu) + (-1)^\mu$

$\mu$	$S_{\mu_0+\mu-1}$	$L_{\mu_0+\mu}$	$P_\mu$	$\kappa(\mu)$
1	57	72	73	11
2	120	126	127	19
3	247	240	239	29
4	502	272	271	43
5	1013	336	337	65
$\vdots$				

The entries of Table 7 may be used to define quark family characteristics: Where  $\chi_{\text{prime}}(\cdot)$  is the characteristic function of prime numbers,  $L_{\text{up}}$  can be said to belong to the family, and be identified with  $L_{\kappa(\mu)}$ , if  $\chi_{\text{prime}}(\kappa(\mu)) = 1$ . This is obvious for  $\mu = 1, 2, 3$ . One further notes that the signum function values,  $\text{sgn}(P_\mu - L_{\mu_0+\mu})$  and  $\text{sgn}(S_{\mu_0+\mu-1} - P_\mu)$ , cancel each other out for  $\mu = 1, 2, 3$ .

But said observations hold out for  $\mu = 4$ : The equations

$$\begin{aligned} \operatorname{sgn}(P_\mu - L_{\mu_0+\mu}) - \operatorname{sgn}(P_\mu - S_{\mu_0+\mu-1}) &= 0, \\ \chi_{\text{prime}}(\kappa(\mu)) - 1 &= 0 \end{aligned} \quad (\mu_0 = \log_2(x_e^{-1} + 1)) \quad (24)$$

are not violated until at  $\mu = 5$ . What might thus constitute the quark family's conservation law would predict that  $L_{43}$  have 2, 31 and 271 among its prime factors and serve as the  $L_{\text{up}}$  of a fourth-generation quark  $t'$ .

It should be noted that the bounds given in Table 6 for the first three generations (next-to-last row) are valid for intra-generational mass ratios only (last row). Ratios of mass for quarks that belong to different generations are distinctly different. One form of heuristics, whose effectiveness would be understood by degrees (cf. 7.1,7.2), draws a link between quark masses and duality controls. These we use as a way of expressing inter-generational quark mass ratios, with the modification that Catalan numbers  $C_x \not> 13$  are mapped to  $\hat{C}_x \equiv 1$ :

$$\begin{array}{llll} \text{measured} & m_t/m_c \approx 135.64 & \text{control} & C_6 = 132 \\ " & m_c/m_u \approx 560.87 & " & 5 \cdot 2^3 \cdot C_4 = 560 \\ " & m_b/m_s \approx 44 & " & C_5 = 42 \\ " & m_s/m_d \approx 19.79 & " & 5 \cdot 2^2 \cdot \hat{C}_3 = 20 \end{array} \quad (25)$$

That, in the light of the above discussion, Eqs.(25) dictate the hypothetical  $t'$  weigh either  $C_7 (= 429)$  or  $5 \cdot 2^4 \cdot C_5 (= 3360)$  top masses is an educated guess at best. Apart from  $t'$  mass, how the two types of mass ratios, inter-generational and intra-generational, intertwine could be ascertained by bound states. It is known that the top quark has too short a lifetime ( $5 \times 10^{-25}$  s) to hadronize.

Instead of forming a bound state  ${}_{\mathbf{b}}^{\bar{t}}$ , say, the top antiquark decays into the bottom quark. Table 3 may be interpreted as a crotonic picture of that failure. First, there is a minority problem: there are only two co-occurring residues to conspire with the pivot, with two down-type targets at their disposal. At  $n = 69$ , two more residues,  $\varphi_{R_3} = 233$  and  $\varphi_{R_4} = 39$  at  $\alpha = 438$  and  $\alpha = 453$ , are available. Their inclusion would solve the minority problem, but yield only one further  $L_{\text{down}} (= 272)$ ; the main down-type target  $L_{\text{down}} = 4320$  stays out of reach. If this interpretation is correct, we can address the co-occurrence example of Table 4. According to Table 6, the up-type kissing number of the charm quark is  $L_{\text{up}} = 10668$ , the main down-type kissing number of the strange quark  $L_{\text{down}} = 336$ . Yet the pivot's target in Table 4 is  $L_{12} = 756$  – which is about  $10668/C_4$ . On the other hand we have this inter-generational mass ratio charm-quark-to-up-quark  $\approx 5 \cdot 2^3 \cdot C_4$  which helps translate “charmed” mass to “up” mass, thusly allowing to consider 756 the  $L_{\text{up}}$  of a meson  $\approx 5 \cdot 2^3$  times as heavy as the average of an up quark and a down antiquark – a description that suits the pion  $\pi^+$ .

One further observation may round out this section. In Table 1,  $\varphi_P^{(991)} = 207646$  connects to  $L_{\text{up}} = 207930$  and  $\varphi_R^{(988)} = 4716$  to the main  $L_{\text{down}} = 4320$ , with a flipped phase  $\psi_R^{(988)} = -4717$ . Can this be interpreted as an attempted bound

state  $\frac{t}{b}$ ? The minority problem can be lifted. We only have to include  $\varphi_{R+}^{(988)}$  ( $= \psi_{R+}^{(988)} = 50$  at  $\alpha_{\varphi_{R+}} = 437$ ,  $\alpha_{\psi_{R+}} = 449$ ),  $\varphi_{R++}^{(991)}$  ( $= \psi_{R++}^{(991)} = 589$  at  $\alpha_{\varphi_{R++}} = 409$ ,  $\alpha_{\psi_{R++}} = 449$ ) and  $\varphi_{R+++}^{(991)}$  ( $= 97$ ,  $\psi_{R+++}^{(991)} = 98$  at  $\alpha_{\varphi_{R+++}} = 377$ ,  $\alpha_{\psi_{R+++}} = 409$ ) which together with the amplitudes  $\varphi_R^{(988)}$  and  $\varphi_P^{(991)}$  sum up to  $L_{29} + (L_{16} + L_{10} + L_9 + L_8)$ . Yet there remains a difference. Table 3 has only co-occurring fluctuations, Table 1 enhanced with the new residues has two fluctuations that contribute at time-like refinement level 988 and three that contribute at 991. For all remarkable correlations arising in the space-like refinements, this might be the footprint of crotonic activity ending in virtual particles – peak amplitude  $\varphi_P^{(992)} = 415294$  makes a  $t\bar{t}$  sea quark pair plausible. By contrast, less-than-perfect correlations but within one level of time-like refinement as in Tables 3-4 seem to be the hallmark of real particles.

## 7. Boundaries and characteristic quantities

In both Sects. 2.1 and 6, the part of duality control was taken by Catalan numbers in conjunction with the numbers  $5 \cdot 2^n$  ( $n \in \mathbb{N}_0$ ). Understood as an expansion factor, the  $5 \cdot 2^n$  is the result of rescaling  $\frac{2^{n+4}}{\pi}$  by a constant factor  $\frac{5\pi}{16} = 1/1.01859\dots$ ; cf. Eqs. (15). The ‘Mersennians’ of  $5, 5 \cdot 2, 5 \cdot 2^2, \dots$  in turn are the numbers  $4, 9, 19, \dots = (p+q)/2$  ( $q = (p-3)/4$ ). To distinguish the latter from regular Mersenne numbers  $M_{\text{reg}} \equiv p = 1, 3, 7, \dots$ , they will be denoted  $M_{5/8} = 4, 9, 19, \dots$ , motivated by the fact  $\frac{5}{8}p$  differs from  $(p+q)/2$  only by the small amount  $\frac{3}{8}$ .

### 7.1. Duality controls: the Catalan number part

Resuming the discussion of labels on the boundary, we recall that out of, in the interordinal case, 192 distinct crotons ensuing from the (enlarged) basis

$$(G_{\rho}^{(7,15)}) = (\underline{1}, 3, \underline{5}, 11, 17, 41, 113),$$

including a null-singularity and neglecting sign reversals, *all* are realized on the enlarged boundary  $\Gamma^{(7,15)}$ , an effect one would expect to carry over to the next level of hybridization,  $p_{i-1} = 15$  and  $p_i = 31$ , thus providing a useful testbed for the specifiability of characteristic physical quantities.

In [Merkel] it was shown that the Catalan number

$$C_q \quad (q = (p-3)/4) \tag{26}$$

is central to croton base numbers keeping time with the successors  $C_{q+1}, C_{q+2}, \dots, C_{2q}$  – a fundamental connection which allows to define a span parameter

$$\Phi^{(p)} = \left( G_{\max}^{(p)} / C_q \right)^{1/q}. \tag{27}$$

Quark constituents are often deemed too artificial to be true elements of nature, but, as we have seen in Sect. 6, if we concentrate on their role as carriers of fractional electric charge,  $x_e^{-1} = 31$  provides a natural frame for them. It therefore comes as no surprise that Eq. (27) supplies up-type *and* down-type interordinal bounds for the electromagnetic coupling constant, the dimensionless quantity  $\alpha$ . When normalized with the factor  $(C_{q_i} - C_{(q_i+q_{i-1})/2})^{-1}$  ( $i = \log_2(x_e^{-1} + 1)$ ), the down-type parameter  $\Phi^{(p_{i-1})}$  provides a tight upper bound

$$(C_7 - C_5)^{-1} \Phi^{(15)} \approx 1/136.88$$

to the current measured value  $\alpha = 1/137.035999$ . And the up-type parameter  $\Phi^{(p_i)}$  in combination with the plus-sign normalizing factor  $(C_{q_i} + C_{(q_i+q_{i-1})/2})^{-1}$  yields an even better lower bound:

$$(C_7 + C_5)^{-1} \Phi^{(31)} \approx 1/137.04$$

The location where  $\alpha^{-1}$  interpolates the interval  $[136.88, 137.04]$  can to good approximation be given by the respective down-type and up-type expressions

Down-type form of  $\alpha^{-1}$ :

$$\alpha^{-1} = (C_7 - C_5)/\Phi^{(15)} + \frac{2f_n + \kappa}{f_{n+1} + \kappa} \Delta_b = 137.035999547\dots$$

Up-type form of  $\alpha^{-1}$ :

$$\alpha^{-1} = (C_7 + C_5)/\Phi^{(31)} - \frac{1}{f_{n+1} + \kappa} \Delta_b = 137.035999547\dots$$

where  $\Delta_b = (C_7 + C_5)/\Phi^{(31)} - (C_7 - C_5)/\Phi^{(15)}$ ,  $\kappa = \frac{3}{8} + \sqrt{\Phi^{(15)}\Phi^{(31)}}$  and  $f_n = 15$ ,  $f_{n+1} = 31$ .

### 7.2. Duality controls: the $M_{5/8}$ part

Obviously, the same controls that regulate the boundary conditions in croton amplitudes and phases – raising the question: Given a boundary, how many  $L_m$ ’s are there for crotons to target at? – are also responsible for intergenerational mass-related selection rules on quark-and-meson  $L_{\text{up}}$ ’s and  $L_{\text{down}}$ ’s, raising the related question: How many Euclidean dimensions out there get involved in particle creation? Key to the approach taken here answering that question is the quotient formed by  $L_\nu - \prod_{i=1}^n(\cdot)$  and  $\prod_{i=1}^{n-2}(\cdot)$  where  $L_\nu$  is least among  $L_m > \prod_{i=1}^n(\cdot)$  and  $\nu'$  is a natural number:

$$\left( L_\nu - \prod_{i=1}^n(\cdot) \right) / \prod_{i=1}^{n-2}(\cdot) = \nu' \quad (\text{natural}). \quad (28)$$

It’s instructive to tabularize the instantiations of Eq. (28) with  $M_{\text{reg}}$  and  $M_{5/8}$  for choices of  $n$  such that  $p_n$  and  $p_{n-1}$  are less or equal  $f_{n+1} (= x_e^{-1})$  and  $f_n (= x_e^{-1})$  respectively:

Table 8: Key particle creation-related dimensions

$n - 2$	$L_\nu$	$\prod_{i=1}^n(\cdot)$	$\prod_{i=1}^{n-2}(\cdot)$	$\nu'$
1	$L_4 = 24$	$1 \cdot 3 \cdot 7 = 21$	1	3
2	$L_{10} = 336$	$1 \cdot 3 \cdot 7 \cdot 15 = 315$	$1 \cdot 3$	7
3	$L_{19} = 10668$	$1 \cdot 3 \cdot 7 \cdot 15 \cdot 31 = 9765$	$1 \cdot 3 \cdot 7$	43
1	$L_{12} = 756$	$4 \cdot 9 \cdot 19 = 684$	4	18
2	$L_{21} = 27720$	$4 \cdot 9 \cdot 19 \cdot 39 = 26676$	$4 \cdot 9$	29

The first observation worth mentioning is that  $\nu$ -sums from the respective parts of the table,  $\Sigma_{r=n-2}^n \nu_r$  and  $\Sigma_{s=n-2}^{n-1} \nu_s$ , are invariant:  $4 + 10 + 19 = 33$  and  $12 + 21 = 33$ . This suggests that the  $\nu_r$  and the  $\nu_s$  can be combined into a basis,  $N_{\text{source}} = (4, 10, 12, 19, 21)$ . With coefficients  $\pm 1$  or 0, linear combinations of its elements with positive result may then be said to span a variety of ‘source dimensions.’ Out of 66 potentially realizable ones, 11 remain unrepresented on  $\text{Bound}(N_{\text{source}})$  – the name connoting a set of labels on the outer nodes of a  $T$ -cube complex ( $T = 5$ ) constructed in the manner of  $\Gamma$  and  $\chi$  –, namely 49, 51,  $\dots$ , 65, and, neglecting sign reversals, two linear combinations yield null-singularities on  $\text{Bound}(N_{\text{source}})$ .

The  $\nu'$  ensuing from the two table parts can in a similar manner be combined into a basis,  $N_{\text{sink}} = (3, 7, 18, 29, 43)$ , spanning ‘sink dimensions.’ Out of 100 potentially realizable ones, 41 remain unrepresented on  $\text{Bound}(N_{\text{sink}})$ : 2, 5,  $\dots$ , 99, and, neglecting sign reversals, one linear combination yields a null-singularity on  $\text{Bound}(N_{\text{sink}})$ . The two boundaries can in turn be combined, to the effect that the number of unrepresentable dimensions shrinks to 22.

The overall picture emerging from these numbers is as follows: The particle creation-potential of the first 100 Euclidean dimensions is governed by the number 11. All other features arising *en route* are identical to or multiples of this number – the  $\nu$ -invariant 33, the unrepresentable 11 ‘source dimensions’ out of 66 potential ones, the number of unrepresentable ‘sink dimensions’ plus the number of null-singularities under the union  $\text{Bound}(N_{\text{source}}) \cup \text{Bound}(N_{\text{sink}})$ , 41 + 3, as well as the number of dimensions staying uninvolved in particle creation even when the distinction between source and sink dimensions is dropped, the said 22 unrepresentable dimensions 49, 55,  $\dots$ , 99. On the other hand, the number of ‘sink dimensions’ denying representation on the single  $\text{Bound}(N_{\text{sink}})$ , 41, to which we may add 1 to account for the one singularity remaining, coincides with  $C_5$ , the interpolating term that makes  $(C_7 \mp C_5)^{-1}$  bound the span parameters  $\Phi^{(p_{i-1})}, \Phi^{(p_i)}$  so tightly they approach the electromagnetic coupling constant in the first place. So it’s worthwhile to go into the details of the dimensional branching process.

At the heart of it resides a unique link leading from  $C_{(q_{i+1}+q_i)/2}$  as starting point to  $C_{(q_i+q_{i-1})/2}$  as end point ( $i = \log_2(x_e^{-1} + 1)$ ). In fact,  $C_{(15+7)/2} = C_{11}$ , in typical interordinal manner, gets down to the last member of the Catalan

number sequence  $(C_3, C_4, C_5, C_6)$  via

$$(C_{11}B(11, 12))^{-1} = 11 \cdot 12 = 132 = C_6, \quad (29)$$

and  $C_6$ , in turn, completes the descent intraordinally to the end point

$$(C_6B(6, 7))^{-1} = 6 \cdot 7 = 42 = C_5 (= C_{(7+3)/2}). \quad (30)$$

How the numbers 11, 12 and 6, 7 work is sort of like in a double strand,  $\begin{array}{ccc} 11 & \cdot & 12 \\ \cdot & \cdot & \cdot \\ 6 & \cdot & 7 \end{array} :$

Horizontally, they serve as upper and lower ties, vertically, as left and right strands. The number of ‘source dimensions’ evolves to  $11 \cdot 6$  (left strand) of which  $11 \cdot 6 - 11$  can be represented on  $\text{Bound}(N_{\text{source}})$ . Panning to the ‘sink side’ (right strand), branching doesn’t end up until at  $12 \cdot 7 + (11 + C_3) = 100$  ‘sink dimensions’ of which, after all,  $12 \cdot 7 - (11 + C_4) = 59$  can be represented on  $\text{Bound}(N_{\text{sink}})$ . The complete  $(G_\rho)^{(15)}$ ’s sequence of Catalan controls  $(C_3, C_4, C_5, C_6)$  is exhausted in the process.

### 7.3. Crotonic implementation

#### Crotonic implementation globally

The goings-on of course have to be implemented crotonically. Take, for example, the creation of the eighteenth dimension: the only certified croton amplitude in the ‘volume’ to match  $L_{18} = 7398$  occurs in a Mersenne fluctuation of Type I (see Table B.16), at time-like refinement level  $n = 1144$  and secondary expansion  $s = 6$ . We note  $1144 = 11 \cdot 104$ . Remarkably, with the the same choice of fluctuation type, crotons creating the remaining basic ‘source’ and ‘sink dimensions’, as far as  $\varphi_\alpha^{(n)}$  to match their kissing numbers are available, are found to share the global property pairing  $11 \mid n$ ,  $s = 6$ , which may be interpreted as being dual to the left-strand effect discussed above:

Table 9: Key particle dimensions via Mersenne fluctuations Type I :  $\lfloor \log_2 C_{63} \rfloor \left( \frac{2^n}{\pi} \right)^{-1}$

$L_\nu$	$\varphi_\alpha^{(n)}$	$L_{\nu'}$	$\varphi_{\alpha'}^{(n')}$
$L_4 = 24$	$\varphi_{315}^{(33=11 \cdot 3)} = 24$	$L_3 = 12$	$\varphi_{67}^{(11)} = 12$
$L_{10} = 336$	$\varphi_{496}^{(737=11 \cdot 67)} = 336$	$L_7 = 126$	$\varphi_{77}^{(55=11 \cdot 5)} = 126$
$L_{19} = 10668$	n/a	$L_{43} = ?$	n/a
$L_{12} = 756$	$\varphi_{330}^{(616=11 \cdot 56)} = 756$	$L_{18} = 7398$	$\varphi_{499}^{(1144=11 \cdot 104)} = 7398$
$L_{21} = 27720$	n/a	$L_{29} = 198506$	n/a

*Crotonic implementation locally*

For a full-scale description of the implementation another type of crotons in the ‘volume’ suit better: where  $\kappa = \frac{3}{8} + \sqrt{\Phi^{(15)}\Phi^{(31)}}$ , (CFR)  $2^{-n}\kappa \rightarrow [\lambda_0^{(n)}; \lambda_\alpha^{(n)}]$ .

As we shall see, a croton  $\lambda_\alpha^{(n)}$  qualifying as a pivot for  $L_m$  has the special property that the gap between it and the target can be bridged by integer addition within a collection of local co-amplitudes  $\lambda_\xi^{(n)}$  – a procedure that is mirrored on a refinement-dependent, *local* boundary  $\Lambda_\alpha^{(n)}$ . For the envisioned relationship we establish the following rules:

(1) When  $\lambda_\alpha^{(n)} > L_m$ ,  $\lambda_\alpha^{(n)}$  qualifies as a pivot with target  $L_m$  if  $\lambda_\alpha^{(n)}/L_m$  does not exceed a prespecified range, say,  $\sqrt{\frac{\lambda_\alpha^{(n)}}{L_m}} \lesssim \frac{16}{5\pi} (= 1.01859\dots)$  as a heuristic, and the local co-amplitudes  $\lambda_\xi^{(n)}$  to include in the collection are located to the pivot’s right; conversely, for  $\lambda_\alpha^{(n)} < L_m$ ,  $\sqrt{\frac{\lambda_\alpha^{(n)}}{L_m}} \gtrsim \frac{5\pi}{16}$  is required, and the inclusions of  $\lambda_\xi^{(n)}$  take place to the left of the pivot;

(2) the prime factorization of  $n$  determines how many co-amplitudes  $\lambda_\xi^{(n)}$  are included; if it contains at least one factor  $p \in M_{\text{reg}}$  ( $p \in M_{5/8}$ ), then the number of co-amplitudes, in a success-dependent way,

(2a) is directly equal to this factor or

(2b) the factor is interpreted as  $p_{j-2}$ , and  $p_j$  is assigned for the number of inclusions.

(1) and (2) are only necessary conditions. A  $\lambda_\alpha^{(n)}$  obeying them has an entourage of co-amplitudes  $\lambda_\xi^{(n)}$  that still have duplicates.  $T$  that are distinct enter the tuple  $(\text{co-}\lambda)_\alpha$  from which the nodes of a  $T$ -cube complex  $\Lambda_\alpha^{(n)}$  as a local boundary get encoded. Either under (2a) or (2b) we get a label  $\Delta_\lambda$  that is equal to  $|\lambda_\alpha^{(n)} - L_m|$ ; if (2b) applies, then, additionally, ‘Catalan tie’ and  $M_{5/8}$  properties have to be deployed to ensure a canonical form for  $\Delta_\lambda$ :

(2b') If co-amplitudes  $\lambda_\xi^{(n)} \in (\text{co-}\lambda)_\alpha$  are multiples of tie numbers 6,7 or 11,12, they induce a sign divide: multiples of 6 (7) and co-amplitudes of the form  $9+4$  ( $9-4$ ) have their signs preserved while all others incur sign inversion; if they instead are upper-tie type multiples, namely of 11 (12), then only they and co-amplitudes of the form  $39+8$  ( $19-4$ ) escape sign inversion.

Let us look into the creation of the eighteenth dimension. For  $L_{18}$ , we reported a match with  $\varphi_{499}^{(1144)} = 7398$  via Mersenne fluctuations of Type I,  $\lfloor \log_2 C_{63} \rfloor \left(\frac{2^n}{\pi}\right)^{-1}$ . As far as can be told, no matches with any  $\lambda_\alpha^{(n)}$  exist for this kissing number, only close pivots. One obeying constraint (1) is  $\lambda_{78}^{(2016)} = 7223$  – a lower-than-target situation. The factor 7 in  $2016 = 2^5 \cdot 3^2 \cdot 7$  directly gives the number of inclusions for  $\lambda_\xi^{(n)}$  on the pivot’s left:  $83, 1, 7, 1, 1, 7, 84, \mathbf{7223}$ .  
Cleaned from duplicates, this yields a quadruple  $(\text{co-}\lambda)_{78} = (84, 7, 1, 83)$  of dis-

tinct co-amplitudes, leading to a label  $\Delta_\lambda$  on  $\Lambda_{78}^{(2016)}$  encoded by

$$(1, 1, 1, 1) \cdot (\text{co-}\lambda)_{78}^t (= 175) \quad (31)$$

to mirror the equation  $L_{18} = \lambda_{78}^{(2016)} + \Delta_\lambda$ .

For the nineteenth dimension, the same online CFR calculator offers a candidate pivot  $\lambda_{341}^{(1736)} = 10808$  with target  $L_{19} = 10668$ . It satisfies constraint (1), and, with  $n = 1736$  factoring as  $2^3 \cdot 7 \cdot 31$ , we encounter a  $p_{j-2}, p_j \in M_{\text{reg}}$  situation, hence constraint (2b) applies and we are led to a string of 31 co-amplitudes  $\lambda_\xi^{(n)}$  to the pivot's (boldface) right,

**10808**, 4, 7, 1, 73, 18, 1, 6, 1, 1, 39, 1, 1, 2, 2, 34, 5, 1, 1, 2, 4, 2, 13, 3, 1, 9, 1, 1, 3, 8, 16, 24.

341 372

$T = 16$  are distinct, so  $(\text{co-}\lambda)_{341} = (4, 7, 1, 73, 18, 6, 39, 2, 34, 5, 13, 3, 9, 8, 16, 24)$ . We recognize that three of them are lower-tie type multiples, namely of 6, and one is equal to  $9 + 4$ . Then, under constraint (2b'),

$$(-1, -1, -1, -1, 1, 1, -1, -1, -1, 1, -1, -1, -1, -1, 1) \cdot (\text{co-}\lambda)_{341}^t (= -140) \quad (32)$$

is a node label  $\Delta_\lambda$  on the local boundary  $\Lambda_{341}^{(1736)}$  that mirrors the equation  $L_{19} = \lambda_{341}^{(1736)} + \Delta_\lambda$ .

Similarly works the creation of the twentieth dimension with a candidate pivot for  $L_{20} = 17400$ ,  $\lambda_{374}^{(1520)} = 17949$ . Again, constraint (1) is obeyed. The factorization of  $n = 1520$  being  $2^4 \cdot 5 \cdot 19$ , it turns out that nineteen co-amplitudes to the pivot's right fail to fill the gap; instead, factor 19 is interpreted as  $p_{j-2} \in M_{5/8}$  and  $p_j = 79$  co-amplitudes to the pivot's (boldface) right are included, i.e.  $\mathbf{17949}, 28, 1, 1, 2, 12, \dots, 407_{374}, 453$ ,  $T = 19$  of them distinct, and a tuple  $(\text{co-}\lambda)_{374} = (28, 1, 2, 12, 8, 3, 5, 4, 7, 45, 9, 32, 22, 17, 6, 15, 20, 14, 407)$  emerges. Again, we recognize co-amplitudes for whom there is sign preservation under constraint (2b'): three that are lower-tie type multiples, namely of 7, and one of the form  $9 - 4$ , so that

$$(1, -1, -1, -1, -1, -1, 1, -1, 1, -1, -1, -1, -1, -1, -1, 1, -1) \cdot (\text{co-}\lambda)_{374}^t (= -549) \quad (33)$$

is a node label  $\Delta_\lambda$  on a new local boundary  $\Lambda_{374}^{(1520)}$ , mirroring  $L_{20} = \lambda_{374}^{(1520)} + \Delta_\lambda$ .

The lower-tie situations bear the imprint of duality controls – the Catalan number part  $(C_6 B(6, 7))^{-1}$  being expressed by the sign preserving in multiples of tie numbers 6 and 7; and the  $M_{5/8}$  part by sign preserving in  $9 \pm 4$  respectively: 13 is the minimal residue in the set of residues  $\{13, 27\}$  ( $= (5 \cdot 2^n - 1 + 2^{n+1}) \bmod C_5$ ) and 5 the minimal one in  $\{5, 11, 9\}$  ( $= (5 \cdot 2^n - 1 - 2^{n+1}) \bmod C_4$ ). Transposed to their upper-tie counterparts, with sign preserving in multiples of tie numbers 11 and 12 and in  $39 + 8, 19 - 4$  respectively, the analogous minimal residue in the set of residues  $\{(11, 23, 47, 95, 59, 119, 107, 83, 35, 71)\}$  ( $= (5 \cdot 2^n - 1 + 2^n) \bmod C_6$ ) as restricted to the interval  $]C_5, C_6[$  would be 47, and the analogous minimal

residue in the set of residues  $\{(7, )15, 31, 21(, 1)\}$  ( $= (5 \cdot 2^n - 1 - 2^n) \bmod C_5$ ) as restricted to the interval  $]C_4, C_5[$  would be 15. In summary, we may conclude minimal-residue selection of the above kind, combined with selection of the tie number with the most multiples in  $(\text{co-}\lambda)_\alpha$ , are part and parcel of the sign arrangement program in local gap filling-in.

More instances of dimensional branching have to be examined before one can definitely say a new invariant is looming here – namely that the number of distinct co-amplitudes having their signs preserved in gap filling-in equals 4, as suggested by Eqs. (31)–(33).

#### *Dimensions (4;18,19,20), (24;46,47,48) and forces*

Before pursuing the case with multiples in Sect.7.4, a peculiar aspect shall be addressed concerning a possible relationship between all three Eqs. (31)–(33) and key particle creation-related dimensions on the one hand and nature’s force coupling constants on the other. Fine-tuning  $(C_7 + C_5)/\Phi^{(63)}$  to  $\alpha^{-1} = (C_7 + C_5)/\Phi^{(63)} - \frac{1}{f_{n+1} + \kappa} \Delta_b$  led to the approximation  $\alpha^{-1} = 137.035999547\dots$

Subtract from this expression  $G_{\max}^{(15)}$  and you get a close approximation of the kissing number  $L_4 = 24$ . Now the same Table 8 that reveals  $L_4$  as the kissing number of the least key particle creation-related source dimension also assigns  $L_{19} = 10668$  to the highest key particle creation-related source dimension (in that table part). Does the latter assignment give us a handle on the glueing (strong) force? Denoting the greatest prime factor of  $n$ ,  $\text{gpf}(n)$ , the fact that  $\text{gpf}(L_{19})$  also determines the  $L_{\text{up}}$  (see Table 6) of the charm quark, the heaviest up-type quark allowing bound states to exist, while at the same time  $L_4$  is the least among the  $L_{\text{down}}$ ’s of the down quark, is encouraging enough for us to formulate the following CFR-related

**Conjecture 3.** *If a dimension  $\nu$  is greatest among particle creation-related source dimensions, it induces the following pattern: (A) there exists a lower pivot  $\lambda_\alpha^{(n_{\nu-1})} < L_{\nu-1}$  with  $\sqrt{\frac{\lambda_\alpha^{(n_{\nu-1})}}{L_{\nu-1}}} \gtrsim \frac{5\pi}{16}$  such that distinct local co-amplitudes  $(\text{co-}\lambda)_\alpha$  are recruited to the left of the pivot and (A')  $(\text{gpf}(L_{\nu-1}))^{-1}$  represents an upper bound to a physical force constant; conversely (B) there exists a higher pivot  $\lambda_\alpha^{(n_{\nu+1})} > L_{\nu+1}$  with  $\sqrt{\frac{\lambda_\alpha^{(n_{\nu+1})}}{L_{\nu+1}}} \lesssim \frac{16}{5\pi}$  such that its  $(\text{co-}\lambda)_\alpha$  in combination with those of  $\lambda_\alpha^{(n_\nu)} > L_\nu$ ,  $\sqrt{\frac{\lambda_\alpha^{(n_\nu)}}{L_\nu}} \lesssim \frac{16}{5\pi}$ , are recruited to the right and (B')  $\text{gpf}(L_{\nu-1})\text{gpf}(L_\nu)L_{\nu+1}^{-1}$  represents a lower bound to a complementary physical force constant.*

Parts (A) and (B) led to Eqs. (31)–(33) and have proven true for them. As to (A'), we refer the reader to Table 6, where  $\text{gpf}(L_{18})$  corresponds to the integer part of  $\alpha^{-1}$ , hence leads to an upper bound for  $\alpha$ ,  $1/137 > 1/137.035999$ . As to (B'), the same table shows that  $\text{gpf}(L_{18})\text{gpf}(L_{19})L_{20}^{-1} = 17399/17400 < 1$ . We are free to interpret 1 as the coupling constant of the glueing force – and

ask if the weak force fit in in this picture as well. Generalizing the fine-tuned calculation of  $\alpha^{-1}$  to<sup>15</sup>

$$(\alpha')^{-1} = (C_{15} + C_{11})/\Phi^{(63)} - \frac{1}{f_{n+1} + \kappa'} \Delta_{b'} = 2626851.2772574808\dots,$$

where  $\Delta_{b'} = (C_{15} + C_{11})/\Phi^{(63)} - (C_{15} - C_{11})/\Phi^{(31)}$ ,  $\kappa' = -\frac{1}{8} + \sqrt{\Phi^{(31)}\Phi^{(63)}}$  for the next higher geometric mean and  $f_{n+1} = 31$ , we note the following: As the fine-tuning  $\alpha^{-1} - G_{\max}^{(15)}$  results in a real number that is only a tiny bit greater than  $L_4 = 24$ , the analogous fine-tuning  $(\alpha')^{-1} - G_{\max}^{(31)}$  produces a real a tiny bit greater than the kissing number  $L_{24} = 196560$ . The 24th dimension then, which is not among the  $F_e$  and  $F_s$ -related source dimensions mentioned in Table 8, might turn out to be  $F_w$ -related and contribute the missing coupling constant to complement the force trio with  $\alpha_w := \alpha' \approx 3.81 \times 10^{-7}$ .

Conjecture 3 deals with the combination of a triad of dimensions with a force duo. To show how bounds to all three couplings could be intertwined, we have to modify that conjecture such that a dimensional triad covers three couplings. To this end, we make a series of qualitative statements.

(C)  $L_{24}$  is the first kissing number to resume the normal successor relation  $L_{m+1} < 2L_m$  after the hiatus  $L_{23}$  where  $L_{24} = 2L_{23} + 10260$ . We may assume the formation law of the hiatus is  $m_{\text{hiat}} = p_k + 2^{k-1}$  ( $p_k \in M_{\text{reg}}$ ); then  $23 = 15 + 8$  would be followed by another hiatus at  $47 = 31 + 16$ .

(D) According to Conjecture 3, the center dimension of the dimensional triad is 19. Assuming a formation law  $m_{\text{cent}} = 2C_{k-1} + p_{k-2}$  ( $p_k \in M_{5/8}$ ), the dimension  $19 = 10 + 9$  would be followed by another center dimension  $47 = 28 + 19$ .

(E) The left companion in the new triad is dimension 46. A serious candidate for the kissing number  $L_{46}$  would be 12 986 152: Mersenne fluctuations of Type I,  $\lfloor \log_2 C_{q_s} \rfloor \left(\frac{2^n}{\pi}\right)^{-1}$ , at secondary expansion  $s = 7$  and time-like refinement levels  $n$  that are multiples of 12, do indeed include the global (matching?) amplitude  $\varphi_{93}^{(1152)} = 12986152$ .

(F) The right companion is dimension 48, which has a *certified* kissing number  $L_{48} = 52416000$ . Because of the assumptions we have made, the unknown kissing number  $L_{47}$  must obey the constraints  $L_{47} < 2L_{46}$  and  $L_{48} \geq 2L_{47}$ . We note in passing that the assumed value  $L_{46}$  has the prime factorization  $12986152 = 2^3 \cdot 1623269$ . If  $\text{gpf}(L_{46})$  is to give rise to a lower bound to the glueing force coupling, it must combine with an  $L_{47}$  that has 31 among its prime factors because the closest analog to the previously found bound  $17399/17400$  would be  $1623269 \cdot 31/52416000 < 1$ . The ansatz to assure this is

$$L'_{47} := 2L_{46} + (8 - 31\eta)10260 \quad (\eta = 1, 2, \dots)$$

where 10260 is borrowed from the hiatus at  $L_{23}$ . As a rule, instances of  $L'_{47}$  will contain also prime factors  $p_j, p_k, \dots > 31$ . In order to eliminate them, we

---

<sup>15</sup>a tedious `int64` computation yields  $G_{\max}^{(63)} = 3,512,576,820,924,177$  from which the value of  $\Phi^{(63)}$  follows; it was shown in [Merkel] that  $\Phi^{(p_n)}$  assumes the limit 4 as  $n \rightarrow \infty$

have to transform  $L'_{47}$  via  $p_j \pm 1, p_k \pm 1, \dots$  into  $L''_{47}$ . For instance,  $L'_{47} := 2L_{46} - 85 \cdot 10260 = 2^2 \cdot 31 \cdot 71 \cdot 2851 \mapsto L''_{47} = 2^2 \cdot 31 \cdot 72 \cdot 2850 \equiv 2^6 \cdot 3^3 \cdot 5^2 \cdot 19 \cdot 31$ . An evolution along these lines does not always succeed – fortunately so, since one of the ‘failures’ turns out to be a lucky strike:  $L'_{47} := 2L_{46} - 54 \cdot 10260 = 2^3 \cdot 17 \cdot 31 \cdot 6029 \mapsto L''_{47} = 2^3 \cdot 17 \cdot 31 \cdot 6028 \equiv 2^5 \cdot 11 \cdot 17 \cdot 31 \cdot 137$ , the latter being the prime factorization of our now preferred candidate at center dimension 47,  $L_{47} := 25\,414\,048$ .

The combined result of our qualitative statements then is the following bounds:

$$\begin{aligned} \text{for } \alpha_w, \quad (\text{gpf}(L_{46}))^{-1} &= 1/1\,623\,269 > 1/2\,626\,851.277257; \\ \text{for } \alpha, \quad (\text{gpf}(L_{47}))^{-1} &= 1/137 > 1/137.035999; \text{ and} \\ \text{for } \alpha_s, \quad \text{gpf}(L_{46}) \text{sgpf}(L_{47})L_{48}^{-1} &= 50\,321\,339/52\,416\,000 < 1 \end{aligned}$$

where  $\text{sgpf}(\cdot)$  connotes ‘second greatest prime factor.’ Provided the postulated values do indeed embody the true kissing numbers  $L_{46}$  and  $L_{47}$ , the new triad preserves the tight bound for the electromagnetic coupling, combining it with loosened bounds for the weak and the strong couplings, respectively. To draw a link between the global and local perspective, we first discuss the tight bounds-only case of the former triad, then proceeding with the loosened bounds case of the second triad. In what follows we use the shorthand  $(\varphi_{\alpha}^{(n; n_{\text{low}} \leq n \leq n_{\text{high}})} | \varphi_{\alpha_{n_{\text{pivot}}}}^{(n_{\text{pivot}})} = \text{pivot})$  for the Mersenne fluctuation  $(\varphi_{\alpha_{n_{\text{low}}}}^{n_{\text{low}}}, \dots, \text{pivot}, \dots, \varphi_{\alpha_{n_{\text{high}}}}^{n_{\text{high}}})$ .

#### Link between local and global implementation for dimensional triad 18,19,20

When  $\nu$  ( $\nu'$ ) is related to a key particle creation-related ‘source’ (‘sink’) dimension, croton amplitudes in the ‘volume’ matching  $L_{\nu}$  ( $L_{\nu'}$ ) (cf. Table 9) are bound to Mersenne fluctuations of Type I,  $\lfloor \log_2 C_{q_s} \rfloor \left(\frac{2^n}{\pi}\right)^{-1}$ , at secondary expansion  $s = 6$  and time-like refinement levels  $n$  that are multiples of 11, suggesting a relationship with the left side of the Catalan double strand, or left strand for short. Here we show that global pivots which the local pivot  $\lambda_{78}^{(2016)} = 7223$  snaps into spring from the *same* type of Mersenne fluctuations. A key feature of this sort of pivots is that they represent the left strand equivalently by time-like refinement levels  $n$  and space-like refinement offsets  $\Delta\alpha (\equiv \alpha_{\psi} - \alpha_{\varphi})$ , where  $\varphi$  denotes amplitude, and  $\psi$  phase. A local pivot  $\lambda_{\alpha_w}^{(n_w)}$  is said to snap into global pivots  $\varphi_{\alpha_v}^{(n_v)}$  and  $\varphi_{\alpha_u}^{(n_u)}$  if it is able to unfreeze them from their frozen-in status they have since expansion went past  $2^{n_u}$  and  $2^{n_v}$ . That is,  $n_w > n_v, n_u$ . For dimension 18, whose kissing number is matched with  $\varphi_{499}^{(1144)} = 7398$  but bound up locally with  $\lambda_{78}^{(2016)} = 7223$ , we find  $\varphi_{\alpha_u}^{(n_u)} := \varphi_{97}^{(90)} = 7569$ . To have this overshoot fit with the local pivot, the excess in amplitude has to be compensated for by a  $\varphi_{\alpha_v}^{(n_v)}$  missing its target by  $-346$ . The global deficient to back this up is with target  $L_{20}$ , comes from within the ranks of a Mersenne fluctuation  $(\varphi_{\alpha}^{(n; 1681 \leq n \leq 1701)} | \varphi_{35}^{(1690)} = \mathbf{17054})$  and incidentally is as ‘leggy’ a pivot therein as the overshoot is in  $(\varphi_{\alpha}^{(n; 79 \leq n \leq 99)} | \varphi_{97}^{(90)} = \mathbf{7569})$ :

Table 10: ‘Leggy’ global pivots (boldface), embedded in their respective frozen-in Mersenne fluctuations ( $\varphi_{\alpha}^{(n; 79 \leq n \leq 99)} \mid \varphi_{97}^{(90)} = \mathbf{7569}$ ), ( $\varphi_{\alpha}^{(n; 1681 \leq n \leq 1701)} \mid \varphi_{35}^{(1690)} = \mathbf{17054}$ ) of type  $\lfloor \log_2 C_{63} \rfloor \left( \frac{2^n}{\pi} \right)^{-1}$

$n$	$\varphi_{\alpha}$		$n$	$n$	$\varphi_{\alpha}(\psi_{\alpha})$		$n$
89	15139		89	1691	34108		1691
88	7569	<b>7569</b>	90	1690	<b>17054</b>	17053 (-17054)	1692
87	3784	3784	91	1689	8526	8526	1693
86	1892	1891	92	1688	4262	4263	1694
85	946	945	93	1687	2131	2131	1695
84	472	472	94	1686	1065	1065	1696
83	235	235	95	1685	532	532	1697
82	117	117	96	1684	265	266	1698
81	58	58	97	1683	132	132	1699
80	28	28	98	1682	66	66	1700
79	13	13	99	1681	32	32	1701
$\vdots$			$\vdots$	$\vdots$			$\vdots$

With the phase at  $n_v = 1692$  (in parentheses) looping into  $\psi_{34}^{(1692)} = -17054$ , we are lucky to find one value,  $|\psi_{34}^{1692}| = 17054$ , that is deficient with respect to the target  $L_{20} = 17400$  by the same amount as  $\varphi_{35}^{(1690)}$ . With  $6 \mid n_v$  and  $5 \mid n_u$ , and also  $(6+5) \mid (n_v + n_u)$ , we come upon the time-like refinement realisation of the left strand depicted in Table 11:

Table 11: Time-like refinement levels for global pivots from fluctuations of type  $\lfloor \log_2 C_{63} \rfloor \left( \frac{2^n}{\pi} \right)^{-1}$  the local pivot  $\lambda_{78}^{(2016)} = 7223$  snaps into

$n$	overshoot & deficient $\varphi_u,  \psi_v $		$\Sigma x \mid \Sigma n, x \mid n$	left strand	
		11   1782	$\mapsto$	tie number 11	
90	7569	5   90	$\mapsto$	inter-tie increment 5	
1692	17054	6   1692	$\mapsto$	tie number 6	

The dual realization of the left strand in terms of space-like refinement offsets works by executing a switch back to the left-leg  $n_v = 1690$ . The effect is as envisioned in the first place:  $\varphi_{35}^{(1690)} = 17054$  is deficient with respect to  $L_{20}$  by -346, but now the tale is told by offsets.

Table 12: Space-like refinement offsets for global pivots from fluctuations of type  $\lfloor \log_2 C_{63} \rfloor \left(\frac{2^n}{\pi}\right)^{-1}$  the local pivot  $\lambda_{78}^{(2016)} = 7223$  snaps into

n	overshoot & deficient			left strand
	$\varphi, \psi$	$\alpha_\varphi, \alpha_\psi$	$\Sigma \Delta \alpha, \Delta \alpha$	
90	7569, -7570	97, 102	11	↔ tie number 11
1690	17054, 17054	35, 41	5	↔ inter-tie increment 5
			6	↔ tie number 6

We conclude that for the dimensional triad 18,19,20 global pivots that are unfrozen by a local pivot provide a picture of the left strand that is complementary to the one based on matching global amplitudes (Table 9). The representations are in terms of time-like refinement levels or space-like refinement offsets, the former aided by switching the ‘standing leg’ and substituting absolute value in phase. The unfreezing encompasses the entire Mersenne fluctuations, not only the pivotal amplitudes. This is suggested by

$$\lfloor L_{20}/2^i \rfloor + \lambda_{\alpha_{w(i)}}^{(w(i))} - \varphi_{\alpha_{v(i)}}^{(v(i))} - \varphi_{\alpha_{u(i)}}^{(u(i))} = \delta \quad (\delta \in \{0, 1\}),$$

where  $w(i) = 2016 \mp i$ ,  $v(i) = \frac{1690-i}{1692+i}$ ,  $u(i) = \frac{88-i}{90+i}$  ( $i = 0, 1, \dots, 9$ ), (13, 27, 55, 112, 225, 451, 902, 1805, 3611, **7223**, 3611, 1805, 902, 451, 225, 112, 56, 27, 13) is the fully traced local fluctuation ( $\lambda_{\alpha}^{(n; 2007 \leq n \leq 2025)} | \lambda_{78}^{(2016)} = \mathbf{7223}$ ) and the expressions  $\lfloor L_{20}/2^i \rfloor$  are the surrogate for the left and right leg of an (auxiliary fourth) fluctuation.

#### Link between local and global implementation for dimensional triad 46,47,48

Within the relatively loose bounds to the weak and strong coupling that characterize the dimensional triad 46,47,48, local amplitudes defined by (CFR)  $2^{-n} \kappa' \rightarrow [(\lambda')_0^{(n)}; (\lambda')_{\alpha}^{(n)}]$ ,  $\kappa' = -\frac{1}{8} + \sqrt{\Phi^{(31)} \Phi^{63}}$ , will have properties that are very different from what we know about  $\lambda_{\alpha}^{(n)}$ . Instead of a prime factorization of  $n$  going by the rules (2)–(2b), the prime factorization of a key amplitude  $(\lambda')_{\alpha_z}^{(n_z)}$  determines a co-structure of dispersed amplitudes  $(\lambda')_{\alpha_y}^{(n_y)}, (\lambda')_{\alpha_x}^{(n_x)}, \dots$  ( $n_z \geq n_y \geq n_x \geq \dots$ ) all of which have to be included to achieve a match with a targeted kissing number. (2c) If this factorization has the form  $v \cdot \text{gpf}(\cdot)$  and  $\text{gpf}(\cdot)$  coincides with  $p \in M_{\text{reg}}$  ( $p \in M_{5/8}$ ), then  $v - 1$  amplitudes join the co-structure. And in case  $v$  coincides also with the inter-tie increment 5, the key local amplitude plus those of the co-structure are found to snap into a global amplitude matching that kissing number so that the interaction may be caught in a dual strand representation in terms of time-like refinement levels and space-like refinement offsets respectively.

We pointed out the possibility of  $L_{46} := \varphi_{93}^{(1152)} = 12\,986\,152$ , a global amplitude

satisfying the property pairing  $12 \mid n, s = 7$  representative of the right strand. To illustrate how this is realized locally, let  $(\lambda')_{15}^{(2913)} = 95$  take the role of key amplitude, noting that its factorization  $95 = 5 \cdot 19$  is meeting the demands. Then the associated space-like refinements  $(\alpha_z)_\varphi = 15$  and  $(\alpha_z)_\psi = 17$  are found to work as cross moduli for the time-like refinement levels and space-like refinement offsets of the dispersed amplitudes that jointly form the co-structure, which are

$$\begin{aligned} (\lambda')_{46}^{(2913)} &= 209\,406 \text{ with } \alpha_\varphi = 46, \alpha_\psi = 51, \\ (\lambda')_{410}^{(1784)} &= 50\,458 \text{ with } \alpha_\varphi = 410, \alpha_\psi = 471, \\ (\lambda')_{400}^{(1678)} &= 44\,750 \text{ with } \alpha_\varphi = 400, \alpha_\psi = 436, \text{ and} \\ (\lambda')_{461}^{(647)} &= 12\,681\,443 \text{ with } \alpha_\varphi = 461, \alpha_\psi = 485. \end{aligned}$$

To begin with the latter realization, we have (key amplitude in parentheses)

Table 13: Space-like refinement offsets of local pivots  $\lambda'$  snapping into  $\varphi_{93}^{(1152)} = 12\,986\,152$

$\lambda'$	co-structure by cross moduli		right strand
	$\alpha_\varphi, \alpha_\psi$	$\Sigma \Delta_\alpha \bmod \alpha_z$	
12 681 443 209 406  (95)	461, 485 46, 51	$12 \equiv (24 + 5)(\bmod 17)$  $(v = 5)$	$\mapsto$ tie number 12
			$\mapsto$ inter-tie increment 5
50 458 44 750	410, 471 400, 436	$7 \equiv (61 + 36)(\bmod 15)$	$\mapsto$ tie number 7

which is flanked by the dual

Table 14: Time-like refinement levels of local pivots  $\lambda'$  snapping into  $\varphi_{93}^{(1152)} = 12\,986\,152$

$\lambda'$	co-structure by cross moduli		right strand
	$n$	$\Sigma n \bmod \alpha_z$	
50 458 44 750  (95)	1784 1678	$12 \equiv (1784 + 1678)(\bmod 15)$  $(v = 5)$	$\mapsto$ tie number 12
			$\mapsto$ inter-tie increment 5
12 681 443 209 406	647 2913	$7 \equiv (647 + 2913)(\bmod 17)$	$\mapsto$ tie number 7

Speaking in terms of expansion in the above example, only 2.35% of the global amplitude  $12\,986\,152$  get unfrozen as usual:  $2^{1152} < 2^{1678} < 2^{1784} < 2^{2913}$ ; 97.65% get preformed by local amplitude  $12\,681\,443$  via  $2^{1152} > 2^{647}$  – perhaps as a raison d’être of crotons seeking targets – or, if you prefer the unfreezing metaphor, ‘unfrozen’ in local time reversal mode.

## 7.4. ‘Field-’, ‘projection-’ and ‘spacetime’ simulacrum

*From croton base numbers to a simulacrally decorated double strand*

Constraint (2b') and the comments that followed it suggest that the entries of the Catalan double strand pattern

$$\begin{array}{ccc} 11 & \cdot & 12 \\ \cdot & & \cdot \\ 6 & \cdot & 7 \end{array}$$

are all on equal grounds – a hypothesis which needs to be checked. This may be done using the subgroups of order 4,  $\{1, 5, 9, 13\}$  (powers of 5) and  $\{1, 15, 33, 47\}$  (powers of 15), of the group of units of the quotient rings  $\mathbb{Z}/16\mathbb{Z}$  and  $\mathbb{Z}/64\mathbb{Z}$ , respectively. Denoting the above quadruples of units by  $(\text{Sim}_{16})$  and  $(\text{Sim}_{64})$ , we arrive at the following decorated version of the double strand:

$$\begin{array}{ll} 11 : & 12 : \\ \text{characteristic multiple:} & \text{characteristic multiple:} \\ (1, -1, 1, 1) \cdot (\text{Sim}_{64})^t = 66 (= 2n_c \cdot 11) & (1, 1, 1, 1) \cdot (\text{Sim}_{64})^t = 96 (= 2n_c \cdot 12) \\ \text{characteristic quantity } 39+8: & \text{characteristic quantity } 19-4: \\ (0, 0, 0, 1) \cdot (\text{Sim}_{64})^t = 47 & (0, 1, 0, 0) \cdot (\text{Sim}_{64})^t = 15 \\ \\ 6 : & 7 : \\ \text{characteristic multiple:} & \text{characteristic multiple:} \\ (1, -1, 1, 1) \cdot (\text{Sim}_{16})^t = 18 (= n_c \cdot 6) & (1, 1, 1, 1) \cdot (\text{Sim}_{16})^t = 28 (= n_c \cdot 7) \\ \text{characteristic quantity } 9+4: & \text{characteristic quantity } 9-4: \\ (0, 0, 0, 1) \cdot (\text{Sim}_{16})^t = 13 & (0, 1, 0, 0) \cdot (\text{Sim}_{16})^t = 5 \\ \\ (n_c = 3) & (n_c = 4) \end{array}$$

Just as the characteristic multiples and projections in the lower half mark sign-preserving co-amplitudes in the gap fillings of lower-tie type – 18 and 13 in Eq.(32), 28 and 5 in Eq.(33) –, the characteristic multiples and projections in the upper half – 66 and 47 in case of 11, and 96 and 15 in case of 12 – anticipate sign-preserving co-amplitudes emerging in gap fillings of the upper-tie type even if we do not, for the time being, know the kissing number pivots that evoke these situations.

The right strand is marked by characteristic multiples with signature  $(1, 1, 1, 1)$  which are called ‘field’ simulacra here; its characteristic projections with signature  $(0, 1, 0, 0)$ , just like their left-strand counterparts with signature  $(0, 0, 0, 1)$ , are accordingly named ‘projection’ simulacra. The characteristic multiples given on the left strand, in being of signature  $(1, -1, 1, 1)$ , may be termed ‘spacetime’ simulacra. The difference between ‘field’ and ‘spacetime’ simulacra is one of their associated  $n_c$ , or number of positive entries in the signature. The label ‘space-time’ perhaps becomes clearer when the time-like refinements are related to space-like refinements – much like in the previous subsection. In Eqs. (32) and (33),  $n$  – the base 2 logarithm of the time-like refinement – is a multiple of  $p_j$  or  $p_{j-2}$  and is linked to the space-like refinements  $\alpha$  and  $\alpha + p_j$  by the

relationship  $|\alpha - C_x| = n_y \cdot 11$ ,  $\alpha + p_j - C_x = n_z \cdot 6$ , where  $n_y, n_z \in M_{5/8}$  or  $M_{5/8} + 1$ :

	Eq. (32)	Eq. (33)
$ \alpha - C_x $	$341 - C_6 = 19 \cdot 11$	$C_7 - 374 = 5 \cdot 11$
$\alpha + p_j - C_x$	$372 - C_6 = 40 \cdot 6$	$453 - C_7 = 4 \cdot 6$

While the second expansion parameter  $s$  in Table 9 has to ‘come out of the woodwork’ –  $C_{63}$  identified as  $C_{2^6-1}$  – to make the left-strand character of time-like parameter pairing  $11 \mid n, s = 6$  apparent, the left-strand affinity of the pairing of space-like parameters in the above table –  $\alpha$  for the pivot,  $\alpha + p_j$  for the rightmost co-amplitude – comes to the fore by letting the lower-tie character retreat into hiding – into index status  $x = 6$  and  $x = 7$  for Eqs. (32) and (33), respectively. The group-theoretic manifestation of left-strand affinity is the said ‘spatio-temporal’ simulacrum, where space-like and time-like aspects combine into one signature.

Although the distinction of simulacral forms may earn them merits of their own on the local level – left-strand affinity and factorization of  $n \rightarrow$  ‘spacetime’ simulacrum, right-strand affinity and factorization of key amplitude  $\rightarrow$  ‘field’ simulacrum –, with respect to *gap filling-in* they are incomplete because only one – what is meant by characteristic – multiple is produced for each tie number and we don’t get to know the (number of) other multiple-type, sign-preserving co-amplitudes contributing to the filling-in. The group-theoretic background however makes the existence of an invariant number for them plausible.

*Bound((Sim<sub>16</sub>)), Bound((Sim<sub>64</sub>)) and  $M_{5/8} + 1$  -complement*

The problem can be narrowed down by the following observations:

First, in analogy to the constructions  $\text{Bound}(N_{\text{source}})$ ,  $\text{Bound}(N_{\text{sink}})$ , we may allow for 4-cubes,  $\text{Bound}((\text{Sim}_{64}))$  and  $\text{Bound}((\text{Sim}_{16}))$ , and check which multiples of 11,12 are node labels on the former and multiples of 6,7 node labels on the latter; it turns out four multiples of 11,12 are represented on  $\text{Bound}((\text{Sim}_{64}))$  and seven multiples of 6,7 on  $\text{Bound}((\text{Sim}_{16}))$ :

$$\begin{aligned} \text{I: } & 33, 48, 66, 96; \\ & 6, 7, 12, 14, 18, 21, 28. \end{aligned}$$

(In  $\text{Bound}((\text{Sim}_{64}))$ , sixty-four out of the numbers 1,2,...,96 remain unrepresented: 3,4,...,12; 20,21,...,27; 35,36,...,45; 50,51,...,60; 67,68,...,78; 82,83,...,93. In  $\text{Bound}((\text{Sim}_{16}))$ , out of the numbers 1,2,...,28, four remain unrepresented: 11,20,24,25.)

The second observation draws on the fact that, while one ‘spacetime’ simulacrum,  $(1, -1, 1, 1) \cdot (\text{Sim}_{64})^t (= 66)$ , suffices to reproduce the left strand

$$\begin{matrix} 11 \\ \cdot \\ 6 \end{matrix},$$

the binary operation ‘+’ on the two of them is required to reproduce the right

$$\begin{matrix} 12 \\ \cdot \\ 7 \end{matrix},$$

namely  $(1, -1, 1, 1) \cdot (\text{Sim}_{64})^t + (1, -1, 1, 1) \cdot (\text{Sim}_{16})^t = 84$ . The latter

being a (Janus-faced) multiple, we can use that operation to find other multiples, but, similar to the constraint (2) for co-amplitudes  $\lambda_\xi^{(n)} \in (\text{co-}\lambda)_\alpha$ , need an  $M_{5/8} + 1$  constraint for them as follows: A multiple of 6, 7, 11 or 12 assuming the form  $(\epsilon_1, \epsilon_2, \epsilon_3, \epsilon_4) \cdot (\text{Sim}_{64})^t \pm (\epsilon_1, \epsilon_2, \epsilon_3, \epsilon_4) \cdot (\text{Sim}_{16})^t$  is admissible in a gap filling situation only if  $[(\epsilon_1, \epsilon_2, \epsilon_3, \epsilon_4) \cdot (\text{Sim}_{64})^t \mp (\epsilon_1, \epsilon_2, \epsilon_3, \epsilon_4) \cdot (\text{Sim}_{16})^t] \in M_{5/8} + 1$ . With only two  $\epsilon_x, \epsilon_y \neq 0$ , we register five solutions:

$$\begin{aligned}
 (1, 1, 0, 0) \cdot (\text{Sim}_{64})^t \pm (1, 1, 0, 0) \cdot (\text{Sim}_{16})^t &= 16 \pm 6 = \frac{22}{10}, \\
 (-1, 1, 0, 0) \cdot (\text{Sim}_{64})^t \pm (-1, 1, 0, 0) \cdot (\text{Sim}_{16})^t &= 14 \pm 4 = \frac{18}{10}, \\
 \text{IIa: } (-1, 0, 1, 0) \cdot (\text{Sim}_{64})^t \mp (-1, 0, 1, 0) \cdot (\text{Sim}_{16})^t &= 32 \mp 8 = \frac{24}{40}, \\
 (0, 1, 0, 1) \cdot (\text{Sim}_{64})^t \mp (0, 1, 0, 1) \cdot (\text{Sim}_{16})^t &= 62 \mp 18 = \frac{44}{80}, \\
 (0, 0, -1, 1) \cdot (\text{Sim}_{64})^t \pm (0, 0, -1, 1) \cdot (\text{Sim}_{16})^t &= 14 \pm 4 = \frac{18}{10};
 \end{aligned}$$

and with  $\epsilon_1, \epsilon_2, \epsilon_3, \epsilon_4 \neq 0$ , one further:

$$\text{IIb: } (-1, 1, -1, 1) \cdot (\text{Sim}_{64})^t \pm (-1, 1, -1, 1) \cdot (\text{Sim}_{16})^t = 28 \pm 8 = \frac{36}{20}.$$

(Terms involving  $\epsilon_w = 0$ , while  $\epsilon_x, \epsilon_y, \epsilon_z \neq 0$ , do not satisfy the condition, nor do terms involving  $\epsilon_w = 1, \epsilon_x, \epsilon_y, \epsilon_z = 0$ . That the number of solutions from I and from IIa+IIb amount to 11 and 6, respectively, while that of solutions from IIa alone coincides with the inter-tie increment 5, testifies to an all-pervasive left strand affinity.)

The equal-grounds condition comes closer into focus now. When we combine contributions from the first bunch (I) with those from the second (IIa+IIb), we have to be careful: just as for the non-characteristic multiple of the right strand, 84, we find  $84 < 2n_c \cdot 12$ , for additional non-characteristic multiples of all tie numbers  $t$  of the Catalan double strand the rule  $m_{\text{add}} < 2n_c t$  may apply. One actually arrives at an equal number of multiples for each tie number, as required:

$$\begin{aligned}
 11 : \quad T &= \{33, 66\} \cup \{22, 44\} & 12 : \quad T &= \{48, 96\} \cup \{24, 36\} \\
 6 : \quad T &= \{6, 12, 18\} \cup \{18, 24, 36\} & 7 : \quad T &= \{7, 14, 21, 28\} \cup \{ \}
 \end{aligned}$$

As could be seen from Eqs. (32) and (33), for lower tie numbers  $t = 6, 7$  the multiples not available to gap filling-in are  $(n_c - 1)t$ : 12 and 21 respectively. Generalizing from that, it appears that, given a suiting gap filling situation, for the remaining tie numbers  $t = 11, 12$  it's the multiples  $n_c t$  that would be non-available – 33 and 48 respectively. While this is in accord with an underlying invariance regarding the number of sign-preserving co-amplitudes, it seems to violate the equal-grounds condition. One has to take note of a peculiarity, though: The contributions  $T$  for the lower tie numbers contain the ‘multiples’ 6 and 7; for the upper tie numbers, the contributions  $T$  do not contain improper multiples. So the equal-grounds condition can be reformed formally by requiring that for all  $t = 6, 7, 11, 12$ , multiple  $(n_c - \delta_{t \in T})t$  is the one that characterizes an amplitude not partaking in gap filling-in, where  $\delta_{e \in S} = 1$  if  $e \in S$ , 0 else.

*In search of more dualities*

For each  $t$  we obtain four multiples from the bases  $(\text{Sim}_{16})$  and  $(\text{Sim}_{64})$  and one characteristic quantity, a quintuple from which one entry, the multiple identifiable as  $(n_c - \delta_{t \in T})t$ , has to be removed to substantiate its non-partaking in gap filling-in. However, as it seems firmly anchored in the simulacral world, we expect to see it pop up in related situations: Simulacra may also be extracted from  $N_{\text{source}} (= (4, 10, 12, 19, 21))$  and  $N_{\text{sink}} (= (3, 7, 18, 29, 43))$  via merger of a pair of basis elements. Going by the  $M_{5/8} + 1$  lead, we may expect a merger to be allowed for  $\delta_x = \delta'_y = 1$  ( $x \neq y$ ) and  $\delta_{v,w,y,z}, \delta'_{v,w,x,z} = 0$  only if one of the expressions  $(\delta_1, \delta_2, \delta_3, \delta_4, \delta_5) \cdot N_{\text{type}}^t \pm (\delta'_1, \delta'_2, \delta'_3, \delta'_4, \delta'_5) \cdot N_{\text{type}}^t \in M_{5/8} + 1$ . Under this constraint, it turns out there are no solutions of type ‘source’, but two of type ‘sink’:

$$(0, 1, 0, 0, 0) \cdot N_{\text{sink}}^t \mp (1, 0, 0, 0, 0) \cdot N_{\text{sink}}^t = \frac{4}{10},$$

$$(0, 0, 0, 0, 1) \cdot N_{\text{sink}}^t \pm (1, 0, 0, 0, 0) \cdot N_{\text{sink}}^t = \frac{46}{40}.$$

It also turns out that, for each type, two order-4 tuples – one simulacral, one auxiliary – emerge from this procedure, homogeneous for type ‘sink’, mixed for type ‘source’,

$$(\text{Sim}_{\text{sink}}^{(2,1)}) = (7 + 3, 18, 29, 43), \quad (\text{Sim}_{\text{source}}^{(5,1)}) = (10, 12, 19, 21 + 4),$$

$$(\text{Aux}_{\text{sink}}^{(2,1)}) = (2, 3, 4, 5), \quad (\text{Aux}_{\text{sink}}^{(5,1)}) = (20, 21, 22, 23),$$

where the superscripts in parentheses mark the places of elements before the confluence, and the auxiliary tuple gives the amplitude decomposition following the polite partition (staircase Young diagram) of the sum of the respective outcomes,

$$\begin{aligned} 4 + 10 &= 2 + 3 + 4 + 5, \\ 46 + 40 &= 20 + 21 + 22 + 23. \end{aligned}$$

The four multiple-type amplitudes 12, 21, 33 and 48 not involved in gap filling-in now have the following ‘projecting-out’ representation:

$11 :$ projection simulacra: $(0, 0, 1, 0) \cdot (\text{Sim}_{\text{sink}}^{(2,1)})^t$ $+ (0, 0, 1, 0) \cdot (\text{Aux}_{\text{sink}}^{(2,1)})^t = 33$ $(0, 1, 0, 0) \cdot (\text{Sim}_{\text{source}}^{(5,1)})^t$ $+ (0, 1, 0, 0) \cdot (\text{Aux}_{\text{sink}}^{(5,1)})^t = 33$	$12 :$ projection simulacra: $(0, 0, 0, 1) \cdot (\text{Sim}_{\text{sink}}^{(2,1)})^t$ $+ (0, 0, 0, 1) \cdot (\text{Aux}_{\text{sink}}^{(2,1)})^t = 48$ $(0, 0, 0, 1) \cdot (\text{Sim}_{\text{source}}^{(5,1)})^t$ $+ (0, 0, 0, 1) \cdot (\text{Aux}_{\text{sink}}^{(5,1)})^t = 48$
$6 :$ projection simulacrum: $(1, 0, 0, 0) \cdot (\text{Sim}_{\text{sink}}^{(2,1)})^t$ $+ (1, 0, 0, 0) \cdot (\text{Aux}_{\text{sink}}^{(2,1)})^t = 12$	$7 :$ projection simulacrum: $(0, 1, 0, 0) \cdot (\text{Sim}_{\text{sink}}^{(2,1)})^t$ $+ (0, 1, 0, 0) \cdot (\text{Aux}_{\text{sink}}^{(2,1)})^t = 21$

Since there are no projection simulacra of type ‘source’ in the lower tie, we register six simulacral representations in all. We may expect six simulacral representations to come out as well when, instead of merger, a deletion scenario is considered: Simple deletion of the  $x$ th element again yields quadruples,  $(\text{Sim}_{\text{source}}^{[x]})$  and  $(\text{Sim}_{\text{sink}}^{[x]})$ . With these constructions at hand, we now find that all of the four multiple-type amplitudes 12, 21, 33 and 48 are representable in  $\text{Bound}((\text{Sim}_{\text{source}}^{[2]}))$ , but only 21 and 33 in  $\text{Bound}((\text{Sim}_{\text{sink}}^{[x]}))$  ( $x = 3, 4, 5$ ), the asymmetry being due to the original non-representability of 12 and 48 in  $\text{Bound}(N_{\text{sink}})$  – which does persist after deletion of one of the basis elements. The ‘indecorous’ double strand, with multiples in  $(\text{Sim}_{\text{source}}^{[2]})$  and, say,  $(\text{Sim}_{\text{sink}}^{[5]})$  representation, then reads thus:

$$\begin{array}{ll}
 \begin{array}{l} 11 : \\ \text{partial R-field simulacrum:} \\ (0, 1, 0, 1) \cdot (\text{Sim}_{\text{source}}^{[2]})^t = 33 \end{array} & \begin{array}{l} 12 : \\ \text{R-spacetime simulacrum:} \\ (-1, 1, 1, 1) \cdot (\text{Sim}_{\text{source}}^{[2]})^t = 48 \end{array} \\
 \begin{array}{l} \text{partial spacetime simulacrum:} \\ (-1, 1, 0, 1) \cdot (\text{Sim}_{\text{sink}}^{[5]})^t = 33 \end{array} & \\
 \\[10pt]
 \begin{array}{l} 6 : \\ \text{projection simulacrum:} \\ (0, 1, 0, 0) \cdot (\text{Sim}_{\text{source}}^{[2]})^t = 12 \end{array} & \begin{array}{l} 7 : \\ \text{projection simulacrum:} \\ (0, 0, 0, 1) \cdot (\text{Sim}_{\text{source}}^{[2]})^t = 21 \\ \text{partial field simulacrum:} \\ (1, 0, 1, 0) \cdot (\text{Sim}_{\text{sink}}^{[5]})^t = 21 \end{array}
 \end{array}$$

Although the outcome is six simulacral representations in either scenario, merger and deletion, the multiples represented differ in detail, the reason being that two Young staircases are used in the former and only one in the latter – in the implicit form  $x = 2, 3, 4, 5$ . Apart from that difference, the scenarios are complementary to one another, in that ‘tied-to-type-sink’ merger and ‘tied-to-type-source’ deletion reliably identify the quartet 12, 21, 33, and 48.

One further complementarity applies lower tie-wise: in the first decorated double strand of this subsection, ‘projection’ simulacra apply to characteristic quantities; in the above double strand they apply to inexpedient (‘projecting-out’) multiples. But there is an unexpected and more profound side to this link between the two double strand representations, which is why we called the deletion-based double strand ‘indecorous’ – for the bottom end of the staircase (at  $x = 5$ ), the simulacra of type ‘sink’ are bound up with the setting familiar from the first decorated double strand of this subsection: the (partial) ‘field’ simulacrum is right-strand affine and the (partial) ‘spacetime’ simulacrum left-strand affine. In contrast, for the top end of the staircase (at  $x = 2$ ), laterally inverted assignment in simulacra of type ‘source’ manifests in the upper tie: the ‘spacetime’ simulacrum turns right-strand affine and the (partial) ‘field’ simulacrum left-strand affine (hence the marking by a prefix R- for reflection). The overall picture and especially the latter unexpected effect imply that Young staircases play an important part in the very foundations of particle creation and crotonic implementation involving gap filling-in.

## 8. Supplementary remarks and outlook

The effectiveness of 4-tuples, come to the fore with sign preserving co-amplitudes in the crotonic process of dimensional molding, may have seemed a bit mysterious, thus far. Mathematically, it owes its existence but to a plain two-stage degeneracy: first, whereas the number of basis elements of  $G_\rho^{(p)}$  ( $p = 15, 31, 63, \dots$ ) increase as 6, 18, 54, ..., the number of basis elements of  $J_\rho^{(p)}$  increase as 4, 18, 54, ... (for details see [Merkel]); second, only the first two elements of the basis  $J_\rho^{(15)} = (-5, 15, -43, 149)$  give rise to order-4 subgroups of the group of units of the quotient rings  $\mathbb{Z}/16\mathbb{Z}$  and  $\mathbb{Z}/64\mathbb{Z}$  (respectively formed by the powers of  $|-5|$ ,  $\{1, 5, 9, 13\}$ , and the powers of 15,  $\{1, 15, 33, 47\}$ ) whereas the remaining elements show quite regular behavior in forming subgroups of *distinct* higher order, *i.e.* powers of  $|-43|$  an order-16 subgroup, and powers of 149 an order-64 subgroup of the group of units of the quotient rings  $\mathbb{Z}/64\mathbb{Z}$  and  $\mathbb{Z}/256\mathbb{Z}$ , respectively. It's worth, globally and locally, panning to a synoptic perspective here on the two stages of degeneracy. As was mentioned in Sect. 2, on  $\Gamma$  – the 6-cube complex ensuing from  $(G_\rho^{(15)}) = (3, 5, 11, 17, 41, 113)$  – 170 out of 190 potentially attainable node labels are realized. On  $\chi$  – the 4-cube complex ensuing from  $J_\rho^{(15)} = (-5, 15, -43, 149)$  –, by contrast, out of 212 potentially attainable ones only 40 are realized. The gap between these numbers, 170–40, was shown (in Sect. 6) to be responsible for the Magnus equation's remarkable ability to account for the ratio  $F_e/F_g$ . Viewing the 172 values failing with  $\chi^{(15)}$  as that gap's uplift by  $C_5$  would be a complementary option (cf.  $C_5$ 's role in subsection 7.1). In view of this, it comes as no surprise that the respectively realized and non-realized node labels  $\leq 96$  on  $\Gamma$  and  $\chi$  correspond to multiples (to-be-projected-out ones in square brackets below) and characteristic numbers of the double strand:

11 :	12 :
multiples:	multiples:
$\Gamma \ni x \notin \chi$ ( $x = 22, 44, 66$ ),	$\Gamma \ni x \notin \chi$ ( $x = 24, 36$ ), $\Gamma \ni 96 \in \chi$ ,
$\Gamma \ni [33] \in \chi$	$\chi \ni [48] \notin \Gamma$
characteristic number:	characteristic number:
$\Gamma \ni 47 \notin \chi$	$\Gamma \ni 15 \in \chi$
6 :	7 :
multiples:	multiples:
$\Gamma \ni x \notin \chi$ ( $x = 6, 18, 24$ ),	$7 \notin \Gamma \cup \chi$ , $\Gamma \ni 14 \notin \chi$ , $\Gamma \ni 28 \in \chi$ ,
$\Gamma \ni [12] \notin \chi$	$\Gamma \ni [21] \notin \chi$
characteristic number:	characteristic number:
$\Gamma \ni 13 \notin \chi$	$\Gamma \ni 5 \in \chi$

Thirteen entries can be identified as node labels realized on  $\Gamma$  but not on  $\chi$  and five as node labels realized on both boundaries – numbers that coincide with the lower-tie characteristic quantities 13 and 5 and whose sum coincides with the number of basis elements in  $G_\rho^{(31)}$ . The rest are one entry each, one not

a label on either boundary and the other identifiable as a node label on  $\chi$  but not on  $\Gamma$ . Of the latter sort there are three more – 106, 164 and 172 – making up a number that matches with the number of basis elements in  $J_\rho^{(31)}$ . The first coincidence brings the number of basis elements of  $G_\rho^{(p)}$  into focus, which is given by the formula

$$2 \cdot 3^{\log_2(p+1)-3}, \quad M_{\text{reg}} \ni p > 7.$$

As was demonstrated in [Merkel], it can equivalently be expressed by an ansatz where two triangular matrices<sup>16</sup> with secondary symmetry, each with at most  $\frac{(q+1)(q+3)}{8}$  distinct entries, are cleaned from redundant entries:

$$2 \left( \frac{(q+1)(q+3)}{8} - s \right), \quad q = (p-3)/4. \quad (34)$$

For  $M_{\text{reg}} \ni p > 15$ , there is a nice twist about this: As the subtrahends  $s$  are keeping company with the units of  $\{1, 5, 9, 13\}$ ,<sup>17</sup> the expressions

$$2 \left( \frac{(q+1)(q+3)}{8} - 5^{\log_2 \frac{q+1}{8}} \right) \quad (35)$$

keep spitting out sums of characteristic quantities per tie – see the table below for their progression:

$p$	31	63	127	255	...
$2 \left( \frac{(q+1)(q+3)}{8} - 5^{\log_2 \frac{q+1}{8}} \right)$	18	62	222	806	...

So far we had:  $13 + 5 = 18$ ,  $47 + 15 = 62$  – if we wish to continue the double strand, we know in advance the next tie should come with the sum of characteristic quantities  $\xi + \zeta = 222$ . The determination of  $\xi$  and  $\zeta$  is straightforward. We may assume they are odd numbers, the left-strand affine lying in the interval  $]C_6, C_7[$  and being the minimum among the remainders  $(5 \cdot 2^n - 1 + 2^n) \bmod C_7$  ( $n \in \mathbb{N}$ ), and the right-strand affine in the interval  $]C_4, C_6[$  and minimal in  $(5 \cdot 2^n - 1 - 2^n) \bmod C_6$ . The left-strand affine's interval can be narrowed down further in that 222 serves as an upper bound:  $]C_6, 222[$ . Twenty out of sixty remainders are odd-numbered, and out of the latter seven match the interval  $]C_6, C_7[$ :

$$(191, (137, 149, 161, 143, 167, )215).$$

<sup>16</sup>  $(G_{\xi+(p+1)/4, \zeta})$  and  $(G_{\xi+(3p+3)/8, \zeta})$ ,  $\xi = 1, 2, \dots, (q+1)/2$ ,  $\zeta = 1, \dots, (q+3)/2 - \xi$ ,

<sup>17</sup> let  $\mathcal{L}_s$  be the set of numbers  $\lfloor \log_2(C_{q*}C_{2q*+1}) \rfloor > s$ , where  $q* \in M_{\text{reg}}$ . Then the least element  $l_{\min} \in \mathcal{L}_s$  is found to satisfy  $l_{\min} - s \equiv u \pmod{16}$  where  $u \in \{1, 5, 9, 13\}$ . For  $\frac{(q+1)(q+3)}{8} = 10$ ,  $s = 1$ , we find  $\lfloor \log_2(C_1C_3) \rfloor - s \equiv 1 \pmod{16}$ ; also for  $\frac{(q+1)(q+3)}{8} = 36$ ,  $s = 9$ ,  $\lfloor \log_2(C_3C_7) \rfloor - s \equiv 1 \pmod{16}$ ; the next instances are  $\frac{(q+1)(q+3)}{8} = 136$ ,  $s = 55$  with  $\lfloor \log_2(C_{15}C_{31}) \rfloor - s \equiv 5 \pmod{16}$ ,  $\frac{(q+1)(q+3)}{8} = 528$ ,  $s = 285$  with  $\lfloor \log_2(C_{63}C_{127}) \rfloor - s \equiv 9 \pmod{16}$ , and so on,

The parenthesising makes it clear: the minimum remainder search requires further constraining by  $2b'$ . That is, the left-strand and right-strand characteristic numbers must respectively be of the form

$$\begin{aligned}\xi &= \xi_0 + 2^{m_\xi} \\ \zeta &= \zeta_0 - 2^{m_\zeta}\end{aligned}\quad (m_\xi > m_\zeta; \xi_0, \zeta_0 \in M_{5/8}).$$

One possibility,  $(79 + 128) + (79 - 64)$ , fails because  $79 + 128$  is not among the above remainders, so the unique solution under this constraint is

$$\begin{aligned}\xi &= 191 = 159 + 32, \\ \zeta &= 31 = 39 - 8.\end{aligned}$$

The solution would be none at all if we could not confirm that the right-strand affine 31 is minimal among the remainders of  $(5 \cdot 2^n - 1 - 2^n) \bmod C_6$ . Again, a parenthesising signals caution: the apparent minimum – 15 for the interval  $]C_5, C_6[$  in the remainders

$$((7, 15, )31, 63, 127, 123, 115, 99, 65(, 3))$$

– is *not* available in being already in use as right-strand affine characteristic number, so 31 becomes the true minimum.

Next, we have to determine the  $t$ 's for the new tie. We have reason to believe that the observed inter-tie increment

$$t' = t + 5$$

is more than mere heuristics: While the twenty values not realizable on  $\Gamma$  – 7, 34, 48, 51, 62, 65, 79, 106, 120, 147, 161, 164, 172, 175, 178, 181, 183, 186, 188, 189 – are not without formation law, the formation law for the 40 values realizable on  $\chi$  is manifestly one of increase by 5: 5, 10, 15, 20; 23, 28, …, 63; 86, 91, …, 126; 129, 134, …, 169; 172, 177, …, 212. So we deduce 16 (= 11 + 5) and 17 (= 12 + 5) as new tie numbers.

The envisioned continuation furthermore demands (i) specifying the characteristic multiples,  $m_c$ , for the new tie numbers and (ii) finding, for them as well as for the new characteristic numbers 191 and 31, equivalents in terms of the units of the order-16 subgroup formed by powers of  $|-43|$  of the group of units of the quotient ring  $\mathbb{Z}/64\mathbb{Z}$ .

As regards (i), we simply assume an increase

$$m'_c = (m + 1)n_c(t + 5),$$

finding

$$\begin{aligned}3n_c \cdot 16 &= 144 \quad \text{for } n_c = 3, \\ 3n_c \cdot 17 &= 204 \quad \text{for } n_c = 4.\end{aligned}$$

Regarding (ii), we note that the sixteen units of the subgroup in question,

$$\{\bar{1}, 43, 57, \bar{19}, \bar{49}, 59, 41, 35, 33, \bar{11}, 25, \bar{51}, \bar{17}, 27, \bar{9}, \bar{3}\} \quad (\Sigma^{\text{sub}} = 480),$$

can be partitioned into two sequences of order 8,

$$(\text{Sim}_{64}^{\text{unbar}}) = (43, 57, 59, 41, 35, 33, 25, 27) \quad (\Sigma^{\text{unbar}} = 320),$$

$$(\text{Sim}_{64}^{\text{bar}}) = (\bar{1}, \bar{19}, \bar{49}, \bar{11}, \bar{51}, \bar{17}, \bar{9}, \bar{3}) \quad (\Sigma^{\text{bar}} = 160),$$

such that the sum of units each realizes  $M_{5/8} + 1$  – the unbarred units 320 and the barred ones 160, making up 480 in all. In order they form simulacral representations for the new tie, the very notion of simulacrum asks for generalization: A simulacrum is now termed ‘spacetime’ or ‘field’ if the number of unbarred units of  $(\text{Sim}_{64}^{\text{unbar}})$  used occupies the lower half of the staircase and a ‘projection’ simulacrum if it occupies the upper half:

‘projection’	1	$\bar{1} + 1$		
”	2	$\bar{2} + 1$		
‘field’		3	$\bar{3}$	
‘spacetime’		4		$\bar{4}$

The number of barred units of  $(\text{Sim}_{64}^{\text{bar}})$  used follows a similar pattern but reacts the switch of halves with unit step lags. The lags are an integral part of the generalization in that they correspond to the  $x = 0$  grades of the  $2^x$ -grading of halves and (halves of) partitions,

$$\begin{aligned} 1 &= (33 + 47)/l, & (33 + 47)/r &= 1, \\ 2 &= \Sigma^{\text{bar}}/l, & \Sigma^{\text{bar}}/r &= 2, \\ 4 &= \Sigma^{\text{unbar}}/l, & \Sigma^{\text{unbar}}/r &= 4, \end{aligned}$$

where  $l = \bar{1} + \bar{19} + \bar{49} + \bar{11}$  and  $r = \Sigma^{\text{bar}} - l$ . Subtract the  $x > 0$  grades whilst retaining the  $x = 0$  ones and you get the original numbers of units of  $(\text{Sim}_{64})$  or  $(\text{Sim}_{16})$  used:

‘projection’	1	$+\bar{1}+1-2 = 1$		
”	2	$+\bar{2}+1-4 = 1$		
‘field’		3	$+\bar{3}-2 = 4$	
‘spacetime’		4	$+\bar{4}-4 = 4$	

The enhanced, decorated double strand then reads

16 :

characteristic multiple  
 ('spacetime' simulacrum):  
 $(1, 1, -1, 1, 0, 0, 0, 0) \cdot (\text{Sim}_{64}^{\text{unbar}})^t$   
 $+(0, 0, 0, 0, 1, 1, -1, 1) \cdot (\text{Sim}_{64}^{\text{bar}})^t$   
 $= 144 (= 3n_c \cdot 16)$   
 characteristic quantity 159+32  
 ('projection' simulacrum):  
 $(0, 1, 1, 0, 0, 0, 0, 0) \cdot (\text{Sim}_{64}^{\text{unbar}})^t$   
 $+(0, 0, 1, 0, 0, 1, 1, 0) \cdot (\text{Sim}_{64}^{\text{bar}})^t = 191$   
 11 :  
 characteristic multiple  
 ('spacetime' simulacrum):  
 $(1, -1, 1, 1) \cdot (\text{Sim}_{64})^t = 66 (= 2n_c \cdot 11)$   
 characteristic quantity 39+8  
 ('projection' simulacrum):  
 $(0, 0, 0, 1) \cdot (\text{Sim}_{64})^t = 47$   
 6 :  
 characteristic multiple  
 ('spacetime' simulacrum):  
 $(1, -1, 1, 1) \cdot (\text{Sim}_{16})^t = 18 (= n_c \cdot 6)$   
 characteristic quantity 9+4  
 ('projection' simulacrum):  
 $(0, 0, 0, 1) \cdot (\text{Sim}_{16})^t = 13$

 $(n_c = 3)$ 

17 :

characteristic multiple  
 ('field' simulacrum):  
 $(0, 0, 0, 0, 1, 1, 1, 0) \cdot (\text{Sim}_{64}^{\text{unbar}})^t$   
 $+(0, 0, 1, 1, 1, 0, 0, 0) \cdot (\text{Sim}_{64}^{\text{bar}})^t$   
 $= 204 (= 3n_c \cdot 17)$   
 characteristic quantity 39-8  
 ('projection' simulacrum):  
 $(0, 0, 0, 0, 0, 0, 0, 1) \cdot (\text{Sim}_{64}^{\text{unbar}})^t$   
 $+(1, 0, 0, 0, 0, 0, 0, 1) \cdot (\text{Sim}_{64}^{\text{bar}})^t = 31$   
 12 :  
 characteristic multiple  
 ('field' simulacrum):  
 $(1, 1, 1, 1) \cdot (\text{Sim}_{64})^t = 96 (= 2n_c \cdot 12)$   
 characteristic quantity 19-4  
 ('projection' simulacrum):  
 $(0, 1, 0, 0) \cdot (\text{Sim}_{64})^t = 15$   
 7 :  
 characteristic multiple  
 ('field' simulacrum):  
 $(1, 1, 1, 1) \cdot (\text{Sim}_{16})^t = 28 (= n_c \cdot 7)$   
 characteristic quantity 9-4  
 ('projection' simulacrum):  
 $(0, 1, 0, 0) \cdot (\text{Sim}_{16})^t = 5$

 $(n_c = 4)$ 

The construction of one more tie on top of the above, with hypothetical tie numbers 21 and 22, could proceed along similar lines. It would involve the units of the order-64 subgroup formed by powers of 149 of the group of units of the quotient ring  $\mathbb{Z}/256\mathbb{Z}$ . However, kissing numbers with index  $> 100$ , whose pivots of local CFR representation origin an enhanced double strand might be a suitable study tool for, are definitely out of reach presently. For kissing numbers with index  $\ll 100$ , the ur-double strand should suffice.

With such prospects, the interplay between local and global CFR-represented pivots and how their carrier Mersenne fluctuations assemble in qphyla becomes a field of study worth aspiring to. Regarding 'sink' dimension 18, we came upon the specific, alloqphyletic condition under which a local pivot snaps into global pivots (see Tables 11 and 12). It would be interesting to find out if this is true of 'source' and 'sink' dimensions alike.

## Appendix A. Crotons on the boundary

Bases of order-31 croton base numbers pop up as a by-product of the matrix constructions  $\mathbf{f}^{(31)} = \mathbf{1}^{\otimes 4} \otimes \mathbf{b}^{(1)} + (G_{\mu\nu}^{(31)}) \otimes c_3$  and  $\mathbf{h}^{(31)} = \mathbf{1}^{\otimes 4} \otimes \mathbf{b}^{(1)} + (J_{\mu\nu}^{(31)}) \otimes c_2$  (for more details of the construction, see [Merkel]). Not all of the matrix elements  $G_{\mu\nu}^{(31)}$  and  $J_{\mu\nu}^{(31)}$  need to be considered because the subquadrants  $UL(LL(\cdot)) = LL(UL(\cdot)) = LL(LR(\cdot))$  just reproduce order-15 croton base numbers. As shown in Fig. A.8, order-31 croton base numbers can be extracted from the non-UR( $LL(\cdot)$ ) parts of quadrants  $LL(G_{\mu\nu}^{(31)})$  and  $LL(J_{\mu\nu}^{(31)})$ :

Figure A.8: Order-31 croton base numbers extracted from matrices of  $\mathbf{f}^{(31)}$  and  $\mathbf{h}^{(31)}$

$$\begin{aligned} LL(G_{\mu\nu}^{(31)}) &= \\ \left( \begin{array}{cccc|cc|cc} \underline{429} & 155 & 43 & 19 & \underline{5} & 3 & \underline{1} & 1 \\ 1275 & \underline{429} & 115 & 43 & 11 & \underline{5} & 1 & \underline{1} \\ 4819 & 1595 & \underline{429} & 155 & 41 & 17 & \underline{5} & 3 \\ 15067 & 4819 & 1275 & \underline{429} & 113 & 41 & 11 & \underline{5} \\ 58781 & 18627 & 4905 & 1633 & \underline{429} & 155 & 43 & 19 \\ 189371 & 58781 & 15297 & 4905 & 1275 & \underline{429} & 115 & 43 \\ 737953 & 227089 & 58781 & 18627 & 4819 & 1595 & \underline{429} & 155 \\ 2430289 & 737953 & 189371 & 58781 & 15067 & 4819 & 1275 & \underline{429} \end{array} \right) \\ LL(J_{\mu\nu}^{(31)}) &= \\ \left( \begin{array}{cccc|cc|cc} -\underline{429} & 117 & -41 & 13 & -\underline{5} & 1 & -\underline{1} & 1 \\ 1547 & -\underline{429} & 143 & -41 & 15 & -\underline{5} & 3 & -\underline{1} \\ -4903 & 1343 & -\underline{429} & 117 & -43 & 15 & -\underline{5} & 1 \\ 18269 & -4903 & 1547 & -429 & 149 & -43 & 15 & -\underline{5} \\ -58791 & 15547 & -4823 & 1319 & -429 & 117 & 41 & 13 \\ 223573 & -58791 & 17989 & -4823 & 1547 & -429 & 143 & -41 \\ -747765 & 194993 & -58791 & 15547 & -4903 & 1343 & -\underline{429} & 117 \\ 2886235 & -747765 & 223573 & -58791 & 18269 & -4903 & 1547 & -\underline{429} \end{array} \right) \end{aligned}$$

Outcomes are the 18-tuples

$$(G_{\rho}^{(31)}) = (19, 43, 115, 155, \underline{429}, 1275, 1595, 1633, 4819, 4905, 15067, 15297, 18627, 58781, 189371, 227089, 737953, 2430289)$$

and

$$(J_{\rho}^{(31)}) = (13, -41, 117, 143, -\underline{429}, 1319, 1343, 1547, -4823, -4903, 15547, 17989, 18269, -58791, 194993, 223573, -747765, 2886235),$$

from which the outer nodes of 18-cube complexes with boundary labels  $\Gamma_x$  and  $\chi_x$  respectively can be formed. Croton amplitudes and phases in the volume,  $\varphi_\alpha^{(n)}, \psi_\alpha^{(n)}$  ( $n \lesssim 3030, \alpha \leq 499$ ), corresponding to labels are given in the order the croton data occurred in the text.

Fig. 1, Mersenne fluctuation  $\Gamma$ -encoded:

$$\begin{aligned}
\varphi_{336}^{(206)} &= 13 = (0, 0, -1, 1, -1, -1, -1, 0, 1, 0, 0, 0, 0, 0, 0, 0, 0, 0) \cdot (G^{(31)})^t \\
\psi_{384}^{(207)} &= -14 = (0, -1, 1, 0, 0, 0, 0, 0, 1, -1, 0, 0, 0, 0, 0, 0, 0, 0) \cdot (G^{(31)})^t \\
\varphi_{326}^{(207)} &= \psi_{363}^{(207)} = 27 = (-1, 0, -1, 0, 1, 0, 1, -1, 0, 0, 1, -1, 0, 0, 0, 0, 0, 0) \cdot (G^{(31)})^t \\
\varphi_{338}^{(208)} &= 56 = (1, 1, -1, 0, 1, 1, -1, 0, 0, 0, 0, 0, 0, 0, 0, 0, 0, 0) \cdot (G^{(31)})^t \\
\psi_{372}^{(208)} &= -57 = (0, 1, -1, 0, -1, -1, 0, 1, -1, 1, 0, 0, 0, 0, 0, 0, 0, 0) \cdot (G^{(31)})^t \\
\varphi_{344}^{(209)} &= \psi_{359}^{(209)} = 114 = (0, 1, 0, 0, 1, 1, 0, -1, 0, 0, 0, 0, 0, 0, 0, 0, 0, 0) \cdot (G^{(31)})^t \\
\varphi_{338}^{(210)} &= 228 = (0, 0, -1, 0, 1, 0, 0, 1, -1, 0, 0, 0, 0, 0, 0, 0, 0, 0) \cdot (G^{(31)})^t \\
\psi_{380}^{(210)} &= -229 = (0, -1, -1, 0, -1, -1, 0, 1, 0, 0, 0, 0, 0, 0, 0, 0, 0, 0) \cdot (G^{(31)})^t \\
\varphi_{366}^{(211)} &= 458 = (0, 0, 1, 0, 1, 0, 0, 1, -1, 0, 0, 0, 0, 0, 0, 0, 0, 0) \cdot (G^{(31)})^t \\
\psi_{356}^{(211)} &= -459 = (1, 0, -1, 1, 1, 0, 0, 0, 1, 0, 0, 1, 0, -1, -1, 1, 0, 0) \cdot (G^{(31)})^t \\
\varphi_{352}^{(212)} &= \psi_{371}^{(212)} = 918 = (0, 1, 1, 0, -1, 1, 0, 0, 1, -1, 0, 0, 0, 0, 0, 0, 0, 0) \cdot (G^{(31)})^t \\
\varphi_{362}^{(213)} &= \psi_{375}^{(213)} = 459 = (-1, 0, 1, -1, -1, 0, 0, -1, 0, 0, -1, 0, 1, 1, -1, 0, 0) \cdot (G^{(31)})^t \\
\varphi_{350}^{(214)} &= \psi_{363}^{(214)} = 229 = (0, 1, 1, 0, 1, 1, 0, -1, 0, 0, 0, 0, 0, 0, 0, 0, 0, 0) \cdot (G^{(31)})^t \\
\varphi_{328}^{(215)} &= \psi_{371}^{(215)} = 114 = (0, 1, 0, 0, 1, 1, 0, -1, 0, 0, 0, 0, 0, 0, 0, 0, 0, 0) \cdot (G^{(31)})^t \\
\varphi_{336}^{(216)} &= 56 = (1, 1, -1, 0, 1, 1, -1, 0, 0, 0, 0, 0, 0, 0, 0, 0, 0, 0) \cdot (G^{(31)})^t \\
\psi_{351}^{(216)} &= 57 = (0, -1, 1, 0, 1, 1, 0, -1, 1, -1, 0, 0, 0, 0, 0, 0, 0, 0) \cdot (G^{(31)})^t \\
\varphi_{328}^{(217)} &= \psi_{343}^{(217)} = 28 = (0, -1, 0, 0, 1, 1, 0, -1, 0, 0, 0, 0, 0, 0, 0, 0, 0, 0) \cdot (G^{(31)})^t \\
\varphi_{324}^{(218)} &= 14 = (0, 1, -1, 0, 0, 0, 0, -1, 1, 0, 0, 0, 0, 0, 0, 0, 0, 0) \cdot (G^{(31)})^t \\
\psi_{391}^{(218)} &= 15 = (-1, -1, 1, 0, 0, 0, 1, -1, 0, 0, 0, 0, 0, 0, 0, 0, 0, 0) \cdot (G^{(31)})^t
\end{aligned}$$

Fig. 1, Mersenne fluctuation  $\chi$ -encoded:

$$\begin{aligned}
\varphi_{336}^{(206)} &= 13 = (1, 0, 0, 0, 0, 0, 0, 0, 0, 0, 0, 0, 0, 0, 0, 0, 0, 0) \cdot (J^{(31)})^t \\
\psi_{384}^{(207)} &= -14 = (1, 0, 1, 0, 0, -1, 0, -1, 0, 0, -1, 0, 1, 0, 0, 0, 0, 0) \cdot (J^{(31)})^t \\
\varphi_{326}^{(207)} &= \varphi_{363}^{(207)} = 27 = (0, 0, -1, 0, 0, 1, 0, 1, 0, 0, 1, 0, -1, 0, 0, 0, 0, 0) \cdot (J^{(31)})^t \\
\varphi_{338}^{(208)} &= 56 = (0, 0, 1, 1, 0, 0, 1, -1, 0, 0, 0, 0, 0, 0, 0, 0, 0, 0) \cdot (J^{(31)})^t \\
\psi_{372}^{(208)} &= -57 = (-1, 1, 0, -1, 0, -1, 0, 1, -1, -1, 0, 1, 0, 0, 0, 0, 0, 0) \cdot (J^{(31)})^t \\
\varphi_{344}^{(209)} &= \varphi_{359}^{(209)} = 114 = (1, 1, 1, -1, 0, 0, 1, 1, 0, 0, 1, 0, -1, 0, 0, 0, 0, 0) \cdot (J^{(31)})^t \\
\varphi_{338}^{(210)} &= 228 = (1, 0, 1, 1, 0, 0, -1, 0, 0, -1, -1, 0, -1, -1, 1, 0, 0) \cdot (J^{(31)})^t \\
\psi_{380}^{(210)} &= -229 = (1, 1, 0, 0, 1, -1, 0, 1, 0, 0, 0, 0, 0, 0, 0, 0, 0, 0) \cdot (J^{(31)})^t \\
\varphi_{366}^{(211)} &= 458 = (1, 0, 1, 1, 1, -1, -1, -1, 0, 0, 0, 0, 0, 0, 0, 0, 0, 0) \cdot (J^{(31)})^t \\
\psi_{356}^{(211)} &= -459 = (1, 1, 1, -1, 1, -1, 1, 0, 0, 0, 0, 0, 0, 0, 0, 0, 0, 0) \cdot (J^{(31)})^t \\
\varphi_{352}^{(212)} &= \psi_{371}^{(212)} = 918 = (0, 1, 0, 0, 0, 1, 0, 0, -1, 1, 0, 1, -1, 0, 0, 0, 0, 0) \cdot (J^{(31)})^t
\end{aligned}$$

Fig. 4, pivot  $\Gamma$ -encoded:

$$\begin{aligned}
\varphi_{448}^{(1556)} &= \psi_{441}^{(1556)} = 1304 = (0, 0, -1, 0, 0, 1, 0, 1, -1, 0, 0, -1, 1, 0, 0, 0, 0, 0) \cdot (G^{(31)})^t \\
\varphi_{442}^{(1557)} &= 2609 = (-1, -1, 0, 0, -1, 1, 1, 0, 0, 0, -1, 1, 0, 0, 0, 0, 0, 0) \cdot (G^{(31)})^t \\
\psi_{413}^{(1557)} &= 2610 = (0, -1, 1, 1, 0, 0, 0, 0, 1, 0, 0, 0, 1, -1, -1, 1, 0, 0) \cdot (G^{(31)})^t \\
\varphi_{401}^{(1558)} &= 5219 = (0, 0, 1, 0, 1, 0, 0, 0, 0, 1, 1, -1, 0, 0, 0, 0, 0, 0) \cdot (G^{(31)})^t \\
\psi_{430}^{(1558)} &= -5220 = (-1, 0, 0, 0, 0, 1, 1, 1, -1, 1, 1, 1, -1, 0, 0, 0, 0, 0) \cdot (G^{(31)})^t \\
\varphi_{407}^{(1559)} &= 2609 = (-1, -1, 0, 0, -1, 1, 1, 0, 0, 0, -1, 1, 0, 0, 0, 0, 0, 0) \cdot (G^{(31)})^t \\
\psi_{430}^{(1559)} &= -2610 = (0, 1, -1, -1, 0, 0, 0, 0, -1, 0, 0, 0, -1, 1, 1, -1, 0, 0) \cdot (G^{(31)})^t
\end{aligned}$$

Fig. 4, pivot  $\chi$ -encoded:

$$\begin{aligned}
\varphi_{448}^{(1556)} &= \psi_{441}^{(1556)} = 1304 = (0, -1, 0, 0, 0, 0, 1, 0, -1, 1, 0, 0, 0, 0, 0, 0, 0, 0, 0, 0) \cdot (J^{(31)})^t \\
\varphi_{442}^{(1557)} &= 2609 = (-1, 0, 1, 1, -1, 0, -1, -1, -1, 0, 0, 0, 0, 0, 0, 0, 0, 0, 0) \cdot (J^{(31)})^t \\
\psi_{413}^{(1557)} &= 2610 = (0, 0, 0, 0, 0, 0, 1, 1, 0, 0, 0, 1, -1, 0, 0, 0, 0, 0, 0) \cdot (J^{(31)})^t \\
\varphi_{401}^{(1558)} &= 5219 = (-1, 0, 0, 0, 1, 0, -1, 0, -1, -1, 1, 0, -1, 0, 0, 0, 0, 0) \cdot (J^{(31)})^t \\
\psi_{430}^{(1558)} &= -5220 = (1, 0, -1, -1, 0, 0, -1, -1, 0, -1, 1, 1, 1, 1, 0, 0, 0, 0) \cdot (J^{(31)})^t \\
\varphi_{407}^{(1559)} &= 2609 = (-1, 0, 1, 1, -1, 0, -1, -1, -1, 0, 0, 0, 0, 0, 0, 0, 0, 0) \cdot (J^{(31)})^t \\
\psi_{430}^{(1559)} &= -2610 = (0, 0, 0, 0, 0, 0, -1, -1, 0, 0, 0, -1, 1, 0, 0, 0, 0, 0) \cdot (J^{(31)})^t
\end{aligned}$$

Fig. 4, residue 2  $\Gamma$ -encoded

Fig. 4, residue 2  $\chi$ -encoded:

$$\begin{aligned}
\varphi_{427}^{(1556)} &= 103 = (1, 1, 0, -1, 1, 1, 0, 1, -1, 0, 1, 1, 1, 0, 0, 0, 0, 0) \cdot (J^{(31)})^t \\
\varphi_{380}^{(1557)} &= \varphi_{403}^{(1557)} = 205 = (0, 0, 0, 0, 1, 0, 0, -1, 0, -1, 1, 0, -1, 0, 0, 0, 0, 0) \cdot (J^{(31)})^t \\
\varphi_{390}^{(1558)} &= \varphi_{423}^{(1558)} = 411 = (0, 0, 0, -1, 0, 0, 0, -1, -1, 0, 1, 0, -1, 0, 0, 0, 0, 0) \cdot (J^{(31)})^t \\
\varphi_{398}^{(1559)} &= \varphi_{419}^{(1559)} = 205 = (0, 0, 0, 0, 1, 0, 0, -1, 0, -1, 1, 0, -1, 0, 0, 0, 0, 0) \cdot (J^{(31)})^t
\end{aligned}$$

Fig. 4, residue 1  $\Gamma$ -encoded:

$$\begin{aligned}
\varphi_{406}^{(1556)} &= 100 = (1, 1, 0, 0, 0, 0, -1, 1, 0, 0, 0, 0, 0, 0, 0, 0, 0, 0) \cdot (G^{(31)})^t \\
\varphi_{428}^{(1556)} &= -101 = (0, 1, 0, 0, 0, 0, 0, -1, 1, 0, 0, 1, -1, 0, 0, 0, 0, 0) \cdot (G^{(31)})^t \\
\varphi_{382}^{(1557)} &= 49 = (0, 1, 1, 0, -1, -1, 1, 0, 0, 0, 0, 0, 0, 0, 0, 0, 0, 0) \cdot (G^{(31)})^t \\
\varphi_{404}^{(1557)} &= -50 = (1, 0, 0, -1, 0, 0, 0, 0, -1, 1, 0, 0, 0, 0, 0, 0, 0, 0) \cdot (G^{(31)})^t \\
\varphi_{392}^{(1558)} &= 24 = (-1, 1, 0, 0, 0, 0, 0, 0, 0, 0, 0, 0, 0, 0, 0, 0, 0, 0) \cdot (G^{(31)})^t \\
\varphi_{424}^{(1558)} &= -25 = (-1, 0, 0, 1, -1, 0, -1, 1, 0, 0, -1, 1, 0, 0, 0, 0, 0, 0) \cdot (G^{(31)})^t \\
\varphi_{400}^{(1559)} &= \varphi_{423}^{(1559)} = 12 = (0, 1, 0, 0, 1, 1, 1, 0, 0, 0, 0, 1, -1, 0, 0, 0, 0, 0) \cdot (G^{(31)})^t
\end{aligned}$$

Fig. 4, residue 1  $\chi$ -encoded:

$$\begin{aligned}
\varphi_{406}^{(1556)} &= 100 = (1, 0, -1, 0, 0, 0, -1, 1, 0, 0, 0, 0, 0, 0, 0, 0, 0, 0) \cdot (J^{(31)})^t \\
\varphi_{428}^{(1556)} &= -101 = (0, 0, 0, 0, 0, -1, 0, 0, -1, 0, -1, -1, 1, -1, 0, 0) \cdot (J^{(31)})^t \\
\varphi_{382}^{(1557)} &= 49 = (1, -1, 0, 1, 0, 1, 0, -1, 1, -1, 0, 0, 0, 0, 0, 0, 0, 0) \cdot (J^{(31)})^t \\
\varphi_{404}^{(1557)} &= -50 = (0, 0, 1, -1, 0, 1, -1, 0, 0, 0, 0, 0, 0, 0, 0, 0, 0, 0) \cdot (J^{(31)})^t \\
\varphi_{392}^{(1558)} &= 24 = (-1, 0, 1, 0, 0, 0, 0, 0, -1, 1, 0, 0, 0, 0, 0, 0, 0, 0) \cdot (J^{(31)})^t \\
\varphi_{424}^{(1558)} &= -25 = (1, 0, -1, 0, 1, -1, 0, 1, 0, 0, -1, 1, 0, 0, 0, 0, 0) \cdot (J^{(31)})^t \\
\varphi_{400}^{(1559)} &= \varphi_{423}^{(1559)} = 12 = (-1, -1, 0, 1, -1, 1, 0, -1, -1, 1, 0, 1, -1, 0, 0, 0, 0, 0) \cdot (J^{(31)})^t
\end{aligned}$$

Fig. 5, Table 2, pivot  $\Gamma$ -encoded:

$$\begin{aligned}
\varphi_{448}^{(1003)} &= 51919 = (-1, 0, 0, 0, -1, 0, -1, 0, 0, 0, 0, 1, 0, 0, 0, 0) \cdot (G^{(31)})^t \\
\varphi_{468}^{(1003)} &= -51920 = (1, -1, 0, 1, 0, 0, 1, 0, 0, 1, -1, 1, 0, -1, 0, 0, 0, 0) \cdot (G^{(31)})^t \\
\varphi_{442}^{(1004)} &= \varphi_{464}^{(1004)} = 103839 = (1, 1, -1, 1, -1, 0, 0, -1, -1, -1, -1, 0, 0, -1, 1, 0, 0, 0) \cdot (G^{(31)})^t \\
\varphi_{438}^{(1005)} &= \varphi_{443}^{(1005)} = 207679 = (1, 0, -1, 0, 1, 1, 0, 1, 0, 0, 1, 0, 0, 0, 1, 0, 0, 0) \cdot (G^{(31)})^t \\
\varphi_{449}^{(1006)} &= \varphi_{447}^{(1006)} = 103839 = (1, 1, -1, 1, -1, 0, 0, -1, -1, -1, -1, 0, 0, -1, 1, 0, 0, 0) \cdot (G^{(31)})^t
\end{aligned}$$

Fig. 5, Table 2, pivot  $\chi$ -encoded:

$$\begin{aligned}
\varphi_{448}^{(1003)} &= 51919 = (-1, 1, 0, -1, 1, 0, -1, 0, 0, 1, 0, 0, 0, -1, 0, 0, 0, 0) \cdot (J^{(31)})^t \\
\varphi_{468}^{(1003)} &= -51920 = (1, 1, -1, -1, -1, 0, 0, 1, 0, -1, 0, -1, 1, 1, 0, 0, 0, 0) \cdot (J^{(31)})^t
\end{aligned}$$

$$\begin{aligned}
\varphi_{442}^{(1004)} &= \psi_{464}^{(1004)} = 103839 = (0, 0, -1, 1, 0, 0, 0, -1, 0, 0, 0, 1, 0, -1, -1, 1, 0, 0) \cdot \\
&\quad (J^{(31)})^t \\
\varphi_{438}^{(1005)} &= \psi_{443}^{(1005)} = 207679 = (1, 0, 0, 0, -1, 0, -1, -1, -1, 0, 0, 0, -1, 0, 0, 1, 0, 0) \cdot \\
&\quad (J^{(31)})^t \\
\varphi_{449}^{(1006)} &= \psi_{447}^{(1006)} = 103839 = (0, 0, -1, 1, 0, 0, 0, -1, 0, 0, 0, 1, 0, -1, -1, 1, 0, 0) \cdot \\
&\quad (J^{(31)})^t
\end{aligned}$$

Fig. 5, Table 2, residue 2  $\Gamma$ -encoded:

$$\begin{aligned}
\varphi_{448}^{(1003)} &= 193 = (0, 0, 0, 1, 0, 0, -1, 1, 0, 0, 0, 0, 0, 0, 0, 0, 0, 0) \cdot (G^{(31)})^t \\
\psi_{469}^{(1003)} &= 194 = (1, 0, 0, 0, 1, 1, -1, 0, -1, -1, -1, -1, 1, 0, 0, 0, 0) \cdot (G^{(31)})^t \\
\varphi_{443}^{(1004)} &= \psi_{465}^{(1004)} = 96 = (-1, 0, 1, 0, 0, 0, 0, 0, 0, 0, 0, 0, 0, 0, 0, 0, 0, 0) \cdot (G^{(31)})^t \\
\varphi_{443}^{(1005)} &= \psi_{465}^{(1005)} = 48 = (0, 0, 0, 0, 0, 0, 1, -1, -1, 1, 0, 0, 0, 0, 0, 0, 0, 0) \cdot (G^{(31)})^t \\
\varphi_{427}^{(1006)} &= 23 = (0, -1, 0, 0, 0, 0, 0, -1, -1, -1, -1, 1, 0, 0, 0, 0) \cdot (G^{(31)})^t \\
\psi_{449}^{(1006)} &= 24 = (-1, 1, 0, 0, 0, 0, 0, 0, 0, 0, 0, 0, 0, 0, 0, 0, 0, 0) \cdot (G^{(31)})^t
\end{aligned}$$

Fig. 5, Table 2, residue 2  $\chi$ -encoded:

$$\begin{aligned}
\varphi_{448}^{(1003)} &= 193 = (-1, -1, 0, -1, 0, -1, 0, 1, 1, -1, 0, 0, 0, 0, 0, 0, 0, 0) \cdot (J^{(31)})^t \\
\psi_{469}^{(1003)} &= 194 = (1, 0, 1, 1, -1, 1, 0, -1, 0, 0, 0, 1, -1, 0, 0, 0, 0, 0) \cdot (J^{(31)})^t \\
\varphi_{443}^{(1004)} &= \psi_{465}^{(1004)} = 96 = (-1, -1, -1, 0, 1, -1, -1, -1, -1, 0, 0, 0, 0, 0, 0, 0, 0, 0) \cdot \\
&\quad (J^{(31)})^t \\
\varphi_{443}^{(1005)} &= \psi_{465}^{(1005)} = 48 = (0, 1, -1, -1, 0, 0, 0, -1, 1, 0, 0, 0, 0, 0, 0, 0, 0, 0) \cdot (J^{(31)})^t \\
\varphi_{427}^{(1006)} &= 23 = (1, 1, -1, -1, 1, 0, -1, 0, 0, 1, -1, -1, -1, -1, 0, 0, 0, 0) \cdot (J^{(31)})^t \\
\psi_{449}^{(1006)} &= 24 = (0, 0, 0, 0, -1, 1, 0, 0, 0, 0, 0, 0, 0, 0, 0, 0, 0, 0) \cdot (J^{(31)})^t
\end{aligned}$$

Fig. 5, residue 1  $\Gamma$ -encoded:

$$\begin{aligned}
\varphi_{479}^{(1003)} &= 58 = (-1, 0, 1, 0, 0, 0, 1, -1, 0, 0, 0, 0, 0, 0, 0, 0, 0, 0) \cdot (G^{(31)})^t \\
\varphi_{477}^{(1004)} &= 117 = (0, 0, 0, 1, 0, 0, 0, 1, -1, 0, 0, 0, 0, 0, 0, 0, 0, 0) \cdot (G^{(31)})^t \\
\varphi_{465}^{(1005)} &= \psi_{477}^{(1005)} = 58 = (-1, 0, 1, 0, 0, 0, 1, -1, 0, 0, 0, 0, 0, 0, 0, 0, 0, 0) \cdot (G^{(31)})^t \\
\varphi_{449}^{(1006)} &= 29 = (0, 0, 1, 0, 0, 0, 0, 0, 1, -1, 0, 0, 0, 0, 0, 0, 0, 0) \cdot (G^{(31)})^t \\
\psi_{473}^{(1006)} &= 30 = (0, 1, -1, 0, 0, 0, -1, -1, 0, 0, 0, -1, 1, 0, 0, 0, 0, 0) \cdot (G^{(31)})^t
\end{aligned}$$

Fig. 5, residue 1  $\chi$ -encoded:

$$\begin{aligned}
\varphi_{479}^{(1003)} &= 58 = (-1, -1, 1, -1, 0, 1, -1, 0, 1, -1, 0, 0, 0, 0, 0, 0, 0, 0) \cdot (J^{(31)})^t \\
\varphi_{477}^{(1004)} &= 117 = (0, 0, 1, 0, 0, 0, 0, 0, 0, 0, 0, 0, 0, 0, 0, 0, 0, 0) \cdot (J^{(31)})^t \\
\varphi_{465}^{(1005)} &= \psi_{477}^{(1005)} = 58 = (-1, -1, 1, -1, 0, 1, -1, 0, 1, -1, 0, 0, 0, 0, 0, 0, 0, 0) \cdot \\
&\quad (J^{(31)})^t
\end{aligned}$$

$$\begin{aligned}\varphi_{449}^{(1006)} &= 29 = (1, -1, 1, 1, 1, 0, 1, 0, 0, 1, 0, -1, 0, 0, 0, 0, 0) \cdot (J^{(31)})^t \\ \psi_{473}^{(1006)} &= 30 = (0, 0, 1, -1, 0, 1, -1, 0, 1, -1, 0, 0, 0, 0, 0, 0, 0) \cdot (J^{(31)})^t\end{aligned}$$

Fig. 6, Table 1, leggy pivot  $\Gamma$ -encoded:

$$\begin{aligned}\varphi_{407}^{(987)} &= \psi_{437}^{(987)} = 12977 = (0, 0, -1, 0, 0, 0, -1, 1, 1, 1, 0, -1, 1, 0, 0, 0, 0, 0) \cdot (G^{(31)})^t \\ \varphi_{411}^{(988)} &= 25955 = (0, 0, -1, -1, -1, 0, 0, 1, 1, 1, 0, 1, 0, 0, 0, 0, 0, 0) \cdot (G^{(31)})^t \\ \varphi_{418}^{(988)} &= 25956 = (0, 0, 0, -1, 0, -1, 0, -1, 0, -1, 0, 1, 1, 0, 0, 0, 0, 0) \cdot (G^{(31)})^t \\ \varphi_{397}^{(989)} &= \psi_{449}^{(989)} = 51911 = (-1, -1, -1, 0, 0, 0, -1, 0, -1, 0, 0, 0, 1, 0, 0, 0, 0) \cdot \\ (G^{(31)})^t \varphi_{433}^{(990)} &= 103823 = (-1, -1, -1, 1, -1, 1, 1, 0, 0, 1, 0, 0, 1, -1, 1, 0, 0) \cdot \\ (G^{(31)})^t \psi_{441}^{(990)} &= 103824 = (0, -1, -1, 1, -1, 1, -1, -1, -1, 0, -1, 0, -1, 1, 0, 0, 0) \cdot \\ (G^{(31)})^t \varphi_{417}^{(991)} &= 207646 = (-1, 1, 0, 1, -1, 0, 1, 1, 0, 0, 0, 1, 0, 0, 1, 0, 0, 0) \cdot (G^{(31)})^t \\ \psi_{457}^{(991)} &= 207647 = (1, 0, 0, -1, -1, -1, 0, 0, 1, 0, 0, 1, 0, 0, 1, 0, 0, 0) \cdot (G^{(31)})^t \\ \varphi_{421}^{(992)} &= \psi_{469}^{(992)} = 415294 = (0, 0, 0, 0, 1, 0, -1, 0, 0, 0, 0, 0, 0, 0, 1, 1, 0, 0) \cdot (G^{(31)})^t \\ \psi_{423}^{(993)} &= \psi_{473}^{(993)} = 207647 = (1, 0, 0, -1, -1, 0, 0, 1, 0, 0, 1, 0, 0, 1, 0, 0, 0) \cdot \\ (G^{(31)})^t \varphi_{443}^{(994)} &= \psi_{475}^{(994)} = 103823 = (-1, -1, -1, 1, -1, 1, 1, 0, 0, 1, 0, 0, 1, -1, 1, 0, 0) \cdot \\ (G^{(31)})^t \varphi_{425}^{(995)} &= 51911 = (-1, -1, -1, 0, 0, 0, -1, 0, -1, 0, 0, 0, 1, 0, 0, 0, 0, 0) \cdot (G^{(31)})^t \\ \psi_{453}^{(995)} &= 51912 = (1, -1, -1, 0, 0, 0, -1, 0, 0, -1, 1, -1, 0, 1, 0, 0, 0, 0) \cdot (G^{(31)})^t \\ \varphi_{431}^{(996)} &= \psi_{477}^{(996)} = 25955 = (0, 0, -1, -1, 0, 0, 1, 1, 1, 0, 1, 0, 0, 0, 0, 0) \cdot (G^{(31)})^t \\ \varphi_{439}^{(997)} &= 12977 = (0, 0, -1, 0, 0, 0, -1, 1, 1, 1, 0, -1, 1, 0, 0, 0, 0, 0) \cdot (G^{(31)})^t \\ \psi_{469}^{(997)} &= 12978 = (1, -1, -1, 1, 1, -1, 0, 0, -1, 0, 0, 0, 1, 0, 0, 0, 0, 0) \cdot (G^{(31)})^t\end{aligned}$$

Fig. 6, Table 1, leggy pivot  $\chi$ -encoded:

$$\begin{aligned}\varphi_{407}^{(987)} &= \psi_{437}^{(987)} = 12977 = (1, 0, -1, 0, -1, 0, -1, 1, -1, -1, 0, 1, 0, 0, 0, 0, 0) \cdot \\ (J^{(31)})^t \varphi_{411}^{(988)} &= 25955 = (-1, -1, -1, 1, 0, 1, 0, -1, -1, 1, 0, 0, 0, 0, 0, 0, 0) \cdot (J^{(31)})^t \\ \varphi_{418}^{(988)} &= 25956 = (1, 1, 0, -1, 0, -1, 1, 0, 1, 0, 1, 0, 0, 0, 0, 0, 0) \cdot (J^{(31)})^t \\ \varphi_{397}^{(989)} &= \psi_{449}^{(989)} = 51911 = (0, -1, 0, 1, 0, 1, 1, 0, 1, 0, 0, -1, 0, 0, 0, 0) \cdot (J^{(31)})^t \\ \varphi_{433}^{(990)} &= 103823 = (1, -1, 1, 0, 0, 1, 0, 0, -1, -1, 1, 0, 1, -1, 0, 0, 0, 0) \cdot (J^{(31)})^t \\ \psi_{441}^{(990)} &= 103824 = (-1, 0, 0, 0, 0, -1, 1, -1, 0, 0, 0, 1, 0, -1, 1, 0, 0) \cdot (J^{(31)})^t \\ \varphi_{417}^{(991)} &= 207646 = (1, -1, 1, 1, -1, 1, 0, 0, 0, 0, -1, 0, 0, 1, 0, 0, 0) \cdot (J^{(31)})^t \\ \psi_{457}^{(991)} &= 207647 = (0, 0, -1, 1, 0, -1, 0, -1, 0, -1, 0, 0, 0, 1, 0, 0, 0) \cdot (J^{(31)})^t \\ \varphi_{421}^{(992)} &= \psi_{469}^{(992)} = 415294 = (-1, -1, 1, 1, 0, 0, 1, 0, 0, 0, 0, 0, 1, 1, 0, 0) \cdot (J^{(31)})^t \\ \psi_{423}^{(993)} &= \psi_{473}^{(993)} = 207647 = (0, 0, -1, 1, 0, -1, 0, -1, 0, -1, 0, 0, 0, 1, 0, 0) \cdot \\ (J^{(31)})^t\end{aligned}$$

$$\begin{aligned}
\varphi_{443}^{(994)} &= \psi_{475}^{(994)} = 103823 = (1, -1, 1, 0, 0, 1, 0, 0, -1, -1, 1, 0, 1, -1, 0, 0, 0, 0) \cdot \\
&\quad (J^{(31)})^t \\
\varphi_{425}^{(995)} &= 51911 = (0, -1, 0, 1, 0, 1, 1, 0, 1, 1, 0, 0, 0, -1, 0, 0, 0, 0) \cdot (J^{(31)})^t \\
\psi_{453}^{(995)} &= 51912 = (0, 0, 0, 0, 1, 0, 0, -1, 0, 1, 0, 0, 0, -1, 0, 0, 0, 0) \cdot (J^{(31)})^t \\
\varphi_{431}^{(996)} &= \psi_{477}^{(996)} = 25955 = (-1, -1, -1, -1, 1, 0, 1, 0, -1, -1, 1, 0, 0, 0, 0, 0, 0, 0) \cdot \\
&\quad (J^{(31)})^t \\
\varphi_{439}^{(997)} &= 12977 = (1, 0, -1, 0, -1, 0, -1, 1, -1, -1, 0, 1, 0, 0, 0, 0, 0, 0) \cdot (J^{(31)})^t \\
\psi_{469}^{(997)} &= 12978 = (-1, 0, 1, -1, 1, 0, 0, 0, 1, 0, 0, 0, 1, 0, 0, 0, 0, 0, 0) \cdot (J^{(31)})^t
\end{aligned}$$

Fig. 6, Table 1, residue 2  $\Gamma$ -encoded:

$$\begin{aligned}
\varphi_{397}^{(987)} &= 9434 = (0, -1, 1, 0, 1, -1, 1, 0, 1, 0, 0, -1, -1, 0, -1, 1, 0, 0) \cdot (G^{(31)})^t \\
\psi_{426}^{(987)} &= -9435 = (-1, 1, 0, 0, 1, -1, 0, 0, -1, 0, 0, 1, 1, 0, 1, -1, 0, 0) \cdot (G^{(31)})^t \\
\varphi_{399}^{(988)} &= 4716 = (0, 0, 1, 1, 0, -1, 0, -1, 0, 0, -1, -1, 0, 0, -1, 1, 0, 0) \cdot (G^{(31)})^t \\
\psi_{410}^{(988)} &= -4717 = (0, 1, 1, 0, -1, 1, 0, 1, 0, 0, 1, 1, 0, 0, 1, -1, 0, 0) \cdot (G^{(31)})^t \\
\varphi_{385}^{(989)} &= 2357 = (0, 1, 0, -1, 0, 0, 0, 0, 1, 0, 0, 1, -1, -1, 1, 0, 0) \cdot (G^{(31)})^t \\
\psi_{438}^{(989)} &= -2358 = (1, 1, 1, 0, 0, 0, 0, 1, 0, 1, 1, 0, 0, 1, -1, 0, 0) \cdot (G^{(31)})^t \\
\varphi_{421}^{(990)} &= 1178 = (0, -1, 0, 0, 1, 0, 1, 0, 0, 0, 0, 1, -1, -1, 1, 0, 0) \cdot (G^{(31)})^t \\
\psi_{430}^{(990)} &= -1179 = (0, 0, 0, 0, -1, 0, 0, 1, -1, 0, 0, 0, -1, 1, 1, -1, 0, 0) \cdot (G^{(31)})^t \\
\varphi_{409}^{(991)} &= \psi_{449}^{(991)} = 589 = (0, 1, 0, 0, 0, -1, -1, 0, -1, 1, 0, -1, 1, 0, 0, 0, 0, 0) \cdot (G^{(31)})^t \\
\varphi_{413}^{(992)} &= \psi_{461}^{(992)} = 294 = (-1, 1, -1, 1, 0, 0, 0, 0, 0, -1, 1, 0, 0, 0, 0, 0, 0) \cdot (G^{(31)})^t \\
\varphi_{405}^{(993)} &= \psi_{461}^{(993)} = 147 = (0, -1, 1, -1, 0, 0, 0, 0, 0, -1, 1, 0, 0, 0, 0, 0, 0) \cdot (G^{(31)})^t \\
\varphi_{435}^{(994)} &= 73 = (1, -1, 0, 0, 1, 0, 1, 0, 0, 1, 0, -1, 0, 0, 0, 0, 0) \cdot (G^{(31)})^t \\
\psi_{446}^{(994)} &= -74 = (0, 1, 0, -1, 0, 0, -1, 1, 0, 0, 0, 0, 0, 0, 0, 0, 0) \cdot (G^{(31)})^t \\
\varphi_{413}^{(995)} &= \psi_{445}^{(995)} = 36 = (-1, -1, 0, 0, 0, 1, 0, 0, 1, 0, 1, 0, -1, -1, 1, 0, 0) \cdot (G^{(31)})^t \\
\varphi_{417}^{(996)} &= \psi_{461}^{(996)} = 17 = (1, 0, 1, -1, 0, 0, -1, 1, 0, 0, 0, 0, 0, 0, 0, 0, 0) \cdot (G^{(31)})^t \\
\varphi_{427}^{(997)} &= \psi_{457}^{(997)} = 8 = (0, 1, 1, 1, -1, 0, -1, 1, -1, 1, 0, 0, 0, 0, 0, 0, 0) \cdot (G^{(31)})^t
\end{aligned}$$

Fig. 6, Table 1, residue 2  $\chi$ -encoded:

$$\begin{aligned}
\varphi_{397}^{(987)} &= 9434 = (1, 0, 0, 0, -1, -1, 0, 0, 0, 0, 0, 0, -1, 0, -1, 1, 0, 0) \cdot (J^{(31)})^t \\
\psi_{426}^{(987)} &= -9435 = (-1, 0, 0, 0, -1, 0, -1, 0, 0, 1, -1, 0, -1, -1, 1, -1, 0, 0) \cdot (J^{(31)})^t \\
\varphi_{399}^{(988)} &= 4716 = (-1, -1, -1, 0, 0, 1, 0, 0, 0, 1, 0, 1, 1, -1, 1, 0, 0) \cdot (J^{(31)})^t \\
\psi_{410}^{(988)} &= -4717 = (0, 0, 0, -1, 0, 0, 0, -1, -1, -1, 1, 0, 1, -1, 1, 0, 0) \cdot (J^{(31)})^t \\
\varphi_{385}^{(989)} &= 2357 = (0, 0, 0, -1, 0, 1, 0, 1, 0, 0, -1, 0, -1, 1, 0, 0) \cdot (J^{(31)})^t \\
\psi_{438}^{(989)} &= -2358 = (-1, 0, 0, -1, 1, 0, 0, -1, 1, 1, -1, -1, 1, -1, 0, 0) \cdot (J^{(31)})^t \\
\varphi_{421}^{(990)} &= 1178 = (0, 0, -1, 0, -1, 1, 1, -1, 0, -1, -1, 0, 0, -1, 1, 0, 0) \cdot (J^{(31)})^t \\
\psi_{430}^{(990)} &= -1179 = (-1, 1, -1, -1, 0, 0, 0, -1, -1, 0, 1, 0, 0, 1, -1, 0, 0) \cdot (J^{(31)})^t \\
\varphi_{409}^{(991)} &= \psi_{449}^{(991)} = 589 = (0, 0, 1, 1, 0, 0, 0, 1, 1, 0, 1, 0, 1, -1, 1, 0, 0) \cdot (J^{(31)})^t \\
\varphi_{413}^{(992)} &= \psi_{461}^{(992)} = 294 = (0, -1, 0, 0, -1, 1, 0, 1, -1, 0, 1, -1, 0, 0, 0, 0, 0) \cdot (J^{(31)})^t
\end{aligned}$$

$$\begin{aligned}
\varphi_{405}^{(993)} &= \psi_{461}^{(993)} = 147 = (-1, -1, 0, 1, 0, 1, -1, 0, 0, 0, 0, 0, 0, 0, 0, 0, 0, 0, 0, 0, 0, 0) \cdot (J^{(31)})^t \\
\varphi_{435}^{(994)} &= 73 = (1, -1, 0, 1, 0, 0, 1, -1, 1, -1, 0, 0, 0, 0, 0, 0, 0, 0, 0, 0, 0, 0) \cdot (J^{(31)})^t \\
\psi_{446}^{(994)} &= -74 = (1, 1, 1, 0, -1, -1, 1, 1, -1, 0, 1, 1, 1, 0, 0, 0, 0, 0, 0, 0, 0, 0, 0, 0) \cdot (J^{(31)})^t \\
\varphi_{413}^{(995)} &= \psi_{445}^{(995)} = 36 = (0, -1, 1, 1, -1, 1, 1, 0, 1, 0, 0, 0, 0, 0, 0, 0, 0, 0, 0, 0, 0, 0, 0) \cdot (J^{(31)})^t \\
\varphi_{417}^{(996)} &= \psi_{461}^{(996)} = 17 = (1, -1, -1, 0, 0, 0, 0, 1, -1, 0, 0, 0, 0, 0, 0, 0, 0, 0, 0, 0, 0, 0, 0) \cdot (J^{(31)})^t \\
\varphi_{427}^{(997)} &= \psi_{457}^{(997)} = 8 = (-1, -1, 1, 1, 0, 0, 0, 0, 0, 1, -1, 0, 0, 0, 0, 0, 0, 0, 0, 0, 0, 0, 0) \cdot (J^{(31)})^t
\end{aligned}$$

Fig. 6, residue 1  $\Gamma$ -encoded:

$$\begin{aligned}
\varphi_{485}^{(990)} &= \psi_{497}^{(990)} = 136 = (-1, 0, 0, 1, 0) \cdot (G^{(31)})^t \\
\varphi_{465}^{(991)} &= 68 = (0, -1, -1, 1, 1, 0, -1, 0, 0, 0, 0, 0, 0, 0, 0, 0, 0, 0, 0, 0, 0, 0, 0, 0, 0) \cdot (G^{(31)})^t \\
\varphi_{465}^{(992)} &= 33 = (-1, 1, -1, 0, 0, 0, -1, 1, -1, 1, 0, 0, 0, 0, 0, 0, 0, 0, 0, 0, 0, 0, 0) \cdot (G^{(31)})^t \\
\varphi_{471}^{(993)} &= 16 = (1, -1, -1, 1, 0) \cdot (G^{(31)})^t
\end{aligned}$$

Fig. 6, residue 1  $\chi$ -encoded:

$$\begin{aligned}
\varphi_{485}^{(990)} &= \psi_{497}^{(990)} = 136 = (-1, -1, -1, 0, -1, 0, 1, -1, 0, 0, 0, 0, 0, 0, 0, 0, 0, 0, 0, 0, 0, 0, 0, 0) \cdot (J^{(31)})^t \\
\varphi_{465}^{(991)} &= 68 = (-1, 1, 0, -1, 1, -1, -1, 0, -1, 0, -1, 0, 0, 0, 0, 0, 0, 0, 0, 0, 0, 0, 0) \cdot (J^{(31)})^t \\
\varphi_{465}^{(992)} &= 33 = (1, 1, 0, -1, 0, 0, -1, 1, 0, 0, 0, 0, 0, 0, 0, 0, 0, 0, 0, 0, 0, 0, 0) \cdot (J^{(31)})^t \\
\varphi_{471}^{(993)} &= 16 = (0, 1, 0, -1, 0, 0, 0, -1, 1, 0, -1, 1, 0, 0, 0, 0, 0, 0, 0, 0, 0, 0, 0) \cdot (J^{(31)})^t
\end{aligned}$$

Table 3, pivot  $\Gamma$ -encoded:

$$\begin{aligned}
\varphi_{72}^{(609)} &= 208430 = (0, 1, 0, 1, 0, 0, 0, 0, 0, 1, -1, -1, 0, 0, 1, 0, 0) \cdot (G^{(31)})^t \\
\psi_{72}^{(609)} &= -208431 = (-1, 0, -1, -1, 0, -1, 1, 0, 0, 0, 0, 1, 0, 0, -1, 0, 0) \cdot (G^{(31)})^t
\end{aligned}$$

Table 3, pivot  $\chi$ -encoded:

$$\begin{aligned}
\varphi_{72}^{(609)} &= 208430 = (0, 0, 1, 1, 0, 1, 0, 1, 0, 0, 0, -1, 0, 0, 1, 0, 0) \cdot (J^{(31)})^t \\
\psi_{72}^{(609)} &= -208431 = (0, 0, 0, 0, 1, -1, 1, 0, 0, 0, 1, 0, 0, 0, -1, 0, 0) \cdot (J^{(31)})^t
\end{aligned}$$

Table 3, residue 2  $\Gamma$ -encoded:

$$\varphi_{78}^{(609)} = \psi_{83}^{(609)} = 66 = (0, 0, 0, 0, 0, 0, 0, -1, -1, -1, -1, 1, 0, 0, 0, 0) \cdot (G^{(31)})^t$$

Table 3, residue 2  $\chi$ -encoded:

$$\varphi_{78}^{(609)} = \psi_{83}^{(609)} = 66 = (0, 1, 0, 0, 1, 0, 0, -1, 0, 1, -1, -1, -1, 0, 0, 0, 0) \cdot (J^{(31)})^t$$

Table 3, residue 1  $\Gamma$ -encoded:

$$\varphi_{58}^{(609)} = 10 = (-1, 0, 1, 0, 0, 0, 0, 0, 1, -1, 0, 0, 0, 0, 0, 0, 0, 0, 0, 0, 0, 0) \cdot (G^{(31)})^t$$

$$\psi_{52}^{(609)} = -11 = (0, 0, 0, -1, 0, 0, 0, 1, -1, 0, 0, -1, 1, 0, 0, 0, 0, 0, 0) \cdot (G^{(31)})^t$$

Table 3, residue 1  $\chi$ -encoded:

$$\varphi_{58}^{(609)} = 10 = (0, 1, -1, 0, 0, 0, 1, 1, 0, 0, 1, 0, -1, 0, 0, 0, 0, 0) \cdot (J^{(31)})^t$$

$$\psi_{52}^{(609)} = -11 = (1, -1, -1, 0, 0, 1, 0, -1, 0, 0, 0, -1, 1, 0, 0, 0, 0, 0) \cdot (J^{(31)})^t$$

Table 3, possible new residues 3 and 4  $\Gamma$ -encoded:

$$\varphi_{438}^{(609)} = 233 = (0, 1, 1, -1, 0, 0, 0, 0, 0, -1, 1, 0, 0, 0, 0, 0, 0, 0) \cdot (G^{(31)})^t$$

$$\varphi_{453}^{(609)} = 39 = (-1, 1, -1, -1, 1, 0, 0, 0, -1, 1, 1, -1, 0, 0, 0, 0, 0, 0) \cdot (G^{(31)})^t$$

Table 3, possible new residues 3 and 4  $\chi$ -encoded:

$$\varphi_{438}^{(609)} = 233 = (-1, -1, 0, 0, -1, 1, -1, 0, 1, -1, 0, 1, -1, 0, 0, 0, 0, 0) \cdot (J^{(31)})^t$$

$$\varphi_{453}^{(609)} = 39 = (1, 0, -1, 1, 0, 0, 0, 0, 0, 0, 0, 0, 0, 0, 0, 0, 0, 0) \cdot (J^{(31)})^t$$

Table 1, possible new residues +, ++ and +++  $\Gamma$ -encoded:

$$\varphi_{437}^{(988)} = \psi_{449}^{(988)} = 50 = (0, 0, 1, -1, 0, -1, 1, 0, 0, 0, 1, -1, 0, 0, 0, 0, 0, 0) \cdot (G^{(31)})^t$$

$$\varphi_{409}^{(991)} = \psi_{449}^{(991)} = 589 = (1, 0, 1, 1, 0, -1, 0, 0, 0, 1, 0, 1, -1, 0, 0, 0, 0, 0) \cdot (G^{(31)})^t$$

$$\varphi_{377}^{(991)} = 97 = (1, 0, -1, 1, 0, 0, -1, 1, 0, 0, 0, 0, 0, 0, 0, 0, 0) \cdot (G^{(31)})^t$$

$$\psi_{409}^{(991)} = 98 = (0, 1, 0, 0, 1, 0, 0, -1, 1, 0, 1, 0, -1, 0, 0, 0, 0, 0) \cdot (G^{(31)})^t$$

Table 1, possible new residues +, ++ and +++  $\chi$ -encoded:

$$\varphi_{437}^{(988)} = \psi_{449}^{(988)} = 50 = (0, 0, -1, 1, 0, -1, 1, 0, 0, 0, 0, 0, 0, 0, 0, 0) \cdot (J^{(31)})^t$$

$$\varphi_{409}^{(991)} = \psi_{449}^{(991)} = 589 = (-1, -1, 0, 0, -1, 1, 0, -1, 1, -1, 0, -1, 1, 0, 0, 0, 0, 0) \cdot (J^{(31)})^t$$

$$\varphi_{377}^{(991)} = 97 = (1, 0, -1, 0, -1, 1, 0, -1, 0, 0, 0, 0, 0, 0, 0, 0, 0) \cdot (J^{(31)})^t$$

$$\psi_{409}^{(991)} = 98 = (-1, 0, -1, 0, 0, -1, 0, 1, 0, 0, 0, 0, 0, 0, 0, 0, 0) \cdot (J^{(31)})^t$$

Table 4, pivot  $\Gamma$ -encoded:

$$\varphi_{239}^{(1000)} = \psi_{269}^{(1000)} = 758 = (0, 0, -1, 0, 1, -1, 0, 1, -1, 1, 0, 0, 0, 0, 0, 0, 0, 0) \cdot (G^{(31)})^t$$

Table 4, pivot  $\chi$ -encoded:

$$\varphi_{239}^{(1000)} = \psi_{269}^{(1000)} = 758 = (1, 0, -1, 0, 1, -1, 1, 0, 0, 0, 1, -1, 0, 0, 0, 0, 0, 0) \cdot (J^{(31)})^t$$

Table 4, residue 1  $\Gamma$ -encoded:

$$\varphi_{356}^{(1000)} = 335 = (1, 0, 0, 0, 0, 0, 0, -1, 1, -1, 1, 0, 0, 0, 0, 0, 0) \cdot (G^{(31)})^t$$

$$\psi_{388}^{(1000)} = -336 = (-1, -1, 0, 1, -1, 0, 0, 0, 0, 0, 0, 0, 0, 0, 0, 0, 0, 0) \cdot (G^{(31)})^t$$

Table 4, residue 1  $\chi$ -encoded:

Table 4, residue 2  $\Gamma$ -encoded:

$$\begin{aligned}\varphi_{135}^{(1000)} &= 5 = (0, 1, 0, 0, 0, 0, 1, -1, 0, 0, 0, 0, 0, 0, 0, 0, 0, 0, 0) \cdot (G^{(31)})^t \\ \psi_{168}^{(1000)} &= -6 = (0, 0, 0, 1, -1, 0, -1, 1, 0, 0, -1, 1, 0, 0, 0, 0, 0, 0, 0) \cdot (G^{(31)})^t\end{aligned}$$

Table 4, residue 2  $\chi$ -encoded:

$$\begin{aligned}\varphi_{135}^{(1000)} &= 5 = (-1, 1, 1, 1, 1, -1, 0, 1, 0, 0, 0, 0, 0, 0, 0, 0, 0, 0, 0) \cdot (J^{(31)})^t \\ \psi_{168}^{(1000)} &= -6 = (0, 0, 0, 1, 1, 0, 0, 0, 0, 0, -1, 1, 0, 0, 0, 0, 0) \cdot (J^{(31)})^t\end{aligned}$$

Both  $G^{(31)}$  and  $J^{(31)}$  lead to various singularity assignments.

For instance

$$0 = (-1, 0, 1, 0, 1, -1, 0, -1, 1, 0, 0, 0, 1, -1, -1, 1, 0, 0) \cdot (G^{(31)})^t$$

$$0 = (0, 0, 0, 0, 1, 0, 1, 1, 0, 1, -1, 1, 0, 0, 0, 0, 0, 0) \cdot (J^{(31)})^t$$

## Appendix B. Crotons in the volume

Table B.15:  $L_m = b_\alpha^{(n)}$  incidences in (CFR)  $\left(\frac{2^n}{\sqrt{2}}\right)^{-1} \rightarrow [b_0^{(n)}; b_\alpha^{(n)}]$  ( $n \leq 3324$ ,  $\alpha \leq 499$ ;  
match=✓; closest pivot=(·); largest  $b_\alpha^{(n)} > L_{31} = (·)$ )

$L_m$ <sup>18</sup>	Type $\sqrt{2}/2^n$	
	$b_\alpha^{(n)}$	in- cidence
2, 6, 12, 24, 40, 72, 126 ( $m = 1, 2, \dots, 7$ )	✓	very high
240	✓	19
272	✓	25
336	✓	9
438	✓	9
756	✓	5
918	✓	1
1422	(1421)	(1)
2340	(2338)	(1)
4320	(4314)	(1)
5346	(5366)	(1)
7398	(7394)	(1)
10 668	(10 596)	(1)
17 400	(17 502)	(1)
27 720	(27 901)	(1)
49 896	(49 780)	(1)
93 150	(94 869)	(1)
⋮		
$> L_{31}$	(2 445 930)	(1)

<sup>18</sup> kissing numbers taken from <http://www.math.rwth-aachen.de/Gabriele.Nebe/LATTICES/kiss.html>

Table B.16:  $L_m = \varphi_\alpha^{(n)}$  incidences in (CFR) type-I/II/III irrationals  $\rightarrow [\varphi_0^{(n)}; \varphi_\alpha^{(n)}]$  (Eqs.(17)–(19);  $n \lesssim 3330$ ,  $2 \leq s \leq 9$ ,  $\alpha \leq 499$ ; match= ✓; closest pivot=(·); largest  $b_\alpha^{(n)} > L_{31} = (\cdot)$ )

$L_m$	Type I		Type II		Type III	
	$\varphi_\alpha^{(n)}$	inci-dence	$\varphi_\alpha^{(n)}$	inci-dence	$\varphi_\alpha^{(n)}$	inci-dence
2, 6, ..., 126	✓	very high	✓	very high	✓	very high
240	✓	131	✓	181	✓	220
272	✓	90	✓	141	✓	163
336	✓	60	✓	93	✓	107
438	✓	47	✓	62	✓	64
756	✓	25	✓	20	✓	25
918	✓	9	✓	21	✓	20
1422	✓	5	✓	6	✓	4
2340	(2341)	(1)	✓	1	✓	4
4320	(4321)	(1)	✓	2	✓	3
5346	(5344)	(1)	(5346 ± 2)	(2)	(5349)	(1)
7398	✓	1	(7399)	(2)	(7398 ± 4)	(2)
10668	(10 674)	(1)	(10 677)	(1)	✓	1
17400	(17 409)	(1)	(17 390)	(1)	(17 398)	(1)
27720	(27 738)	(1)	(27 733)	(1)	(27 717)	(1)
49896	(49 679)	(1)	(50 216)	(1)	(49 888)	(1)
93150	(92 646)	(1)	(93 489)	(1)	(92 677)	(1)
⋮						
207930	—	—	(207 679)	(1)	(208 430)	(1)
⋮						
$> L_{31}$	$(12\ 986\ 152)$ $= L_{46}?$	(1)	(3 614 855)	(1)	(9 996 953)	(1)

**References**

- [Merkel] U.Merkel: [arXiv:math/0608423v41](https://arxiv.org/abs/math/0608423v41), 2016
- [Green] H.S.Green, Phys.Rev. **90**, 270 (1953)
- [Higin] D.Higinbotham,G.A.Miller,O.Hen,K.Rith,CernCourier **53**(4),35(2013)
- [Cohn] H.Cohn,Y.Jiao,A.Kumar,S.Torquato,Geometry&Topology **15**,2235(2011)